Response of a stiff monopile in cohesionless soil to the offshore loading conditions

Master Thesis

M.Sc. Structural and Civil Engineering
School of Engineering and Science
Aalborg University

Aleksandra Lada

June, 2014

School of Engineering and Science
Sohngårdsholmsvej 57
9000 Aalborg
Telefon 994085 30
Fax 98 1425 55
http://bsn.aau.dk/

Title:

Response of a stiff monopile in cohesionless soil to the offshore loading conditions

Project period:

M.Sc. 3rd and 4th semester,
autumn 2013 - spring 2014

Author:

Aleksandra Lada

Supervisor:

Lars Bo Ibsen

PhD Fellow Giulio Nicolai

Page Numbers: V - 56

Appendix Numbers: 57 - 168

Finished: 10-06-2014

Preface

This thesis is submitted as a Master thesis and it was conducted in the period from September 2013 till June 2014. The thesis's title is "Response of a stiff monopile in cohesionless soil to the offshore loading conditions". The thesis is submitted as a fulfillment of the requirements for graduating a Master program on Department of Civil Engineering at Aalborg University, Denmark.

The thesis consists of three scientific papers and appendices related to the work. First two articles are related to the laboratory work and the third one focuses on the finite element analysis. The laboratory manual is attached as one of the appendices.

The following chapters are named by numbers. Section and subsection correspond to the number of the chapter. Figures and tables are also related to the corresponding chapters. As an example, the second figure that is presented in the third chapter is named "Figure 3.2.". All equations are named with a subsequent number. The appendices are numbered by letters. Each article has its own numbering for figures and tables by relating them to the corresponding sections. Equations are numbered with a subsequent number, starting with (1) for each article. All articles are printed with its individual page numbering. However, the number of pages of each paper is considered in the page numbering of the thesis.

All computational programs used to get relevant information for the thesis (and articles) are gathered on the attached CD, together with a pdf version of the thesis.

A list of references used in the thesis is given before appendices. Each article has its own reference list at the end. The position used only in papers are not present in the reference list of the thesis.

The supervisors, Professor Lars Bo Ibsen and PhD Fellow Giulio Nicolai are thanked for their help during the project. A student of Aalborg University, Szymon Gres is thanked for his co-operation during the first semester and his assistance in the laboratory tests.

Summary

The wind energy is currently one of the leading source of the renewable energy. The offshore conditions are more favorable for the energy production, as the stronger and less turbulent wind is working on the turbine. Also the site is less limited, what results in the increasing market of the offshore wind farms. However, the costs of offshore wind turbines exceed the costs of onshore structures and therefore the cost optimization is one of the challenges in the renewable energy sector. As the cost of the foundation constitutes a significant part of the total costs, the developing of the foundation concept can be meaningful for the expanding offshore wind turbine industry.

The most often used concept of the offshore foundation is a monopile. The current standards used for the design of the monopile, [API, 2005] and [DNV, 2011] recommend the use of the p-y curve approach. The method is based on few full-scale tests of slender piles. The standards poorly account for the cyclic loads, which are prevailing for offshore conditions. The standards do not include the load characteristics and the number of cycles in the prediction for the pile response. The only recommendation is the reduction of the soil resistance as an effect of the cyclic loads. Today the large diameter monopiles are used for the offshore wind farms. Their behaviour under the lateral loads is described as a rigid, which contradicts to the flexible behaviour of slender piles.

Currently the subjects related to the design of the offshore monopiles are investigated with a strong interest. Many researchers have analyzed the influence of the number of cycles or load characteristics on the monopile behaviour. The currently state of art reveals that the design of the large-diameter monopile based on the p-y curve approach is questionable and provide inaccurate results.

In order to evaluate the effects of the long-term laterally loads on the stiff monopile the number of small-scale tests have been performed in the laboratory at Aalborg University. Tests are characterized with the magnitude and the direction of loading. The results are analyzed in order to assessed the accumulated rotation and the change in stiffness. Those both values can significantly influence the design of the monopile for offshore wind turbines. The post-cyclic tests provide a relevant information on the change in the ultimate soil resistance.

Additionally a finite element analysis, FEA, is conducted in the geotechnical program PLAXIS 3D. The results are used for analyzing the differences in the behaviour of stiff and flexible piles. Different simulations are performed in order to assess the influence of parameters such as a pile diameter, a pile length and a load eccentricity on the ultimate pile capacity.

Contents

1 Offshore wind turbines

Recently a renewable energy concept is becoming more popular and lot of effort is put on reduction of the usage of fossil fuels, which come from limited resources. In addition, the emission of gas causing the greenhouse effect has become a serious issue. Therefore clean energy industry records steady growth and contributes significantly to the global energy production. Figure 1.1 presents the increase of generated energy from renewable resources from 2000 to 2012 in Europe.

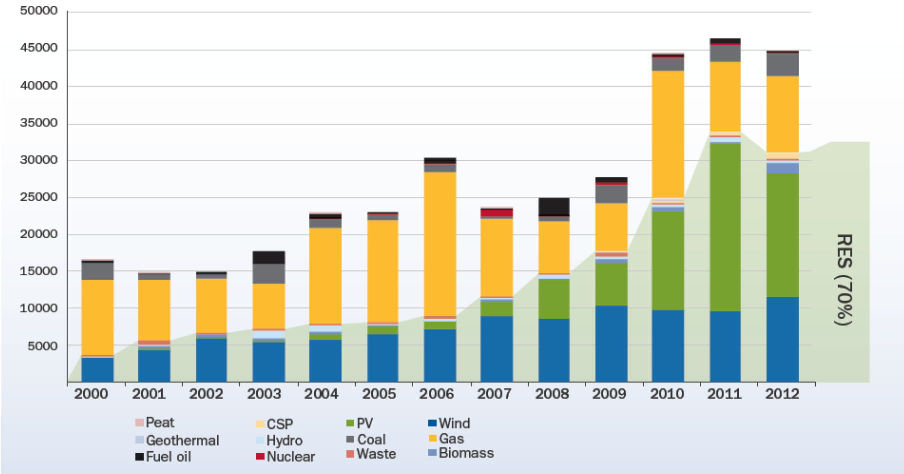

Figure 1.1. Growth of the renewable energy contribution [EWEA, 2013]

One of the most rapidly developed renewable energy resource is wind, which currently is increasing its extent, when it comes to both, onshore and offshore wind turbines. The contribution of wind power in the total energy production has grown from 2.2 % in 2000 to 11.4 % in 2012 [EWEA, 2013]. The huge effects is being made in order to increase this statistics even more. The specific goals have been made by the World Wind Energy Association for upcoming years, which force all countries to enlarge the total wind capacity. Figure 1.2 presents the annual installation of onshore (blue) and offshore (red) wind turbines.

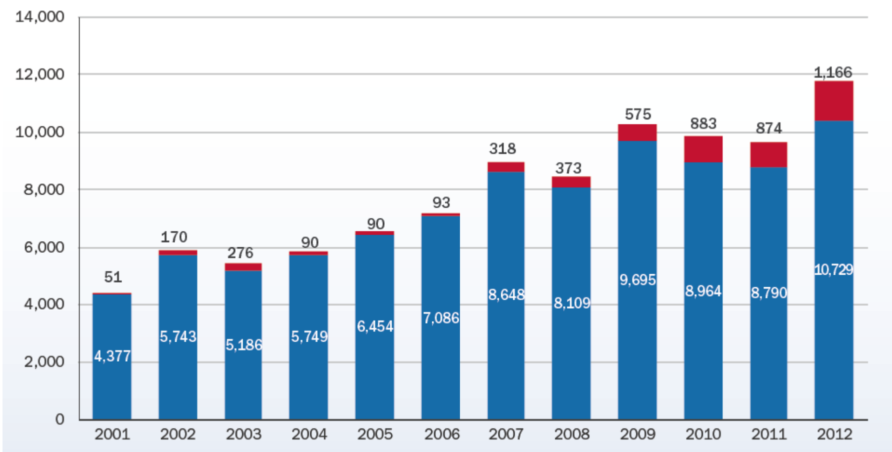

Figure 1.2. Annual instalation of wind turbines [values in MW] [EWEA, 2013]

Wind turbines do not emit CO_2, what makes them environmental friendly. However, they produce noise, which can be disturbing for neighboring areas. Furthermore, the visual effect of wind turbines is often considered as disadvantage. For countries with vastly utilized land sector, where coastal area access is granted, the concept of offshore wind farms is a reasonable alternative, though expensive. The energy captured offshore must be delivered to the coastline by using expensive installations. All of periodic inspections and repairs requires the use of vessels. Nevertheless, offshore wind farms have several strong advantages like higher wind speeds with less turbulence and location far away from human neighbors. Moving wind turbines offshore allows bigger structures, as the seabed is not used for any other purpose and the site is not limited by other factors. All this cause that the power output can be greater comparing with onshore turbines.

1.1 Foundation concepts

Nowadays there are many different foundations used for offshore wind turbines. Different concepts in majority originate from the oil and gas sector. The main difference between those structures and offshore wind turbines is the self-weight, which is significantly smaller for the latter ones. This indicates smaller vertical loads. Hence the wind turbines are subjected to the lateral load on the great heights (wind loads on the rotor), the overturning moment is a dominant force. The differences between this two kinds of structures reveal the need for further and deeper research and improvements of the offshore wind turbine design.

The choice of appropriate foundation must be made based on thorough analysis of site condition, including water depth, sea conditions and soil conditions. Offshore wind turbines are subjected to stronger loads comparing to turbines situated onshore. The sufficient connection with the seabed must be provided, so the wind turbine will not be moved in irreversible extent. Furthermore, the cost of the foundation is considered to be approximately 20 - 30 % of the total cost for offshore turbine. Therefore foundation design is a critical part of the entire project.

The most common foundation used are gravity foundations, monopiles, tripod and jacket foundations, see Picture 1.3.

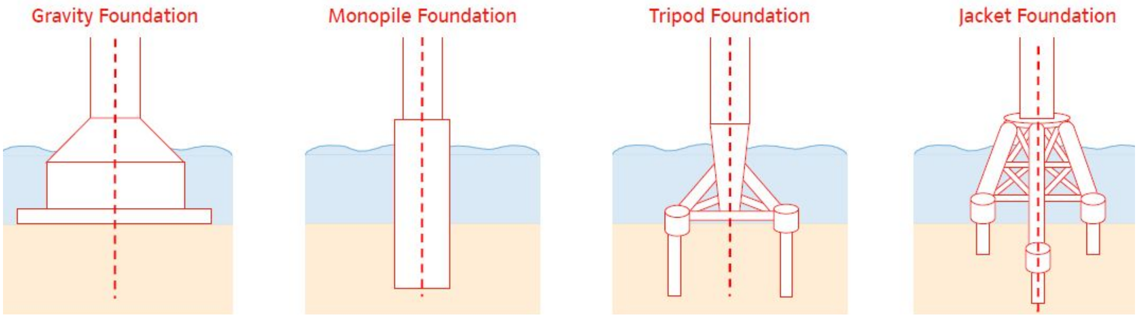

Figure 1.3. Different types of foundation for offshore wind turbines [Miceli, 2012]

The first two concepts are preferable in shallow, or intermediate waters. The gravity based foundation concept is based on its self-weight, which must be sufficient to resist the loads working on the structure and on itself. It is solution that does not require huge costs when it comes to installation. Monopiles use the earth pressure from surrounded soil in order to resist the applied loads.
The jacket and the tripod foundation are the most optimal solution for deeper water levels. Both use the earth pressure as monopiles, however their construction is more complex and adjusted to more difficult site conditions.
For the deepest water the floating foundation concept was established. The possibility of creating a wind farms far from the shore line, where the wind is stronger is undoubtedly a great advantage. However, the maintenance of turbines becomes more problematic. This concept is still in the developing phase.
Currently, the bucket foundation focuses the attention of engineers. Developing new technology is cost and time effective, though it creates an extremely strong foundation through the use of a suction technique. With those features the bucket foundation can easily compete with other concepts and it might become the most often used foundation for offshore wind turbines in the future. Yet, it is a foundation suitable for water depth of 0 - 25 m. Figure 1.4 presents a concept of the bucket foundation.

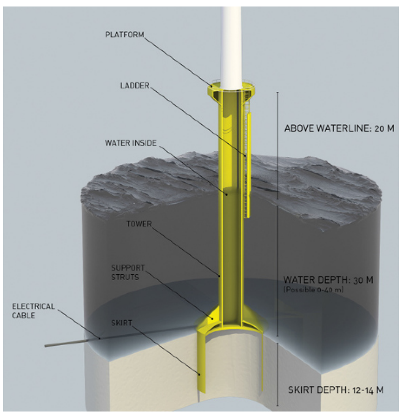

Figure 1.4. The bucket foundation concept from DONG Energy [Thomsen, 2012]

1.1.1 Monopile for offshore wind turbines

The monopile concept is considered as the most preferable foundation for offshore wind turbines. A monopile foundation was the first used solution, when the turbines were moved from onshore to offshore. As it became a success, the monopiles have started to be used in a bigger scale as a simple, cost-effective and reliable solution.

The foundation is based on steel large diameter piles, empty inside. Currently the diameter of monopiles reaches 4-6 m. Piles are inserted into the seabed by using different methods. Most often they are driven in with the use of a hammer or drilled and grouted in a previously prepared hole. The typical length of monopiles is presently around 20-35 m. They are used in the water depth up to 25 m. The thickness of a pile is also of a big importance, as it should be adequate for resisting an axial and lateral loads and also stresses occurring during installation. A pile with the connection to the ground inside and outside of a tube creates a sufficient base for a wind turbine. What is more, the design of monopile is not complicated, as its simple shape provides the easiness when defining the loads. However, the provided installation methods are one of the disadvantages for the monopile concept, as the process is slow and causes some environmental problems.

Figures 1.5 and 1.6 present the monopile concept used in Horns Rev II wind farm situated in the North Sea (27 to 41 km from the west coast of Jutland in Denmark). Horns Rev II, completed in September 2008, was the first farm built furthest offshore in comparison to any other wind farm in the world at that time. Apart from a steel hollow pile the design contains the transition piece with the working platform on the top and the access ladder. Both parts are connected offshore by a grout joint. The installation of one pile with transition piece is a long process, what is another disadvantage of the concept.

Figure 1.5. Large diameter piles and transition pieces [DONG, 2014]

Figure 1.6. Offshore wind turbines on monopiles [DONG, 2014]

For the offshore wind turbines foundation there is a risk of scour, especially when the material in the seabed is rather frictional. The shear stress around the foundation are the reason of sediment transport. The material that flows from its original place around the foundation decreases the stability of the structure. However, this aspect is not a scope of this thesis, therefore it will not be analyzed in details.

1.2 Environmental loading conditions

The offshore wind turbines are subjected to the strong, cyclic, environmental loads, primarily from wind and waves. Concerning a monopile foundation, the vertical load from self-weight of a pile and a wind turbine is small in comparison to the large lateral loads and the overturning moment. Therefore a big importance is made in order to provide an efficient and precise calculation method, regarding cyclic lateral loading.

An important aspect concerning offshore wind turbines is its sensitivity to rotation, as even for the small rotation a wind turbine looses its ability of effective energy production. Therefore requirements for Serviceability Limit State, SLS, set the limits on the permanent accumulated rotation. This limit is often set by the designers to be $\pm 0.5°$.
Additionally, as the structure is exposed to the cyclic loading, the dynamic analysis is an important aspect of the design. The efficiency of a wind turbine is reduced as an effect of vibrations. The first natural frequency of the wind turbine should lie between the dominating forces frequencies, so that the resonance will not occur.
For the extreme waves a typical range of frequency is between 0.07 to 0.14 Hz, whereas the frequency from wind load is normally below 0.1 Hz [Sørensen, 2012].
Due to the aerodynamics of the structure some excitation can be observed in the rotational frequency. As an example, the rotor of a 5MW wind turbine creates 12.1 rotation per minute, what correspond to the frequency of 0.2 Hz. The rotor frequency is often denoted as 1P, wheres 3P frequency (around 0.6 Hz) corresponds to the frequency that the rotor blades pass the tower. This frequency varies from different wind turbines, 1P: 0.15 - 0.3 Hz. Smaller excitation can be observed for 1P, whereas larger excitations can be seen from blades passing the tower, 3P.
The eigenfrequency of the structure depends not only on the stiffness of the tower and the foundation, but also on the stiffness of the interaction between the pile and soil. The most often foundations are design in the way that the eigenfrequency of the complete structure is between 1P and 3P, which is denoted as soft-stiff design. This is illustrated in Figure 1.7.

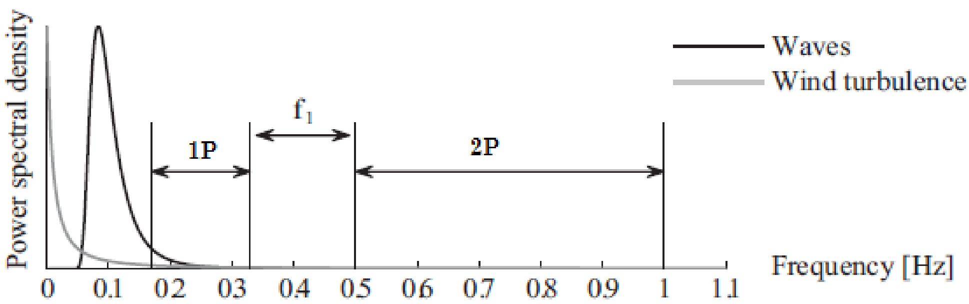

Figure 1.7. The natural frequency, f_1, of a soft-stiff wind turbine design [LeBlanc, 2009]

Another possible option is a soft-soft design, where the eigenfrequency is below 1P, however this gives a risk of resonanse between the structure and the loads eigenfrequency. A stiff-stiff design, with eigenfrequency above 3P, is the most safe, though the most expensive solution.

As the structure is subjected to a large number of cycles, the design should be based also on the Fatigue Limit State analysis, FLS. For the FLS the steel materials used for structure, the tower and the monopile, are required to be assessed. The FLS design should also include the calculation for rotation and the changes in stiffness according to increasing number of cycles.

Apart from the dominant forces, wind and wave loads, there are more that can affect the design. First of all the water current should be analyzed, as the created loads can significantly increase the erosion around the pile foundation. For the localization, where the strong current might be present, the scour protection on the seabed around the monopile is required. Secondly, when the offshore wind turbine is planned to be installed in the localization, where the development of the ice and the drifting ice are of a high probability, the design condition should take them into account as well.

1.3 Current design standards

The full design of the foundation should consider four different design limit states, described below [DNV, 2011].

- ULS - Ultimate Limit State, where the maximum load-carrying resistance must be obtained.
- FLS - Fatigue Limit State, where the failure as an effect of cyclic loading is checked.
- ALS - Accidental Limit State, where the damage due to an accidental event or operational failure is checked.
- SLS - Serviceability Limit State, where the criteria for normal operation must be satisfied.

As mentioned before, the most important is the SLS and FLS design. Both should provide the proper operation of the turbine, resulting in the effective energy ptoduction.

The behaviour of laterally loaded pile is controled by the interaction between the pile and the soil. There are different existing methods that can be used for the analytical pile design, and they can be categorized in four groups [Fan and Long, 2005]:

1. The limit state method: used for ULS design, where the ultimate soil resistance is proportional to the depth and the pile diameter.
2. The subgrade reaction method: giving the linear relation between the soil resistance and the horizontal deflection with the Winkler approach used.
3. The p-y curve method: giving the non-linear relation between the soil resistance and the horizontal deflection with the Winkler approach assumed and with the possibility of obtaining the ultimate soil resistance.
4. The elasticity method: giving the pile response with the preserving of the soil continuity, but only in elastic region - valid only for small strain.

The most often used design standards for monopiles embedded in sand are DNV [2011] and API [2005], where the p-y curve method is used. The choice of this method was dictated by its simplicity and the good accuracy when comparing to full-scale results of slender piles.

The assessment of the lateral displacement of the monopile foundation, and hence its rotation, is made with the use of the Winkler approach. The approach models the pile as en elastic beam, where the uncoupled springs are implemented as en elastic foundation. The stiffness of each spring is obtained from the p-y curves. The concept is presented in Figure 1.8.

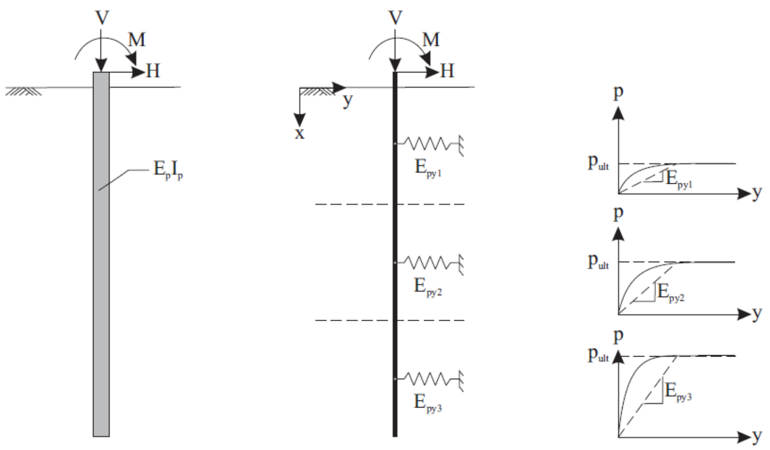

Figure 1.8. The Winkler approach with p-y curves [Augustesen et al., 2009]

The non-linear p-y curves are given by equation (1.1). The stiffness of p-y curves, which is normally denoted as the modulus of subgrade reaction, increases with the depth and decreases with the deflection. The expression is however highly empirical as it was fitted to the results of only few tests.

$$p = A \cdot p_u \cdot tanh\left(\frac{k \cdot x}{A \cdot p_u} \cdot y\right) \tag{1.1}$$

where

p	The soil resistance [kN/m^2]
y	The horizontal deflection [m]
x	A specific depth [m]
p_u	The ultimate soil resistance [kN/m^2]
k	The initial modulus of subgrade reaction [kN/m^3]
A	A factor to account for a loading condition [-]

For the cyclic loading a degradation of the ultimate resistance is assumed. A factor A is then set to be 0.9. The initial modulus of subgrade reaction and the ultimate soil resistance are given in the appendix A.

There are some limitation and unknowns concerning the p-y curve approach. The main one is based on the fact, that the piles used nowadays for offshore wind turbines are stiff, and the rigid behaviour deviates significantly from the flexible behaviour of the slender piles. Therefore the analyze of large-diameter piles cannot be only based on this approach and it requires a thorough study. Others limitation can be found in the appendix A.

The p-y curve approach pays not sufficient attention on the stiffness of pile-soil system. From the assumed formulation, there are no changes of the stiffness due to the cycles. The relation between the soil resistance and the pile head deflection is constant for cyclic loading, and it is only dependent on the soil properties and the pile diameter. No interest is made for the dependency on the others pile properties, on the load characteristics and on the number of cycles. Therefore, there are many researches being performed in order to find a unique solution for the cyclic laterally loaded monopiles. Some of the researches are presented in companion papers.

The behaviour of laterally loaded pile can be also assessed by using a numerical approach. Different Finite Element Models, FEM-s, have been already used, where the deformations and stresses can be obtained, and the ultimate soil resistance can be calculated. Models can be made as 2D or 3D and due to its complexity, they are time consuming and require an adequate computational power. The detailed information of the PLAXIS models used for the purpose of this report can be found in appendix E on page 166.

Main aims of the thesis 2

The renewable energy is under a strong development, what involves the new technologies and also the improvement of existing ones. However, the energy produced from alternative sources is still only a small part of the total income in this field. The wind energy is covering a significant part of the total renewable energy and currently, the offshore wind turbines are more vastly used, as this energy production is more effective. Therefore, the reduction of the costs related to the structure and its installations is very desirable, especially for the foundation cost, as it covers a big part of the total costs for an offshore wind turbine.

In this thesis the monopile foundation is analyzed, as it is the most often used solution for the offshore wind turbines. The offshore monopiles are mainly subjected to the cyclic loading, which is poorly accounted in the current standards for laterally loaded monopiles. The wind turbines are really sensitive to rotation and vibration, which can reduce their efficiency. Therefore, it is important to predict the accumulated rotation for the foundation and to find an accurate way to calculate the change in the stiffness of the pile-soil system. Such a prediction can help in avoiding the resonance between the structure and the main loading excitations. A more precise design of the monopiles can significantly contribute to the cost reduction.

One of the main aims of the thesis is an acquaintance with the theory for laterally loaded piles, especially with attention paid on the non-slender piles that behave rigidly under the lateral loading conditions. The other of main aims focuses on the laboratory research of a laterally loaded monopile. The stiff monopile embedded in dense sand is the base for the tests, where the accurate force measurements and the prediction of the pile rotation on the seabed is enabled. Small-scale tests performed at Aalborg University are used for assessing the accumulated rotation and the change in stiffness and in the ultimate capacity for the soil-pile system as an effect of the long-term cyclic loading. Moreover, the numerical simulations in the geotechnical finite element program PLAXIS have been performed in order to investigate the differences in the behaviour of a flexible and a stiff pile and also for assessing the influence of the pile properties on the ultimate capacity.

The main part of the Master thesis consists three scientific papers, where the laboratory and the numerical results are given and analyzed. Each of the papers contains the short state of art related to the content and the conclusions based on the results.

The research work 3

3.1 Article no. 1

Title:

Response of a stiff monopile for a long-term cyclic loading

Authors:

Lada A., Gres S., Nicolai G. and Ibsen L. B.

Number of pages:

14

Response of a stiff monopile for a long-term cyclic loading

Aleksandra Lada Szymon Gres Giulio Nicolai Lars Bo Ibsen
Aalborg University
Department of Civil Engineering

Abstract

In the Geotechnical Laboratory at Aalborg University a number of small scale tests have been performed to analyze the behavior of a rigid monopile subjected to a long-term cyclic lateral loading. Only a dense state of sand is considered. A cyclic loads cause the permanent displacement of soil and rotation of a pile, effecting in the accumulated rotation and the change in soil-pile stiffness. These aspects, as poorly accounted in current standards, require thorough analysis. The design methods and a current state of art in cyclic loading field is discussed. One of the aims of the article is to validate the method established by LeBlanc (2010) in order to confirm its reliability. In addition, the results of performed tests are presented to obtain the further conclusion on the cyclic behavior of monopiles.

1 Introduction

In the past few years a strong impact has been put on the contribution of the renewable energy sources in the total energy consumption. According to the statistics, the wind power is the leading renewable energy resource in Northern Europe. In Denmark, the data shows that wind energy contributes 27% to total electricity consumption and by 2025 it should rise to 50% [EWEA, 2013]. Among the wind energy structures the offshore wind turbines, OWT, withstand the most harsh and various environmental conditions, therefore a strong influence should be put on their design and the cost optimalization.

The foundation concept for OWT structures is very dependent on the site parameters. There are several types of foundations used: gravity based foundation, monopile foundation, jacket, tripod foundation and bucket foundation. For the average water depth, 30-40m, the most common type of a foundation is a steel monopile. It consists of a large diameter steel tube driven directly into the seabed and connected with a tower through a transition piece. Currently used monopiles have diameters in range 4-6m and slenderness ratio around 5. Average length of a monopile foundation is 15-40m.

The monopile foundation concept for offshore wind turbines originates from the offshore oil and gas sector. However, the physical behavior and the loading type differ. An offshore wind turbine structure is exposed to a strong long-term cyclic lateral loading through it's lifetime due to environmental loads. The number of loading cycles that a structure must withstand varies depending on the situation. Storms cause approximately 100 cycles, where the FLS is assessed for 10^7 cycles. As a consequence, it

leads to rotation of a monopile and rearrangement of soil particles, causing changes in the natural frequency of a soil-structure system. As a result, it strongly influences the design criteria of all parts of a wind turbine. Hence the main design factor for OWT is serviceability limit state and a long-term cyclic lateral loading contributes to permanent deformations in soil and changes in the soil stiffness, therefore it is essential to predict the effects of horizontal loading on monopile foundation.
The 1g tests have being performed in the Geotechnical Laboratory at Aalborg University. A high-quality experimental equipment allows to perform static and both one-way and two-way cyclic tests for the pile under different long-term horizontal loading, with accurate displacements measurements.

In the article results of tests performed by LeBlanc (2010) are compared with new test results in order to confirm the reliability of used methods. Another aim of the article is to draw further conclusion regarding the behavior of cyclic loaded monopiles.
The current research was started by M.G. Onofrei and H.Ravn Roesen in 2012 and their results, among others, are used in further analysis.

2 Current design standards

Current design standards for monopile foundations embedded in sand are based on the empirically derived p-y curves approach,[API, 2005] and [DNV, 2011]. The approach was originally presented by Reese et al.(1974) and subsequently improved and re-formulated by Murchison and O'Neil (1984) by the full scale tests carried out on the Mustang Islands. Physically, p-y curves implemented to Winkler approach are described as series of uncoupled springs, showing a non-linear relation between the lateral displacement of the pile and the soil resistance. A non-linear soil behavior corresponds to the subgrade reaction modulus function. The numerical solution to this problem is provided by solving the 4th order differential equation for a beam deflection.
Recent design regulations define hyperbolic formulation for constructing the non-linear p-y curves for monopiles in sand, dependent on the ultimate soil resistance and the soil stiffness.

$$p(y) = A \cdot p_u \cdot tanh\left(\frac{k \cdot z}{A \cdot p_u \cdot y}\right) \qquad (1)$$

where

A	The loading coefficient
k	The initial modulus of subgrade reaction
p_u	The ultimate soil resistance
z	The soil depth

For a cyclic lateral loading coefficient A is equal 0.9. This indicates that the ultimate soil resistance is reduced. The method was empirically derived from few full scale test of very slender, flexible piles ($L/D = 34.4$). Currently used monopiles for OWT have the slenderness ration around 5. According to Poulos & Hull (1989) a pile behaves as a rigid when the equation (2) is fulfilled, whereas the flexible pile behavior is expected for piles that satisfied the equation (3), [Sørensen *et al.*, 2012].

$$L < 1.48 \cdot \left(\frac{E_p I_p}{E_s}\right)^{0.25} \qquad (2)$$

$$L > 4.44 \cdot \left(\frac{E_p I_p}{E_s}\right)^{0.25} \qquad (3)$$

For offshore steel monopiles in dense sand these expressions are presented in Figure 2.1. A thickness of a monopile wall is expressed as a function of a pile diameter, $t = D/80$. The limit values of Young's modulus for the dense sand, E_s, are considered.

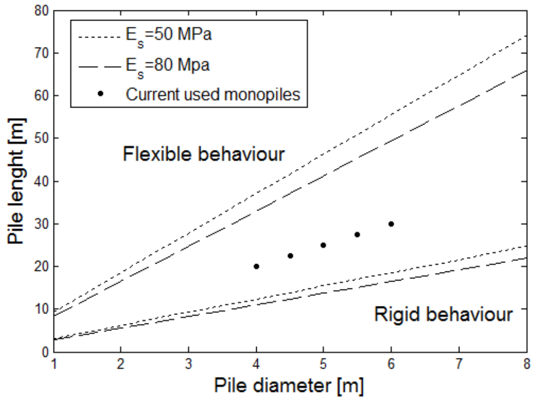

Figure 2.1: Criterion for a pile behavior

Even though, the currently used piles are not precisely fitted to rigid behavior, unquestionable they cannot be analyzed as flexible. Presently, the monopiles used offshore are considered as rigid. The difference in those two behavior of laterally loaded pile is presented in Figure 2.2. Due to different deformation pattern the soil-pile interaction changes, which could possibly influence the p-y curve formulation.

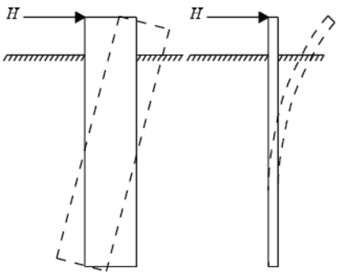

Figure 2.2: Difference between the rigid and the flexible pile behavior [Sørensen *et al.*, 2012]

In addition, OWT during its lifetime is subjected to a large number of cycles leading to accumulated rotation and hardening (or softening) of the soil. Moreover, the pile rotation and changes in soil stiffness are dependent on the direction and the magnitude of loading, which is presented hereafter. However, the p-y curve formulation neglects the influence of these loading parameters. Therefore current design standards are not reliable in describing the long term cyclic effects on a rigid monopile foundation. Methodology for cyclic loaded piles still requires further investigation.

3 State of art

Recently a number of research have been conducted in order to estimate the influence of a cyclic lateral loading on a monopile foundation. The number of proposed methods is vast, from full scale tests to the advanced numerical models and different kind of small-scale experiments. Some of the studies related to analyzed problem are presented.

Little & Briaud [1998] conducted research focuses on effects of a cyclic loading on piles lateral displacement. Obtained results are based on 6 full scale tests on slender piles with different material properties such as reinforced concrete, pre-stressed concrete and steel. These piles were subjected to $10-20$ number of cycles. The data was analyzed by using the cyclic p-y curve approach presented by Little & Briaud (1987), which describes a power law dependency between the number of cycles and the pile displacement.

$$y_N = y_1 \cdot N^{\alpha} \tag{4}$$

where

y_N	The lateral displacement after N cycles
y_1	The lateral displacement after 1^{st} cycle
α	The cyclic degradation parameter

Results from research lead to the following conclusions:
- the traditional p-y curve approach overestimates a pile displacement during cyclic loading,
- a pile displacement obtained by the cyclic p-y curve approach are undervalued in compari-

son to the measured data,
- a pile-soil stiffness has a major influence on soil displacements,
- a soil densification occurs after the first series of cycles (around 10 cycles) resulting in a stiffer response during the second series.

Long & Vanneste [1994] analyzed results of 34 full scale tests conducted in the Tampa Bay, Florida, in order to investigate effects and parameters influencing a pile response to a repetitive lateral loading. Piles were subjected to varying number of cycles (50-100 cycles). The invented method includes the effects of loading characteristics, a pile installation method and a soil density. The equation (5), based on Little&Briaud solution, involves deterioration of a static p-y curve resistance to account all mentioned effects.

$$p_N = p_1 \cdot N^{(\alpha-1)t} \tag{5}$$

where

p_N	The soil resistance after N cycles
p_1	The soil resistance after 1^{st} cycle
α	The degradation factor
t	The degradation parameter

A pile deflection obtained by using deteriorated static p-y curve method is more accurately fitted to full scale tests than deflection calculated by using the standard p-y curve approach.

Lin & Liao [1999] conducted a study in evaluating a strain accumulation for repetitive laterally loaded piles in sand. The data was obtained from 20 full scale tests performed for piles with varying slenderness ($L/D = 4.1 - 84.14$), number of cycles between $4 - 100$ cycles and different installation methods. The results confirmed that the cyclic strain ratio is determined by the load characteristics, the pile installation method, the soil properties and a relation between soil/pile stiffness. By definition of strain, cyclic strain ratio can be used to calculate pile head displacement ratio as following:

$$\frac{\varepsilon_N}{\varepsilon_1} = 1 + t \cdot ln(N) \tag{6}$$

where

ε_N	The soil resistance after N cycles
ε_1	The soil resistance after 1^{st} cycle
t	The degradation parameter

The formula was additionally validated by 6 full scale tests. The predicted and measured displacements were in a good fit for the most of cycles, however during the last stage of loading there were some differences. It is assumed that it was caused by an increase of the soil density with the number of cycles.

LeBlanc *et al.* [2010] introduced an innovative approach based on 1g small-scale laboratory tests, where the predicted accumulated rotation and the change in stiffness of a pile-soil system were analyzed in relation to the load characteristics and the soil density. The tested pile was subjected to 8 000 - 60 000 number of cycles in realistic time frame. Different loading combinations were analyzed. Obtained results were scaled to the full scale through scaling law, allowing an accurate comparison to other results from full-scale tests.
The difference in the isotropic stress level between a small scale and a full scale test was included. A corresponding friction angle was achieved by lowering the relative soil density. The influence of the effective vertical stress was considered in shear modulus calculations. This experiment was conducted on a mechanical rig, where the cyclic loading characteristics were controlled by a system of pulleys and wires between the pile and weight hangers. Tests were performed with a use of the rigid cooper pile, $(L/D = 4.5)$, embedded in dry sand. The research was performed for $I_D = 4\%$ and $I_D = 38\%$, corresponding to the loose and medium-dense state in full scale respectively. The deflections were measured by two dial gauges.

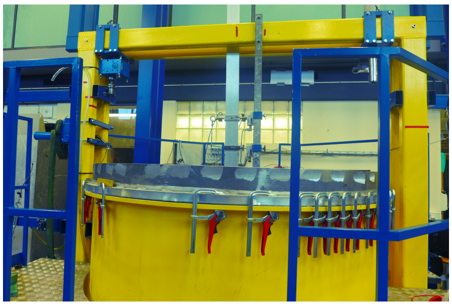

Figure 3.1: The mechanical rig used for tests

The analyzed data revealed an exponential correlation between the accumulated rotation and the number of cycles. Subsequently, the accumulated rotation was dependent on the magnitude and the loading direction. The obtained results showed that the maximum value for accumulated rotation is between one way and two way loading, which contradicts the general beliefs that the largest accumulated rotation is for one way cyclic loading. For the soil stiffness the logarithmic increase with the number of cycles was revealed. This change was observed as independent on the soil density, but only related to the load characteristics. This increase undermines the existing regulations used in standards, [DNV, 2011], indicating the degradation of p-y curves due to a cyclic loading.

4 Test Set-up

Based on the equipment used by LeBlanc (2010), a similar rig has been constructed in the AAU laboratory. The research equipment is illustrated in Figure 3.1.

A cylindrical container is filled with sand of properties presented in Table 4.1. These parameters were obtained by previous tests performed in the laboratory. The inner diameter of the container is 2000 mm and the depth is equal to 1200 mm. At the bottom a drainage system is installed in order to provide saturation of sand. The system includes pipes and the gravel layer of 300 mm, covered by the geotextile.

Table 4.1: Properties of the sand used at Aalborg University Laboratory

Property	Value
Specific grain density, d_s [g/cm^3]	2.64
Maximum void ratio, e_{max} [-]	0.858
Minimum void ratio, e_{min} [-]	0.549

In order to simulate the offshore conditions, the sand must be fully saturated and dense. Before each test a hydraulic gradient is applied and a loose state of sand is obtained by reducing the effective stress. Next sand is vibrated mechanically in order to achieve a small void ratio. The density of soil is established through performing cone penetration tests, [Ibsen *et al.*, 2009]. The variation of the relative densities, I_D, from different tests is presented in Table 4.3. From the results it can be concluded that the soil conditions are similar between each performed test. The target results of I_D lay between 80 to 90 %, what indicates a dense state of sand.

Table 4.2: The variation of the relative soil density

Number of tests	μ_{I_D}	σ_{I_D}
15	88.34 %	4.12 %

An open-ended, aluminum pile is used for tests. The pile characteristics are presented in Table 4.3. The reason of chosen eccentricity is due to the expected eccentricity level of wave loads acting on a pile in the most common cases [Onofrei *et al.*, 2012]. The pile behavior is assumed to be rigid. The small variation of the load eccentricity, $\pm$ 5 mm, that can be caused by different level of soil, are included in the calculations of the moment on the seabed.

Table 4.3: Characteristics of the pile

Property	Length [mm]
Embedded length, L	500
Diameter, D	100
Slenderness ratio, $\frac{L}{D}$	5
Thickness, t	5
Load eccentricity, a	600 ± 5

The monopile is installed in sand by using an electrical motor working with the velocity of 0.02 mm/s. This ensures a small disturbance of the soil.

The different part of the rig are presented in Figure 4.1 and described hereafter.

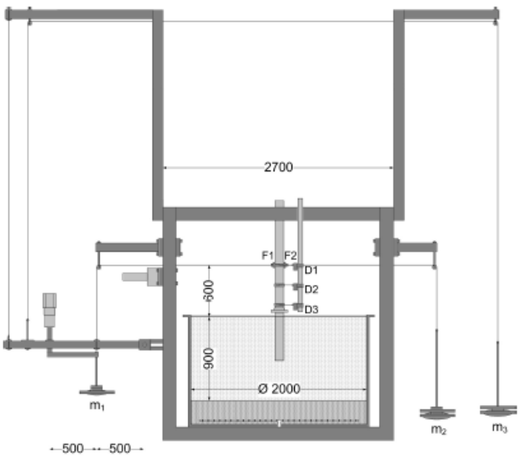

Figure 4.1: A test set-up with the dimensions and the localizations of transducers [Onofrei *et al.*, 2012]

At the top of the pile a rigid tower with force transducers is mounted, F_1 and F_2. A steel frame situated above the container consists of a system of pulleys and wires, that are used to transfer the loads from weights, m_1, m_2 and m_3, to the rigid tower. A beam with three displacement transducers, D_1, D_2 and D_3, is fixed to the steel frame in order to measure the displaced position of the pile. This information are used to extrapolate a rotation to the ground level. Two types of loading are performed, indicating the two different loading systems.
The static loading is a displacement controlled test performed with the use of a motor attached to the steel frame. The motor creates a pulling horizontal force acting on the tower, which is recorder by F_1. The main aim of this test is to obtain the ultimate resistance moment of soil, M_R. The speed of pulling is equal to 0.02 mm/s, so in case of creating the excess pore pressure, it can easily dissipate.
A cyclic loading is initiated by m_1 and m_2, which create forces recorded by F_1 and F_2. The mass m_3 is a counter-weight of the rig. The mass m_2 is directly connected to F_2 through a wire and a pulley, what result in the force equal to $m_2 g$. On the other side the mass m_1 is put on a rotating hanger, controlled by a motor with the loading frequency of 0.1 Hz. This correspond to a common wave loads frequency [Onofrei *et al.*, 2012].

The rotating hanger works on a lever connected to the frame through a pinned joint. When the motor starts to rotate m_1, the force increases until it reaches the maximum value, when the mass is in the most further position, equation (7). While the cycle is continued, the force decreases till minimum, when the mass returns to the starting position - the most closest to the force transducers, equation (8).

$$F_{max} = 3 \cdot m_1 g - m_2 g \tag{7}$$

$$F_{min} = m_1 g - m_2 g \tag{8}$$

An accurate determination of the loading magnitude is difficult due to the loss in force. Partly, it can be caused by the friction in the mechanical system. In addition, some losses appear due to the lever tilting. As long as the wire connecting F_1 and the lever is of a fixed length, every time when the pile rotates, the position of the lever will change in some small extent.

5 Tests methodology

A presented research methodology is based on the concept described by LeBlanc *et al.* [2010]. A comparison with the full-scale is not a part of the research, therefore no scaling law is used.

All tests are identified by the load characteristic parameters ζ_b, equation (9) and ζ_c, equation (10). The cyclic loading parameters describe the magnitude and direction of loading respectively. The visual interpretation is illustrated in Figure 5.1.

$$\zeta_b = \frac{M_{max}}{M_R} \quad (9)$$

$$\zeta_c = \frac{M_{min}}{M_{max}} \quad (10)$$

where

M_{max}	The maximum moment[Nm]
M_{min}	The minimum moment [Nm]
M_R	The static moment capacity [Nm]

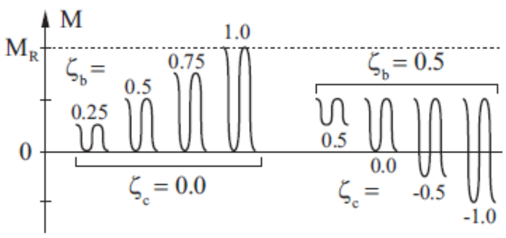

Figure 5.1: Characterization of cyclic loading [LeBlanc *et al.*, 2010]

The value of the static moment capacity is obtained from a static loading test. The value of M_R is determined in reference to moment-rotation curves. The moment of failure is identified for the maximum value, before the magnitude starts to decrease. The results of static tests are illustrated in Figure 5.2.

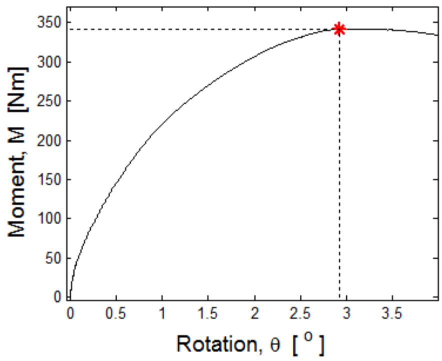

Figure 5.2: The static test results

The applied magnitude of loading is determined in reference to FLS, where ζ_b for the typical design load for OWT fluctuates around value of 0.3. The assumed range of ζ_c is $-1 < \zeta_c < 1$, where $\zeta_c = 1$ describes the one-way loading and $\zeta_c = -1$ describes the two-way loading. The research pays attention on the negative values of ζ_c, regarding to the conclusion made by LeBlanc *et al.* [2010], that the worse cyclic conditions are obtained for tests with loading between one-way and two-way.

The data obtained in tests provide information about the change in stiffness during the cyclic loading, k, and the accumulated rotation after long-term cyclic loading, $\Delta\theta(N)$. The assumptions concerning these two parameters are described in following sections. The method for determining both values is presented in Figure 5.3.
During the cyclic test 50 000 load cycles are applied. The FLS is assessed for 10^7 number of cycles, however such a big number of cycles

is time consuming. The adopted number of cycles is assumed to be sufficient for describing the behavior of monopiles for FLS.

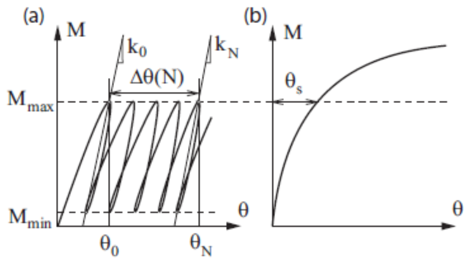

Figure 5.3: A method for determining stiffness and accumulated rotation [LeBlanc *et al.*, 2010]

In order to fully refer to the research performed by LeBlanc *et al.* [2010] the sand should behave as drained during the loading. As far as for static tests this is provided by the small velocity of pulling, the conditions during cyclic tests must be analyzed. Therefore, the results of first cycle in each test, the maximum moment and the corresponding rotation, are plotted and compared with the static results. Figure 5.4 indicates that during the cyclic tests, the drained condition is preserved. The only result that does not fit to the static curve is from the test characterized with $\zeta_b = 0.41$, where the sand behaviour can be interpreted as a partially drained.

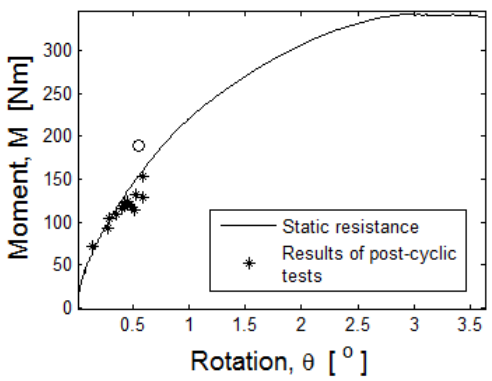

Figure 5.4: The reference static test with the results for first cycle in each cyclic test

6 The accumulated rotation

A method for describing accumulated rotation is express by equation (11), using the power law of the same form as it was done in LeBlanc *et al.* [2010].

$$\frac{\Delta\theta(N)}{\theta_0} = \frac{\theta_N - \theta_0}{\theta_0} = T_b \cdot T_c \cdot N^n \qquad (11)$$

where

θ_0	The rotation after 1^{st} cycle
θ_N	The rotation after N cycle
T_b and T_c	Dimensionless functions
n	The power fitting parameter

It was already proved by others researchers, that the power dependency between the accumulated rotation and the number of cycles gives a good fit with the real tests values.
The magnitude of the rotation caused by cyclic loading should be normalized by the corresponding rotation from the static tests, θ_s, Figure 5.3. However, some differences between static moment capacity was revealed after performing few static tests in the AAU laboratory, as there are always some small discrepancies in the test set-up between performed tests. Furthermore, while the two-way cyclic tests are being performed, there is a risk of a small negative rotation to occur before the 1^{st} cycle, what might have effects on the initial rotation. Therefore, the initial rotation is used when normalizing $\Delta\theta(N)$.

LeBlanc *et al.* [2010] revealed that a power fitting parameter for all loading conditions can be set to $n = 0.31$. However, this fit is no longer valid for dense sand, what is illustrated in Figure 6.1 for one-way and two-way loading tests ($\zeta_c = -0.55$).
The fitting parameter is therefore adjusted for each singular test. So far, no dependency between power fitting parameters and load characteristics have been found, however the mean value for all tests is $n = 0.14$, which is a

half of the value given by LeBlanc.

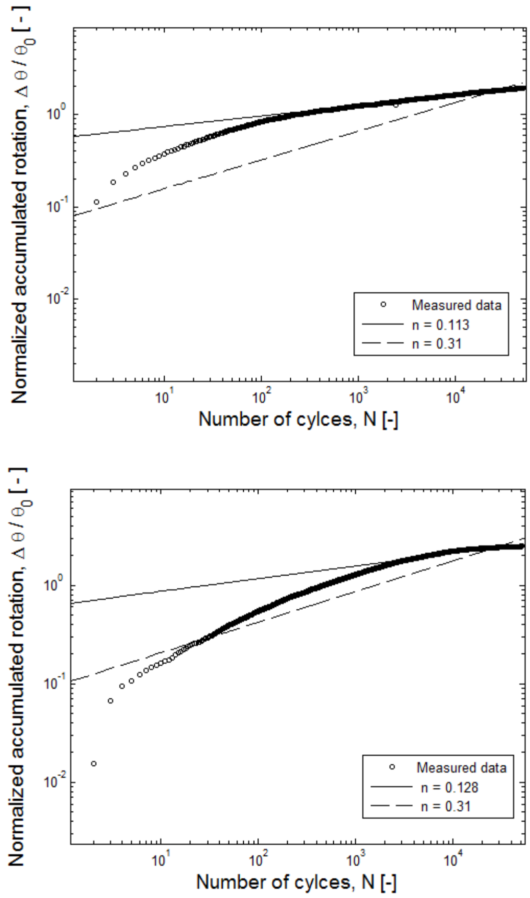

Figure 6.1: Normalized rotation for one-way loading test (upper plot) and two-way loading test (lower plot)

T_b and T_c functions depend on the load characteristics and soil density. T_b can be obtained by performing tests with $\zeta_c = 0$ and varying ζ_b. Figure 6.2 presents the relation of T_b for performed tests in correlation to the results obtained by LeBlanc *et al.* [2010]. The change in soil relative density seems to increase the values of T_b, what could indicate the increase of the accumulated rotation. However, as a different power fitting parameter is applied, the value of accumulated rotation cannot be solely based on T_b value.

It is assumed that $T_c(\zeta_c = 0) = 1$. As for the static test no accumulated rotation is expected, therefore $T_c(\zeta_c = 1) = 0$. The same is predicted for two-way cyclic loading, as the load is equal in both direction, $T_c(\zeta_c = -1) = 0$. The rest of the values are empirically determined by fitting to the laboratory results. Only the negative values of ζ_c are analyzed. Figure 6.3 illustrates the tests results, along with the trend found by LeBlanc *et al.* [2010].

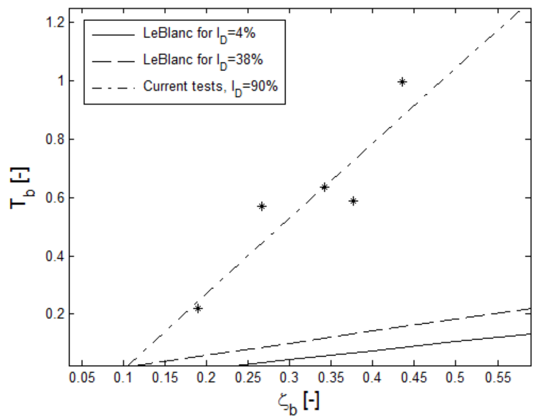

Figure 6.2: A dimensionless functions T_b

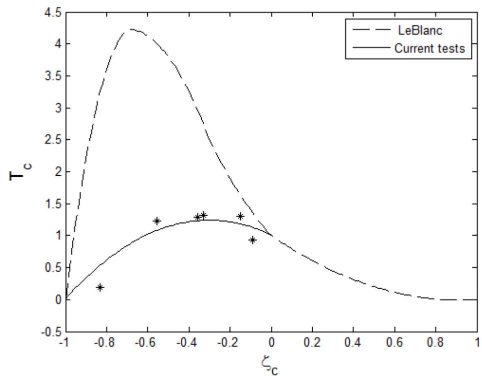

Figure 6.3: A dimensionless function T_c

Despite that the values of T_c are smaller in comparison with LeBlanc *et al.* [2010], it does not indicate that the accumulated rotation is smaller for denser sand, as it depend on both,

T_b and T_c. Both these values could be also affected by a power fitting parameter. However, the shapes of functions are similar, with extreme values for tests between one-way and two-way loading.

More results of accumulated rotation with dependency on ζ_c are presented in Figure 6.4 with logarithmic axes and in Figure 6.5 with normal axes. Selected tests are described by $\zeta_b \approx 0.3$.

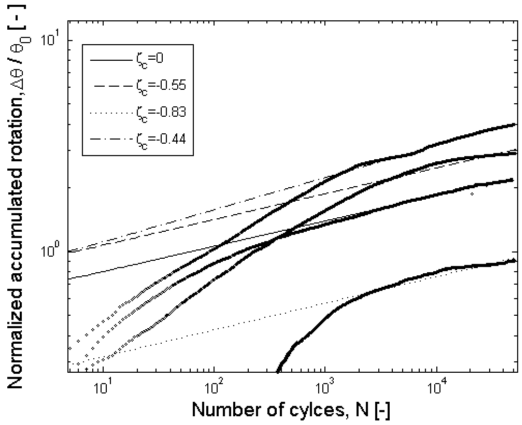

Figure 6.4: The increase of accumulated rotation for varying ζ_c - logarythmic axes

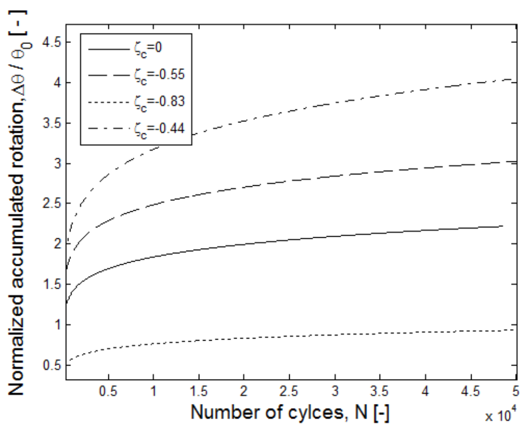

Figure 6.5: The fitting function for accumulated rotation for varying ζ_c - normal axes

The value of $\Delta\theta$ / θ_0 is overestimated by the power function for the first loading cycles, but a good fit is provided for a large number of cycles, what is crucial for FLS design. The accumulated rotation gets the biggest value for $\zeta_c = -0.44$, whereas the smallest increase is observed for $\zeta_c = -0.83$. Similar observation was obtain by LeBlanc *et al.* [2010], where the maximum accumulated rotation was obtained for loading condition between one-way and two-way. When the fitting functions are plotted in normal axes a significant accumulated rotation can be observed for couple first cycles and more constant behavior is found with increasing N.

Generally, the values of $\Delta\theta$ / θ_0 are bigger for dense sand in comparison to loose and medium-dense sand.

7 The change in stiffness

The stiffness in relation to the number of cycles, k_N, is described by the equation 12, likewise in the research of LeBlanc *et al.* [2010].

$$k_N = k_0 + A_k \cdot ln(N) \tag{12}$$
$$k_0 = K_b(\zeta_b)K_c(\zeta_c) \tag{13}$$

where

A_k	A dimensionless parameter
k_0	The initial stiffness
K_b and K_c	Dimensionless functions

Even though a larger scatter of data is noticeable for stiffness results, they can be fitted to above mentioned function. The dimensionless parameter A_k was found to be constant for results obtained by LeBlanc *et al.* [2010], $A_k = 8.02$, not depending on I_D.

Figure 7.1 presents the results for dense sand, where the data are fitted for fixed value of A_k in comparison to the best possible fit. The results reveal that for dense sand the parameter A_k is of larger value. The parameter is obtained for each test.

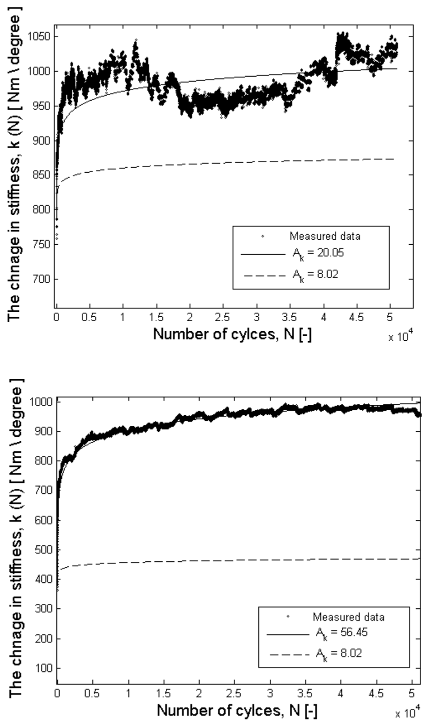

Figure 7.1: The change in stiffness for one-way loading test (upper plot) and two-way loading test (lower plot)

A large discrepancy of A_k is observed, but clearly there is an increase in A_k for increasing ζ_b, what can be found in Figure 7.2. No such a dependency was found for different values of ζ_c.

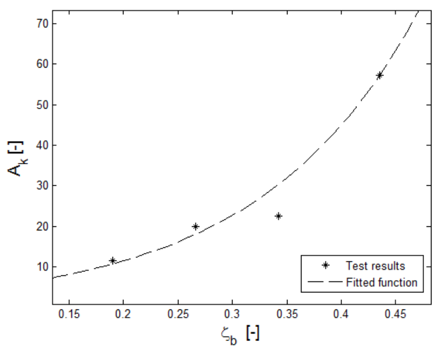

Figure 7.2: The increase of A_k as a function of ζ_b

According to LeBlanc *et al.* [2010] the dimensionless function K_b and K_c are only dependent on the load characteristics. In order to distinguish between two functions it is assumed that $K_c(\zeta_c = 0) = 1$, so the values of K_b are found for one-way cyclic loading and the rest of tests results are extrapolated. Functions are presented in Figure 7.3 and 7.4 along with the results obtained by LeBlanc *et al.* [2010].

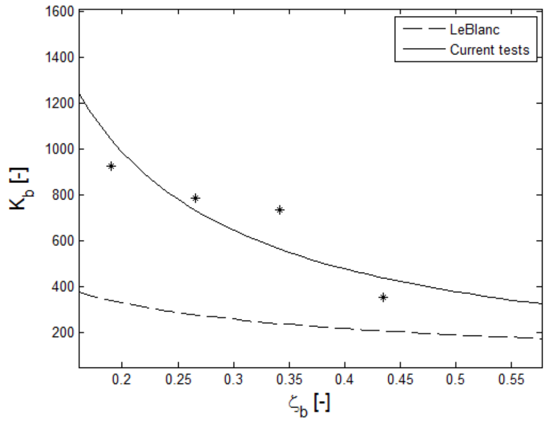

Figure 7.3: The dimensionless functions K_b

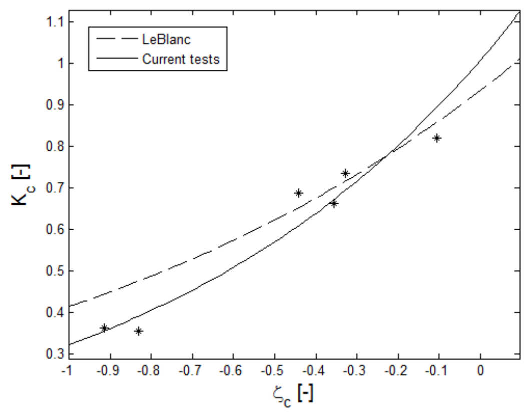

Figure 7.4: The dimensionless functions K_c

The results for dense sand indicate the increase in the initial stiffness comparing to loose and medium sand. The values of K_c, despite a visible scatter of data, seem to fit the curve obtained by LeBlanc *et al.* [2010], whereas there is a significant increase in the values of K_b. The same trend is preserved, as an increase of ζ_b decreases the value of K_b. It can be concluded that values of K_c are independent on I_D, however this does not hold for values of K_b.

More results of the change in stiffness for changing ζ_c are presented in Figure 7.5. Selected tests are described with $\zeta_b \approx 0.3$.
The biggest increase of stiffness is observed for one-way cyclic loading, whereas the smallest increase occurred for the two-way loading test. The same behaviour was obtain by LeBlanc *et al.* [2010]. Furthermore, the most of soil stiffness is mobilized during first loading cycles. This behavior indicates a high, nonlinear increase is soil stiffness, that occurs due to cyclic sequence of loading and unloading, which might influence the relative soil density around the pile by increasing it. With increasing N, the value becomes more constant.

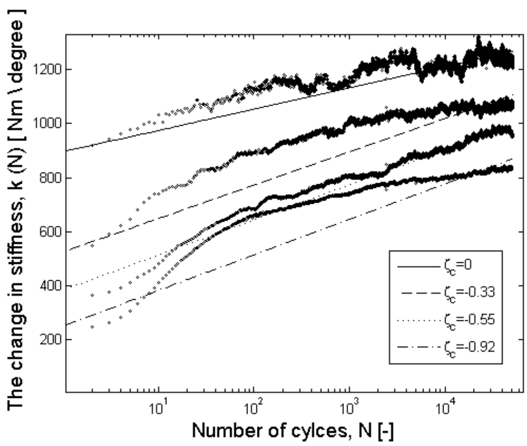

Figure 7.5: The change of stiffness for varying ζ_c

Generally, the increase of stiffness is found to be much bigger for dense sand in comparison to loose and medium-dense sand.

8 The post-cyclic soil resistance

The results reveals that the ultimate resistance almost always increases as a result of large number of cycles, Figure 8.1. The increase might be caused by the previously mentioned rise in the soil stiffness in the cyclic loading. The significant increase of the static stiffness is also noticed from the figure.

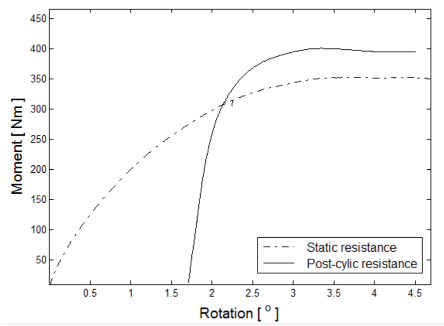

Figure 8.1: The change in soil ultimate resistance for one-way loading test

The results of post-cyclic resistance for all tests are plotted in Figure 8.2. All of the points exceed the ultimate bearing capacity given by the static tests. The average increase of the bearing capacity is assessed for around 10%.

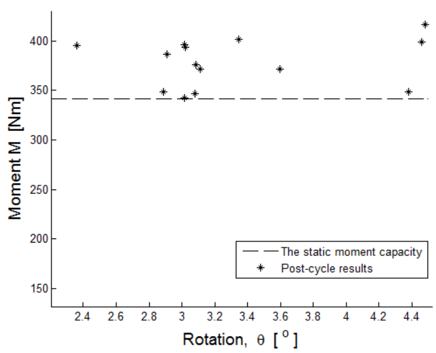

Figure 8.2: The results of the post-cyclic resistance for different tests

9 Conclusions

The presented paper provides the results of small scale tests conducted on the rigid pile foundation in dense, saturated sand. The monopile is subjected to a long-term cyclic lateral loading. The article relates to the results obtained by LeBlanc *et al.* [2010] for laterally loaded pile in loose and medium dense sands.

In the research the accumulated rotation and the change in cyclic stiffness are analyzed. Both illustrate that the loading characteristics have a significant effects on the pile behavior under a cyclic loading conditions. This finding is an important aspect for a future pile design, as the current standards do not include the load characteristics while designing a monopile subjected to the cyclic loading.
The function for the accumulated rotation established by LeBlanc *et al.* [2010] was modified for dense sand. The power dependency for a growing number of cycles reveals the maximum accumulated rotation for tests between one-way and two-way loading, as it was obtained for medium and loose sand. However, the magnitude of accumulated rotation increases for dense sand.
The logarithmic function for the change in soil stiffness obtained by LeBlanc *et al.* [2010] was also modified for piles embedded in dense sand. The increase of stiffness is found to be significantly bigger for dense sand comparing to medium and loose sand.
The results reveal that first cycles are important for a whole cyclic process, as the most of rotation is mobilized in these first cycles. This is undoubtedly influenced by the nonlinear increase of stiffness in its initial cyclic part. As the soil-pile system becomes more stiff, the accumulated rotation is more constant for larger number of cycles.

Furthermore, a series of post-cyclic tests revealed the increase of post-cyclic bearing capacity for both one-way and two-way cyclic loading. Following results contradicts current design standards, which involves degradation of stiffness for p-y curves by factor of 0.9 for including the effects of cyclic loading.

For more thorough summary of cyclic loading behavior of offshore monopiles in dense sand further research, focused on larger diversification of load characteristics, ought to be conducted. Finally, in order to create the general design method, obtained data must be compared with full scale results to verify proposed solutions.

References

API, American Petroleum Insitute. 2005. *Recommended practice for planning, designing and constructing fixed offshore platform*. Downloaded: 10-10-2013.

DNV, Det Norske Veritas. 2011. *Design of Offshore Wind Turbine Structures*. Downloaded: 10-10-2013.

EWEA, The European Wind Energy Association. 2013. *Wind in power - 2012 European Statistics*. URL: `http://www.ewea.org/`. Downloaded: 06-03-2014.

Ibsen, L. B., Hanson, M., Hjort, T., & Thaarup, M. 2009. MC- Parameter Calibration for Baskarp Sand No. *Department of Civil Engineering, University of Aalborg*.

LeBlanc, C., Houlsby, G.T., & Byrne, B.W. 2010. Response of stiff piles in sand to long-term cyclic lateral loading. *Geotechnique 60*, **No.2**, 79–90.

Lin, S., & Liao, J. 1999. Permanent Strains of Piles in Sand due to Cyclic Lateral Loads. *Journal of Geotechnical and Geoenvironmenral Engneering*, 798–802.

Little, Robert L., & Briaud, Jean-Louis. 1998. Full scale cyclic lateral load tests on six single piles in sand. *US Army Engineering District, Final Raport*.

Long, J.H., & Vanneste, G. 1994. Effects of Cyclilc Lateral Loads on Piles in Sand. *Journal of Geotechnical Engineering*, **Vol.120, No.1**, 225–244.

Onofrei, M.G., Roesen, H. Ravn, & Ibsen, L. Bo. 2012. Small-Scale Modelling of Monopiles in Sand Subjected to Long-Term Cyclic Load. *Department of Civil Engineering, Aalborg University*.

Sørensen, S.P.H., Brødbæk, K.T., Møller, M., & Augustesen, A.H. 2012. Review of laterally loaded monopiles employed as the foundation for offshore wind turbines. *DCE Technical Reports, Department of Civil Engineering, Aalborg University, Aalborg, Denmark*, **No.137**.

3.2 Article no. 2

Title:

The stiffness change and the increase in the ultimate capacity for a stiff pile resulting from the cyclic loading

Authors:

Lada A., Nicolai G. and Ibsen L. B.

Number of pages:

9

The stiffness change and the increase in the ultimate capacity for a stiff pile resulting from a cyclic loading

Aleksandra Lada Giulio Nicolai Lars Bo Ibsen
Aalborg University
Department of Civil Engineering

Abstract

Today the knowledge concerning a monopile design under a cyclic loading is uncertain and the current standards might lead to the failure problems or to an uneconomical design. An inappropriate prediction of the stiffness for pile-soil system might lead to vibration problems resulting from the resonance that can occur between the natural frequency of the wind turbine and the frequencies of cyclic loads.
In the paper the experimental results of small-scale tests on a stiff monopile are presented to outline the change in stiffness during the cyclic loading and the change in the ultimate pile capacity. The results confirm the increase of stiffness and the increase in bearing capacity resulting from cyclic loading. Performed analysis provides a better understanding of the problem and reveals some correlations that can be useful in the future design of stiff monopiles.

1 Introduction

Problems concerning energy are well-known and require a continuously increasing focus on renewable energy sources. During last years a huge rise of installed wind capacity has been reported [WWEA, 2013]. The wind turbine concept gives a non-limited resource of the energy, reducing problems of CO_2 production. Situating the wind farms offshore results in a less turbulent, stronger wind, which allows a more effective energy production. However, the costs of offshore wind turbines greatly exceed the costs of onshore structures and therefore, a strong impact should be put on the cost stabilization.

A significant part of the total costs for an offshore wind turbine concerns the foundation design. Currently, the most often used solution in the offshore area is a monopile concept. As far as the installation process is well-known, the behavior under the cyclic loading from wind and waves is poorly accounted in the literature. An increasing knowledge concerning this aspect might lead to notably changes in costs of offshore wind turbines and the cost decrease will contribute to an increase of competitiveness of the offshore wind energy in the general energy market.

The results of small-scale tests are presented in order to analyze the changes in stiffness for soil-pile system and the ultimate soil-pile resistance influenced by cyclic loading. They are preceded with the description of current standards for laterally loaded piles and also with a short state of art concerning this issue. The analysis demonstrates that both, the soil-pile stiffness and the post-cyclic resistance increase due to the long term cyclic loading conditions. This will affect not only limit state designs, but also the eigenfrequency of the wind turbine.

THE STIFFNESS OF WIND TURBINE

The reliability of the foundation design can be attributed to the better understanding of the stiffness for the soil-pile system. The stiffness is important as it contributes to the eigenfrequency of the whole turbine. As the wind turbines are sensitive to vibration that affects the proper operation of a turbine, it is extremely important to avoid the resonance, that can occur between the eigenfrequency of the structure and the frequencies coming from cyclic loads. Moreover, the action of the rotor exerts the aerodynamic loads at frequencies of 1P, which is the rotor frequency and 3P, which is the frequency at which the blades pass the tower. Consequently, the wind turbines are designed in a manner that their frequency does not lie close to these loads frequencies, as soft-soft structure, soft-stiff structure and stiff-stiff structure as indicated in Figure 1.1.

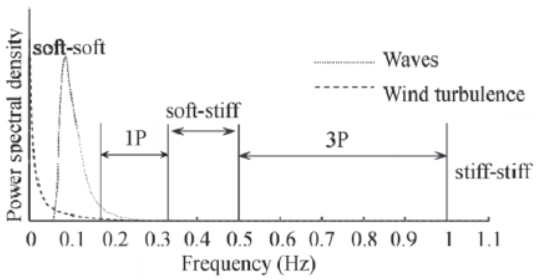

Figure 1.1: Typical design ranges for offshore wind turbines [Kirkwood & Haigh, 2014]

The most safe solution is the stiff-stiff, though the most expansive. Currently, the soft-stiff solution is chosen by the most of designers. However, the sufficient stiffness of the structure must be provided. As long as the stiffness of the tower and the monopile can be calculated, determination of the stiffness for soil-pile interaction is rather problematic. The most often used analytical approach for laterally loaded piles is the p-y curve method outlined in DNV [2011] and API [2005].

THE P-Y METHOD

Current standards use the Winkler approach, where the lateral soil capacity is presented as a system of uncoupled springs. The stiffness of each spring is obtained from the p-y curve, which show the relation between the mobilized resistance of surrounding soil, p, and the lateral displacement, y. This relation for pile embedded in cohesionless soil is estimated based on the full-scale tests results of slender piles, [Reese *et al.*, 1974], [O'Neill & Murchinson, 1983]. Equation (1) describes this dependency.

$$p = A \cdot p_u \cdot tanh\left(\frac{k \cdot X}{A \cdot p_u} \cdot y\right) \tag{1}$$

Here p_u stands for the static ultimate resistance, X for the depth below soil surface and k is the initial modulus of subgrade reaction, that can be determined based on the friction angle. A factor for the cyclic loading is set to 0.9 what means, that the ultimate soil resistance is assumed to degrade as an effect of cyclic loads.

The ultimate resistance is obtained from equation (2) for a shallow depth and equation (3) for a deep depth. The depth is considered to be deep, when the value of shallow depth soil resistance becomes bigger belong those two. Coefficients C_1, C_2 and C_3 are based on the friction angle.

$$p_{us} = (C_1 \cdot x + C_2 \cdot D) \cdot \gamma' \cdot x \tag{2}$$

$$p_{ud} = C_3 \cdot D \cdot \gamma' \cdot x \tag{3}$$

The equations shows that the response of laterally loaded pile is only dependent on the pile diameter, D, but not on the embedded length, L, or the eccentricity of the load, e.

The stiffness obtained from the p-y curve is decreased for cyclic loading, $A = 0.9$. The approach does not account for the magnitude, the direction of loading and for the number of cycles. Another aspect is the usefulness of the method for currently design monopiles. The method was originally designed for a slender piles, that behave flexible under the lateral loads. Today monopiles has a significantly smaller slender ratio and their response on the lateral load is considered to be rigid. The behaviour of stiff monopile under the lateral load is presented in Figure 1.2. The displacement at the pile toe that occur for a rigid pile results in additional shear stress, which increase the lateral resistance. Therefore the use of the method for large diameter piles is doubtful.

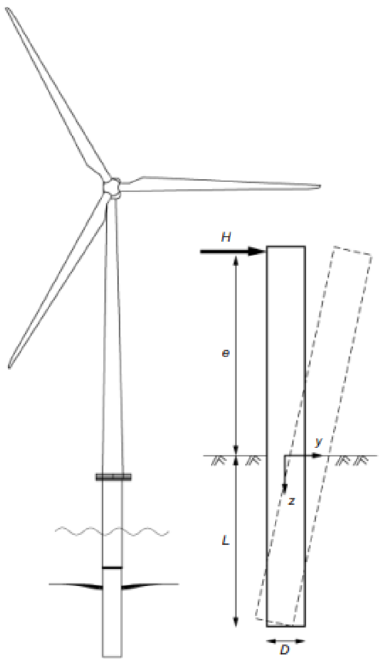

Figure 1.2: A rigid monopile for offshore wind turbine [LeBlanc *et al.*, 2010]

CURRENT PRESENTED CONCEPTS

Recently the behaviour of cyclic laterally loaded monopiles is investigated with a strong interest. The change in stiffness as an effect of lateral cyclic loads has been already analyzed by many researchers. Especially small scale tests and numerical models are used as both are more cost-efficient solutions in comparison with full-scale models.

The change in stiffness effecting from cyclic loading was confirmed in papers of Little & Briaud [1998]. The research based on the results of full-scale slender piles indicates the stiffer response in the second series of cycles as a result of sand densification in the first, preceding series of cycles.
Long & Vanneste [1994] after exploring 34 full-scale tests of both, slender and stiff piles, deduced that the soil resistance is decreased by performed cycles. However, it is stated in limitation that the soil densification might happen for loading ratio below 0 (between one and two-way loading).
Klinkvort *et al.* [2010] by performing a centrifuge small-scale test on a stiff pile has proved that the soil bearing capacity indeed increases as a response of the cyclic loads. The small increase in secant stiffness was observed, even though the data were scattered significantly.
All these tests were performed with a small number of cycles, not sufficient for assessing the long-term effects for offshore turbines.

The rig adjusted for performing more cycles was used by LeBlanc *et al.* [2010]. The stiff pile embedded in dry sand of loose and medium-dense state was tested for the accumulated rotation and the change in stiffness as an effect of long-term cycles (N=8 000 - 60 000). The logarithmic dependency between the increase in stiffness and the number of cycles has been found. This trend is also related to the load magnitude and the direction of loading, but independent on the soil density.
The same approach and similar equipment was used by Abadie & Byrne [2014] and Lada *et al.* [2014]. The stiffness increase as a logarithmic function of the number of cycles was found to be dependent on the soil density. In

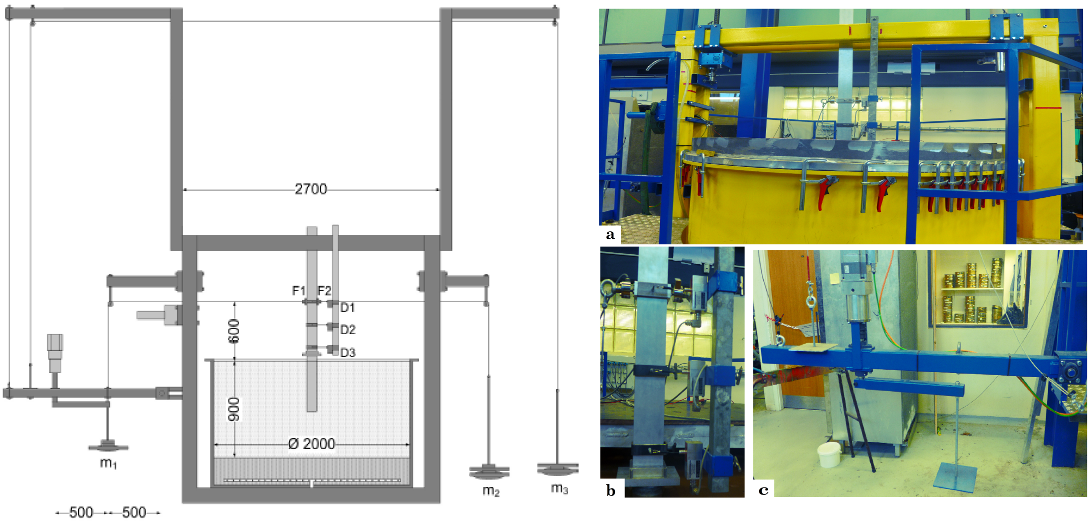

Figure 1.3: The set-up: sketch with dimensions (left picture), the sand container (a), the displacement and force transducers (b) and the cyclic loading side (c)

the small-scale centrifuge test performed by Kirkwood & Haigh [2014] this changes of stiffness are explained by forming of locked in soil stresses around the pile caused by a reversal in loading. Therefore, while designing offshore wind turbines, a strong attention should be paid on the possible migration of the natural frequency of the soil-pile system.

2 Small-scale tests

A series of small-scale tests have been performed at Aalborg University. The rig provided by the Geotechnical Laboratory allows to conduct proper tests, with a number of cycles exceeding 50 000. Therefore, the results can be used to analyze the monopile response for a long-term lateral cyclic loading conditions.

EXPERIMENTAL MODEL

The rig used in the research was based on the mechanical equipment used by LeBlanc *et al.* [2010]. Such a setup allows for performing both static and cyclic tests. Figure 1.3 presents the experimental rig.

The Aalborg University Sand No. 1 of investigated properties given in Table 2.1 is used.

Table 2.1: The soil properties for Aalborg University Sand No.1

Property	Value
Specific grain density, d_s [g/cm^3]	2.64
Maximum void ratio, e_{max} [-]	0.858
Minimum void ratio, e_{min} [-]	0.549
Particle size, d_{50} [mm]	0.14
Uniformity coefficient, $\frac{d_{50}}{d_{100}}$ [-]	1.78

Table 2.2: The characteristic properties of pile

Property	Value
Pile diameter, D [mm]	100
Embedded pile length, L [mm]	500
Wall thickness, t [mm]	5
Load eccentricity, e [mm]	605
Slenderness ratio, L/D [-]	5

Soil is prepared before each test in the same manner, so the comparison between tests is reliable. The preparation provides a saturated, dense sand state, with the relative density, I_D aimed for 80-90 %. Such a soil state is considered to be an adequate simulation of offshore conditions.

An open-ended aluminum monopile is used for all tests. The pile properties are given in Table 2.2. The soil stiffness is predicted to be around 4 MPa, so according to the most often used criterion proposed by Poulos and Hull (1989), the rigid response of the pile due to lateral load is expected [Sørensen *et al.*, 2012]. The more thorough description of the soil preparation and the equipment is given in the paper [Lada *et al.*, 2014].

EXPERIMENTAL PROGRAM

The static tests are performed in order to determine the ultimate pile capacity, M_R. The results of cyclic tests are used for investigation of the accumulated rotation and the change in stiffness due to the increasing number of cycles. After each cyclic test, the post-cyclic static test is conducted and the results are used for investigation of the change in the ultimate resistance. For both loading conditions, static and cyclic, the drained behaviour of the sand is assumed.

The effects of cyclic tests are investigated by using the approach presented by LeBlanc *et al.* [2010]. Tests are described by the loading characteristics, ζ_b and ζ_c, which are determined by equation (4) and (5).

$$\zeta_b = \frac{M_{max}}{M_R} \tag{4}$$

$$\zeta_c = \frac{M_{min}}{M_{max}} \tag{5}$$

Here, the maximum and the minimum moment of cyclic loading is denoted as M_{max} and M_{min}.

In order to provide realistic conditions the target ζ_b for the most of tests is set to be close to 0.3. 30 % of the ultimate capacity and around 10^7 cycles is used to assess the Fatigue Limit State, FLS. However, such a number of cycles would be too time consuming, therefore a number of $5 \cdot 10^4$ cycles is assumed to be relevant.
Different values of ζ_b are prescribed for tests, when the dependency of the results on this parameter is assessed.

3 Results and discussion

The increase of the bearing capacity as a result of cyclic loading was already proved in others papers, [Klinkvort *et al.*, 2010] and [Lada *et al.*, 2014]. However, any dependency for this increase has been presented. By analyzing the results of small-scale tests some relationships between the change in the ultimate capacity and the loading characteristics are observed.

The post-cyclic soil resistance is normalized by the static ultimate capacity and plotted versus ζ_b in Figure 3.1. A linear dependency is observed, where almost all of the chosen data fit to the function. When the loading amplitude is increased, the bigger increase in the resistance is obtained. The test with $\zeta_b = 0.514$ was stopped after 8 000 cycles due too excessive tilting of the lever in the equipment. Nevertheless, it is already seen that the value of post-cyclic resistance increases significantly.

When plotting the results in relation to ζ_c also a specific trend is observed. The results are presented in Figure 3.2. The selected tests are described by $\zeta_b \approx 0.3$. A small increase in the soil resistance is obtained after the tests between one-way and two-way cyclic loading, whereas a significant change in bearing capacity is found after the tests characterized by ζ_c close to -1 or to 0.

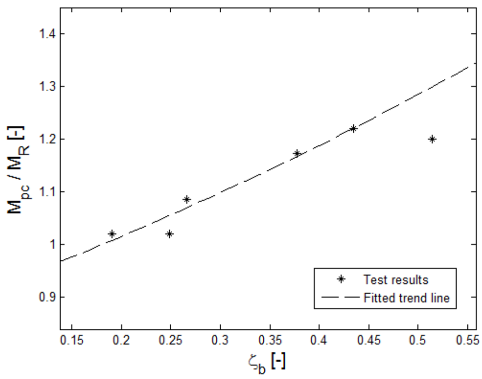

Figure 3.1: Normalized post-cyclic soil resistance dependency on ζ_b

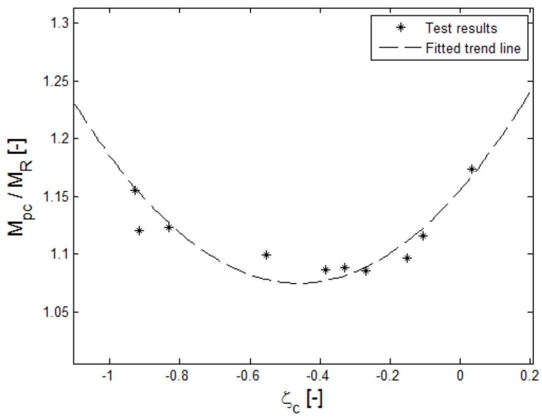

Figure 3.2: Normalized post-cyclic soil resistance dependency on ζ_c

The change in the ultimate capacity might be interpreted as an increase in the stiffness of the soil. The change in stiffness for 50 % strength in the post-cyclic tests was investigated, but no correlation with the load characteristics was obtained. Also the influence of the load characteristics on the value of cyclic unloading stiffness was assessed. The results of cyclic stiffness after around 50000 cycles are presented in Table 3.1. From overall tests the minimum increase of stiffness was assessed for 34 % for a one-way cyclic test. The maximum increase was found for a two-way loading test with $\zeta_c = -0.915$. The stiffness results of tests between one-way and two-way loading lie between those two values, however no correlation for them was found. No clear correlation was found with ζ_b as well.

The dependency was however found for the change in the unloading cyclic stiffness. The ratio between the unloading stiffness after the last one cycle and the first one cycle is plotted in Figure 3.3. The chosen tests are described with $\zeta_b \approx 0.3$.

Table 3.1: The results of cyclic unloading stiffness, $\zeta_b \approx 0.3$

ζ_c	$k_{N,unload}$ [Nm ^{o}]	$\frac{k_{N,unload}}{k_{1,unload}}$ [-]
0.03	1 061.70	1.34
-0.107	783.63	1.48
-0.152	1 122.70	1.80
-0.268	951.03	2.64
-0.329	1 065.51	2.03
-0.383	1 070.33	2.15
-0.554	958.79	2.50
-0.915	833.50	3.32
-0.929	918.47	2.71

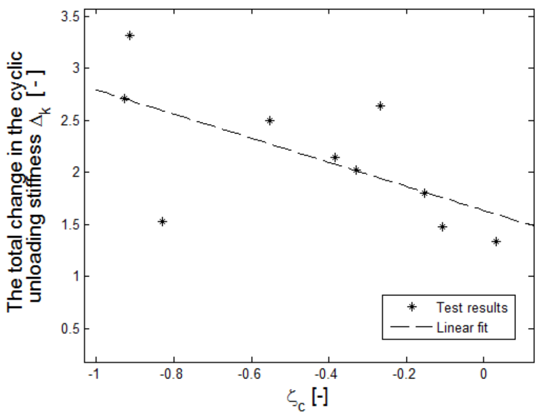

Figure 3.3: The total increase in the unloading, cyclic stiffness

The chosen trend is not perfectly fitted to the data, however it can be concluded, that when approaching $\zeta_c = -1$ the change in the cyclic unloading stiffness become bigger for given tests. No dependency for the change in stiffness on ζ_b is found. It can be concluded that apart of the stiffness, there might be some others parameters that influence the post cyclic resistance.

The analysis shows that due to the cyclic loading the final stiffness is always bigger than the initial one. However, in some tests the increasing tendency in stiffness was changed into the falling trend. As a result, the biggest increase of the stiffness do not always correspond to the biggest number of cycles, but to the number of cycles between. This shows that during a life-time of a turbine the cyclic loading changes significantly the stiffness and therefore, some fluctuations in the soil-pile system stiffness should be included in the design.

The dependency between the number of cycles and the post-cyclic resistance is also investigated. The test group considered was loaded with the same weights, aiming in one-way cyclic loading with the magnitude of around 30 % of ULS. The results are presented in Figure 3.4.

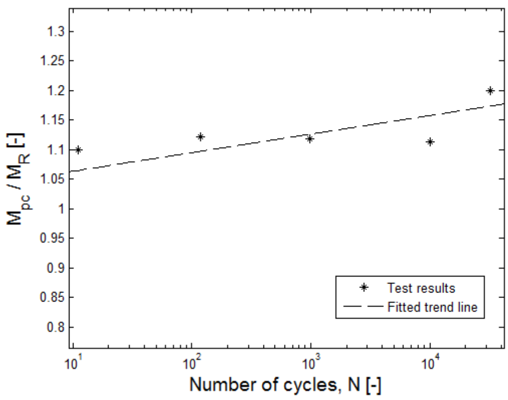

Figure 3.4: The increase of ultimate resistance due to the number of cycles

Clearly, it can be concluded that there is a relationship between the change in the ultimate bearing capacity and the number of cycles. It seems like the cycles strengthen the soil, and when the number of cycles increase, the increase of the ultimate bearing capacity is observed. A logarithmic function of N was adjusted to the data and the reasonable fit is obtained.
The result of post-cyclic resistance after a test with 10 000 cycles differs from the logarithmic function. However it should be underlined that many external and internal factor can influence the test results and some of them can differ from the expectation.
As far as the rest of results are in a good fit with the function, following statement are concluded:

- The bearing capacity of soil-pile system increase logarithmically with the number of cycles,
- The logarithmic dependency should be still investigated and confirmed with more test results.

The same tests are used for the investigation of the stiffness changes with the increasing number of cycles. The results of the rotational stiffness from the post-cyclic tests are plotted in Figure 3.5. The tangential stiffness for 50 % of ULS is taken as the representative value. The rotational stiffness from the static tests is also plotted for the number of cycle N=1.

In the same manner, the cyclic unloading stiffness changes in tests are plotted against the increasing number of cycles, and also a logarithmic dependency is obtained, Figure 3.6.

The change in the ultimate capacity due to the cyclic loading is clearly related to the increasing stiffness of the soil-pile system. The increase of the stiffness can be clarified with the fact that the plastic strains that occur during the cycles might expand the yielding surface. As the soil become stronger, it possesses a greater stiffness.

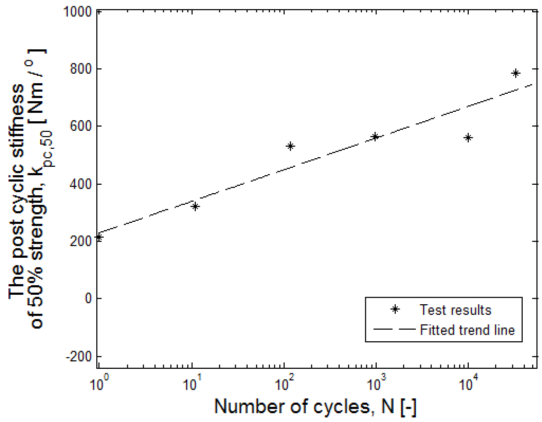

Figure 3.5: The change in stiffness for post cyclic tests

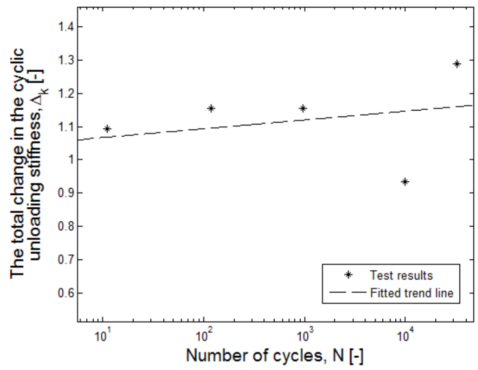

Figure 3.6: The increase of the rotational stiffness due to the number of cycles

Nevertheless, those increasing dependency with the number of cyclces should be still investigated in order to define, whether the logarithmic function of cycles can be used in predicting the post-cyclic resistance and the change in stiffness for the design of offshore wind turbines.

4 Conclusion

Nowadays the use of offshore wind turbines is increasing, as it gives an unlimited source of energy that can be produced more effectively in comparison to the onshore wind farms. Therefore, the design of the foundation must be developed in order to limit the total costs of turbines and also to provide their operation to be undisturb and more efficient.

The design of the monopiles for offshore turbines is normally based on p-y curve approach, where the ultimate soil-pile capacity has a big impact on the relation between the soil resistance and the corresponding lateral deformation of the pile. Contrary to the recommended practice, where the ultimate capacity is degraded, the results of small scale tests show that the soil become stronger due to the cyclic loading. The relation between the increase in the ultimate soil resistance and the load characteristics, ζ_b and ζ_c, is found. As an effect of cycles, the soil capacity increases more when bigger load magnitude is applied. Also it is concluded that the most of increase happens for a one-way and two-way loading tests, whereas the tests between show a smaller growth. Additionally, the logarithmic relation between the increase in the ultimate capacity and the number of cycles was found.

The small scale tests results reveal also the change in the rotational stiffness. The logarithmic function was also obtained as a good fit for the relationship between the number of cycles and both, the total change in the cyclic unloading stiffness and the post cyclic stiffness of 50 % strength. The dependency between the changes in stiffness and the load characteristics was difficult to obtained. Only a clear increase of the total change in cyclic stiffness was found when ζ_c approaches -1. This indicates a stronger sand densification for two-way loading in comparison to one-way loading, where the smallest increase of the stiffness is found. However, it contradicts to the findings concerning the post-cyclic resistance, as the maximum increase is observed not only for the two-way loading but also for the one-way loading.

The accurate prediction of the soil-pile system is extremely important for the design of the whole structure. Most often the design predicts the eigenfrequency of the turbine to lie between 1P and 3P. The change in stiffness increases the eigenfrequency, which lead to problems related to the resonance occurring between the loading frequencies and the natural frequency of the turbine.

References

Abadie, C.N., & Byrne, B.W. 2014. Cyclic loading response of monopile foundations in cohesionless soil. *Physical Modeling in Geotechnics - Gaudin & White*, **ISBN 978-1-138-00152-7**, 779–784.

API, American Petroleum Insitute. 2005. *Recommended practice for planning, designing and constructing fixed offshore platform*. Downloaded: 10-10-2013.

DNV, Det Norske Veritas. 2011. *Design of Offshore Wind Turbine Structures*. Downloaded: 10-10-2013.

Kirkwood, P.B., & Haigh, S.K. 2014. Centrifuge testing of monopiles subject to cyclic lateral loading. *Physical Modeling in Geotechnics - Gaudin & White*, **ISBN 978-1-138-00152-7**, 827–831.

Klinkvort, R.T., Leth, C.T., & Hededal, O. 2010. Centrifuge modeling of a laterally cyclic loaded pile. *Physical Modelling in Geotechnics Ű Springman, Laue & Seward*, **ISBN 978-0-415-59288-8**, 959–964.

Lada, A., Gres, S., Nicolai, G., & Ibsen, L. Bo. 2014. Response of a stiff monopile for a long-term cyclic loading. *Department of Civil Engineering, Aalborg University*, **part of a Master thesis**.

LeBlanc, C., Houlsby, G.T., & Byrne, B.W. 2010. Response of stiff piles in sand to long-term cyclic lateral loading. *Geotechnique 60*, **No.2**, 79–90.

Little, Robert L., & Briaud, Jean-Louis. 1998. Full scale cyclic lateral load tests on six single piles in sand. *US Army Engineering District, Final Raport*.

Long, J.H., & Vanneste, G. 1994. Effects of Cyclilc Lateral Loads on Piles in Sand. *Journal of Geotechnical Engineering*, **Vol.120, No.1**, 225–244.

O'Neill, M.W., & Murchinson, J.M. 1983. An Evaluation of p-y Relationships in Sand. *a report to the American Petroleum Institute*.

Reese, L.C., Cox, W.R., & Koop, F.D. 1974. Analysis of Laterally Loaded Piles in Sand. *Proceeding of the Sixth Annual Offshore Technology Conference, Houston, Texas*, **paper no. OTC 2080**, 473–484.

Sørensen, S.P.H., Brødbæk, K.T., Møller, M., & Augustesen, A.H. 2012. Review of laterally loaded monopiles employed as the foundation for offshore wind turbines. *DCE Technical Reports, Department of Civil Engineering, Aalborg University, Aalborg, Denmark*, **No.137**.

WWEA, World Wind Energy Association. 2013. *Small Wind World Raport*. URL: `http://www.wwindea.org`. Downloaded: 25-03-2014.

3.3 Article no. 3

Title:

The behaviour of a stiff monopile foundation subjected to a lateral load

Authors:

Lada A., Nicolai G. and Ibsen L. B.

Number of pages:

10

The behaviour of the stiff monopile foundation subjected to the lateral loads

Aleksandra Lada Giulio Nicolai Lars Bo Ibsen
Aalborg University
Department of Civil Engineering

Abstract

The article focuses on the analysis of a large-diameter monopile foundation for offshore wind turbine based on the numerical model results. The case describes the behaviour of a monopile in sand subjected to a lateral loading conditions. The effects of the pile diameter, the length and the load eccentricity on the results are investigated. Additionally, the cyclic nature of load is also taken into consideration. The cyclic loading leads to an accumulated rotation, thus the SLS design must ensure that the maximum permanent rotation does not exceed the limit value for a given wind turbine. The approach analyzed by LeBlanc *et al.* [2010] and Lada *et al.* [2014] is discussed in the way of its use as a preliminary design.

1 Introduction

The monopile foundation is the most often used concept for wind turbines in the offshore conditions. The greater demand for the renewable energy is the reason why bigger and more effective turbines are introduced in the offshore field. This has a significant influence on the foundation design. Not only the vertical load from the turbine itself are bigger, but also the overturning moment working cyclically on the pile increases. As the wind working on the rotor has its center at a greater height, the arm for the load increases.

Nowadays a large diameter monopiles are used for offshore wind turbines and they are considered highly successful. Nevertheless, the current design of monopile embedded in sand leaves a lot to be desired. The most often used standards, DNV [2011] and API [2005] recommend the p-y curve design, which describes the non-linear relationship between the soil resistance and the lateral pile deflection at each depth below the seabed. The method is based on the full-scale tests of slender piles and it found its confirmation to a greater or lesser extent by other full-scale tests. However, the increase of the diameter was found by other researchers to change the behaviour of pile under lateral load and therefore the results of pile deflection do not fit the p-y curve any longer.

Currently, the attention of many engineers is devoted to the consideration of the cyclic loads in the design standards. Both, API [2005] and DNV [2011] recommend only the decrease of the ultimate soil resistance, when accounting for a cyclic loading. Nor the load characteristics, neither the number of cycles are included.

THE STATE OF ART

The comparison between the p-y method and a fine element method for the response of a large-diameter pile subjected to a lateral load was performed by Lesny *et al.* [2007]. The models of two piles, D= 1 m and D= 6 m, embedded in non-cohesive soil were investigated. An elasto-plastic material behavior assuming the Coulomb friction law was the basis for the analysis. Both piles were designed by providing sufficient length for a rigid fixation and the limited pile head rotation, $\alpha_{lim} = 0.7°$. As long as for smaller pile both results are quite comparable, for the large-diameter pile the results varies significantly. The p-y curve approach overestimates the pile-soil stiffness of a larger pile at a great depth, questioning the use of this method. Both piles were characterized by different diameters and embedded lengths, therefore it seems to be reasonable to state, that both these parameters influence the response of horizontally loadded piles.

In the research of Achmus *et al.* [2009] the numerical model was used in the analysis of laterally-loaded monopile. The results of drained cyclic triaxial tests on cohesionless soil was applied in the model, so the cyclic condition could be reconstructed. As the increase of plastic strain with the number of cycles was observed, it was interpreted as a decrease in soil secant stiffness. Therefore the model was named the degradation stiffness model. The soil was modeled as en elasto-plastic with a Mohr-Coloumb failure criteria and both, dense and medium dense sand were analyzed.
Due to an investigation of different pile lengths, the difference in the behaviour of a stiff and a slender pile was observed. Due to applied cycles the increase of deformation and the lowering of the rotation point of a pile was noticed. From the results it was stated that the pile performance is very much dependent on the embedded pile length, whereas the increase of the pile diameter from 5 m to 7.5 m decreases the accumulated displacement of the pile only slightly. The design criterion considering the zero-toe-kick in order to minimize the risk of accumulated deformation under cyclic loading was claimed to be inadequate for the stiff piles. The piles with the same length, but different diameters were investigated and the stiffer pile that behaves more rigid had a smaller deformation on the mudline. Additionally, a strong dependence between the magnitude of the applied load and the accumulated displacement was found.

Many others publications describe the numerical models used in analyzing the response of laterally loaded piles. Some of them suggest the new expressions for p-y curves for the large diameter piles. Generally, a more rigid behaviour for less slender piles is proved. This results in the overestimation of the p-y curve stiffness on the great depth and cause also the underestimation of the rotation on seabed, [Abbas *et al.*, 2008],[Augustesen *et al.*, 2009],[Onofrei & Ibsen, 2010].

SUBJECTS OF INTEREST

The numerical model has been made and the results of performed simulations are used to analyze the behaviour of a large diameter pile. The strong attention is also paid on the dependency of pile properties, like the diameter and the length and also the load eccentricity on the pile design.
In order to account for a cyclic loading a new approach based on LeBlanc *et al.* [2010] and Lada *et al.* [2014] accompanied with a numerical calculation is presented.

2 The numerical model of monopile

For numerical calculation a geotechnical program PLAXIS 3D is used, as it is able to simulate the soil condition with a good accuracy. The analysis is focused on the laterally loaded monopile embedded in a drained sand.

From a different available material models in PLAXIS 3D, the Soil Hardening Small Strain model is chosen, as a one of more advanced. The model assume the hardening of soil due to the plastic strains. The hardening due to compression and the hardening due to deviatoric loads (shear hardening) are distinguished in the model. Those two loads and also reloading of soil are controlled by different stiffness parameters, E_{50}, E_{oed} and E_{ur}. The relation between the axial strain and the deviatoric stress is modelled to be hyperbolic. Additionally the model adopts the dependency between the stiffness and the stress level, by the parameter m.

In contrast to the basic Hardeing Soil model, a non-linear decrease of the stiffness due to the plastic strains is included. This change is controlled with the small-strain shear modulus, G_0, and the parameter providing the level of shear strain at which the reduction of the secant shear modulus to about 70 % is observed, $\gamma_{0.7}$. [Brinkgreve *et al.*, 2012]

MATERIAL PARAMETERS

The advanced model requires a large number of input soil parameters in order to provide a realistic prediction of the soil behaviour. Three different state of sand are used in simulations: dense, medium dense and loose sand. The relative density, I_D, are chosen to be 85 %, 40 % and 5 % respectively. The required soil parameters are obtained from the data of the cone resistance, q_c. There is no specific location chosen and no data from CPT available, therefore the data of q_c are evaluated based on I_D, equation (1) [Lunne *et al.*, 2007]. The atmospheric pressure, p_a, is set to be 100 kPa.

$$I_D = \frac{1}{2.96} ln \left[\frac{\frac{q_c}{p_a}}{24.94 \cdot \left(\frac{\sigma'_{v0} \cdot \left(\frac{1+2 \cdot K_0}{3} \right)}{p_a} \right)^{0.46}} \right] \quad (1)$$

The consolidation of the sand is assessed in order to provide a reliable formulations for the rest of the parameters. The friction angle is obtained from relation in equation (2). The pore pressure is neglected, so the total cone resistance, q_t, is equal to q_c.

$$\varphi' = 17.6 + 11 \cdot log \left(\frac{\frac{q_t}{p_a}}{\left(\frac{\sigma'_{v0}}{p_a} \right)^{0.5}} \right) \quad (2)$$

The stiffness parameters are given in the dependency on the oedometer stiffness, E_{oed}, obtained from equation (3) for normally consolidated sand and from equation (4) for overconsolidated sand. The secant stiffness E_{50} is related to the oedometer stiffness through the Poisson's ratio as it is indicated in equation (5) and the unloading-reloading stiffness, E_{ur}, can be approximated with equation (6).

$$E_{oed} = q_c \cdot 10^{1.09 - 0.0075 \cdot I_D} \quad (3)$$

$$E_{oed} = q_c \cdot 10^{1.78 - 0.0122 \cdot I_D} \quad (4)$$

where I_D is in %.

$$E_{50} = E_{oed} \cdot \frac{1 - \nu - 2\nu^2}{1 - \nu} \quad (5)$$

$$E_{ur} = 3 \cdot E_{50} \quad (6)$$

The shear modulus obtained from equation (7) is set as the small-strain shear modulus. $\gamma_{0.7}$ is calculated according to recommendation for the program [Brinkgreve *et al.*, 2012].

$$G = 1634 \cdot q_c^{0.25} \cdot \sigma'^{0.375}_{v0} \quad (7)$$

In order to avoid numerical instabilities, the value of cohesion is set to be 0.1 kPa. The list of soil parameters used in the programm are presented in Table 2.1. The reference values for stiffness are chosen as the ones corresponding to $\sigma'_{v0} = 100$ kPa.

Table 2.1: Soil parameters used in PLAXIS

I_D [%]	5	40	85
φ [^{o}]	32.56	37.55	44.49
e [-]	0.843	0.734	0.595
γ [kN/m^3]	18.90	19.46	20.28
OCR [-]	0.67	1.43	3.98
K_0 [-]	0.462	0.485	0.788
E_{50}^{ref} [MPa]	18.30	103.520	142.60
E_{oed}^{ref} [MPa]	25.84	132.61	150.00
E_{ur}^{ref} [MPa]	54.91	310.57	427.80
ν_{ur} [-]	0.21	0.21	0.21
G_0^{ref} [MPa]	69.04	93.25	177.00
$\gamma_{0.7}$ [-]	2.14e-7	1.71e-7	1.44e-7
R_{inter}	0.57	0.61	0.71

For the monopile a steel material is used. The stiffness is set to 210 GPa and the Poisson's ratio to 0.3. The wall thickness is chosen to be 0.06 m. The additional extension of pile is made in order to apply the horizontal load on the sufficient arm, creating the appropriate moment on the seabed. The stiffness of the pile extension is chosen to be much larger and its unit weight is chosen to be small, so there will be no effect of the additional part on the pile-soil interaction.

PLAXIS MODEL

The model boundaries was chosen based on the numerical model used by Abbas *et al.* [2008]. Chosen boundaries can be seen in Figure 2.1.

The model is divided into number of elements, so that the finite element calculations can be performed. Two different kinds of elements are used in the program to simulate an accurate soil behaviour and a pile behaviour. The third kind of elements are used for the interface between pile and soil, what is really useful for investigating the soil-pile interaction. The parameters for soil on the interface are obtained by using the reduction factor $R_{inter} = tan(\delta)/tan\varphi$, where δ is the angle of soil friction on the pile wall.

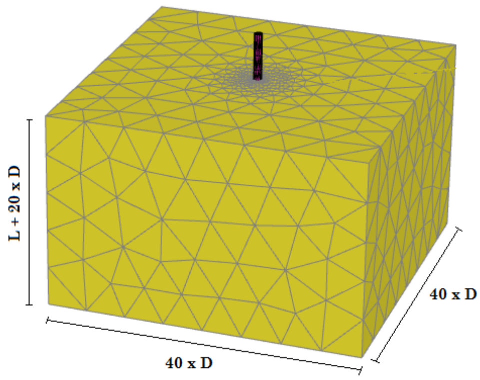

Figure 2.1: The model boundaries with the mesh example

The overall mesh is chosen to be coarse. As the most interesting results are expected near the pile, therefore the mesh is refined in the surroundings of the pile. There are two chosen region for mesh refining. The region closer to the pile is more refined. After performing a convergence analysis an appropriate Fineness-Factor is chosen for the soil volumes close to the pile and the pile surface. An example of meshed model is presented in Figure 2.1.

CALCULATION PHASES

The calculation for a laterally loaded monopile are divided into five calculation phases. The analysis is initiated by the initial phase, where the initial soil stress are obtained. In the phase a K_0 procedure is used. This phase is followed by the nil-step phase, where no changes in activating parts is made, but the plastic calculations are used. The phase has no physical meaning and it is used only in order to obtain an equilibrium of stress before applying the load. In the third phase, the construction phase, the plates are activated and in the next phase the vertical load is applied in order to simulate the self-weight of the wind turbine. In both phases the plastic calculation are chosen. In the final loading phase the horizontal load is additionally activated. The load is applied as a point load.

The determination of exact failure in the numerical calculation is impossible. Therefore the failure is assessed for a 4 ^{o} of the pile rotation on the seabed. In case, where the calculation fails before obtaining the sufficiently large displacement, the tolerable numerical error is slightly increased.

3 The analysis of results

TEST PROGRAM

Different aspects of the pile behaviour are assessed and therefore different geometries and model properties are chosen for simulations. The test programs can be seen in Table 3.1

Table 3.1: Test program for PLAXIS simulations

Model	D [m]	L [m]	e [m]	I_D [%]
1	1	11	1.2L	85
2	5	11	1.2L	85
4	6	25	1.2L	85
5	7	25	1.2L	85
6	5	30	1.2L	85
7	5	35	1.2L	85
8	5	25	1.0L	85
9	5	25	1.4L	85
10	5	25	1.2L	40
11	5	25	1.2L	5

PILE BEHAVIOUR

In order to assess the difference in the behaviour of the rigid and the slender pile the results of model 1 and 2 are investigated. In both cases the same length of the pile was chosen, but there is a difference in the pile diameter. The horizontal load is applied at the same height. The dense state of sand is chosen. The lengths of piles were chosen based on criterion proposed by Poulus and Hull (1989), where the pile behaviour is assessed as a rigid or flexible according to the soil and the pile stiffness and the pile geometry.

The ULS was found for both situations. The difference in the behaviour is analyzed when 30 % of the ultimate moment capacity is applied to the piles. The different patern of deformation is presented in Figure 3.1.

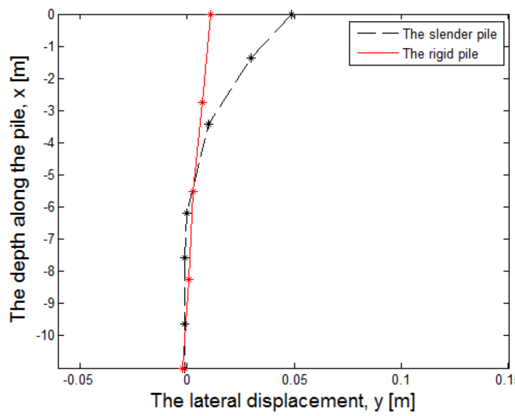

Figure 3.1: The different pattern of behaviour for the rigid and the slender pile

Clearly, the slender pile gives the flexible response, whereas the rigid pile gives more stiff response. For the pile with the large-diameter there is a visible deformation on the pile top resulting in additional shear stresses. Even though the much larger force is applied for the stiff pile, the displacement on the seabed are significantly smaller. It can be concluded that the large diameter piles have a better lateral performance in comparison to the slender piles.

DEPENDENCY OF PILE PROPERTIES

The diameter of monopile is changed while keeping the others properties fixed. The effects of the diameter on the ultimate moment capacity on the seabed are presented in Table 3.2. The ultimate soil-pile resistance is important for the design, as it is used for the p-y curve. As the rotation of the pile on the seabed is often assessed for SLS, the change in the moment capacity on the seabed are interesting to inspect.
It can be clearly stated that the diameter has a significant effect on the moment capacity on the seabed. The diameter increase of 20 % gives a rise of more than 42 % in the moment capacity.
Additionally, the displacement of the pile, while applying 30 % of ULS from the main model (model no 3) are inspected in Figure 3.2.

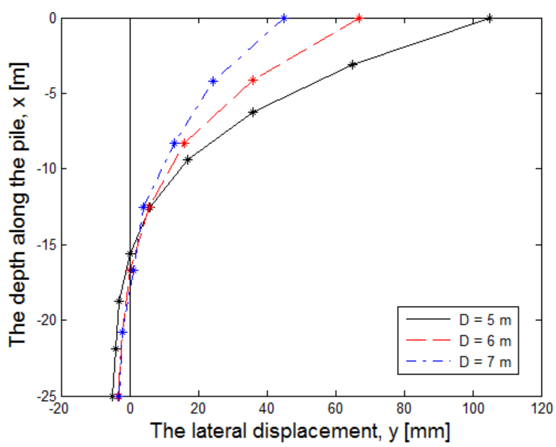

Figure 3.2: Pile deformations for varrying D, L = 25m, e = 1.2L - H = 19.3 MN

It can be seen that the pile behaves more rigidly for all cases and the increase in the diameter gives a better pile performance.

The same analysis is performed for different pile lengths, while keeping other properties fixed. The results of the ultimate moment capacity can be seen in Table 3.3 and the deformation for the same applied horizontal force are plotted in Figure 3.3.

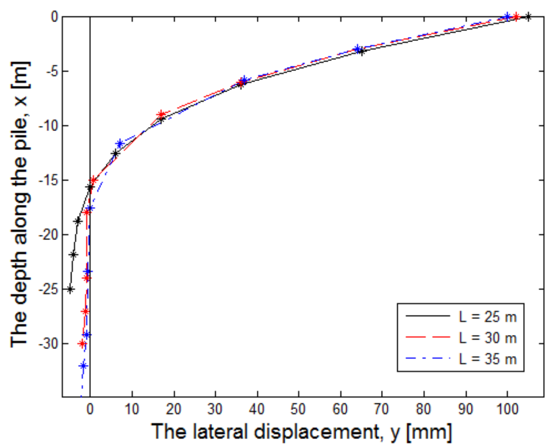

Figure 3.3: Pile deformations for varrying L, D = 5m, e = 1.2L - H = 19.3 MN

The increase in the length has an influence on the ultimate capacity by increasing it. The 20 % increase of length gives a 13 % increase of the moment capacity. It can be concluded that the change in the diameter is more effective for increasing the ultimate capacity. From the deformation graph it can be concluded that for applied 30 % of the ultimate moment, the difference in the displacement on the seabed does not varry significantly.

The load eccentricity is also inspected in order to assess its influence on the moment capacity. The results can be seen in Table 3.4. The change in the load eccentricity have also an effect on the ultimate capacity of the soil-pile system, however this parameter among others is assessed to be the least meaningful.
On the other hand, where the deformation of the pile for the same horizontal load is applied on the pile, it can be seen that the

load eccentricity has a bigger influence on the displacement on the seabed in comparison with the change of the length, Figure 3.4.

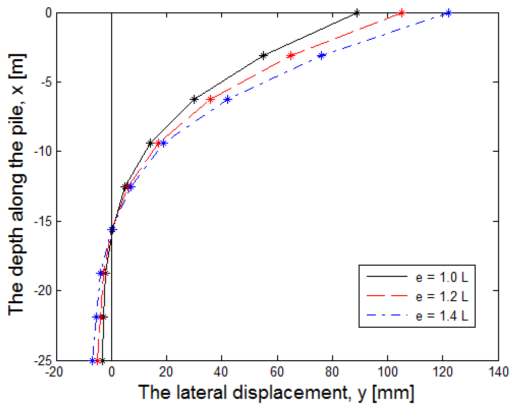

Figure 3.4: Pile deformations for varrying e, D = 5m, L = 25 m - H = 19.3 MN

As the change in the ultimate capacity is smaller, but the change in the deformation of the pile is more significant, the explanation for this is searched somewhere else. After inspecting the stiffness no change in the initial part is observed when the pile length is increased. When the load eccentricity is increased, the decrease in the rotational stiffness in its initial part is revealed. The results are presented in Figure 3.5.

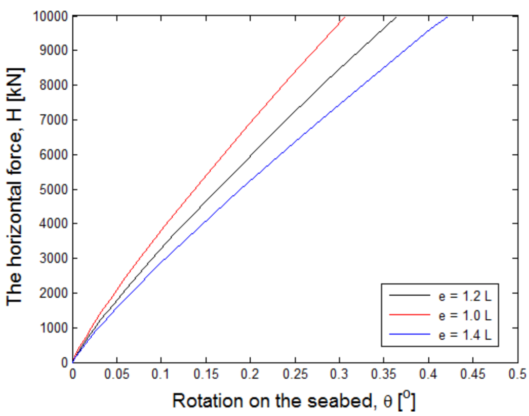

Figure 3.5: The inspection of the initial rotational stiffness

Table 3.2: Results of the ultimate moment capacity for different pile diameters

Pile diameter, D [m]	Moment capacity, M_R [MNm]
5	1934.49
6	2754.50
7	3395.91

Table 3.3: Results of the ultimate moment capacity for different pile lengths

Pile length, L [m]	Moment capacity, M_R [MNm]
25	1934.49
30	2183.78
35	2262.05

Table 3.4: Results of the ultimate moment capacity for different load eccentricity

Load eccentricity, e [m]	Moment capacity, M_R [MNm]
1.0 L	1835.38
1.2 L	1934.49
1.4 L	2008.36

Finally the difference in the soil density on the ultimate capacity are inspected. The results for all three chosen relative densities are indicated in Table 3.5. The soil density is found to be the factor affecting the ultimate capacity significantly.

Table 3.5: Results of the ultimate moment capacity for different soil densities

Relative density, I_D [%]	Moment capacity, M_R [MNm]
5	467.24
40	1106.20
85	1934.49

4 The cyclic lateral load

LeBlanc *et al.* [2010] proposed a new method for determining an accumulated rotation for a long-term cyclic loaded monopile. Based on this research, the monopile response for lateral load in medium-dense and loose sand can be obtained. The approach was modified by Lada *et al.* [2014] for a dense sand. In both researches the cyclic test are described with the loading characteristics ζ_b ($\zeta_b = M_{max}/M_R$) and ζ_c ($\zeta_c = M_{min}/M_{max}$).

ACCUMULATED ROTATION DUE TO THE CYCLIC LOADING

For the accumulated rotation an exponential dependency on the number of cycles was revealed. The displacement due to the cyclic loads can be approximated from equation (8).

$$\frac{\Delta\theta(N)}{\theta_s} = \frac{\theta_N - \theta_0}{\theta_s} = T_b \cdot T_c \cdot N^n \qquad (8)$$

For medium-dense and loose state of sand the parameters n was chosen to be 0.31. For dense sand the value was found to be smaller and it differs between tests. However, the mean value can be chosen, $n = 0.14$. The dimensionless functions can be predicted based on Figure 4.1 and Figure 4.2.

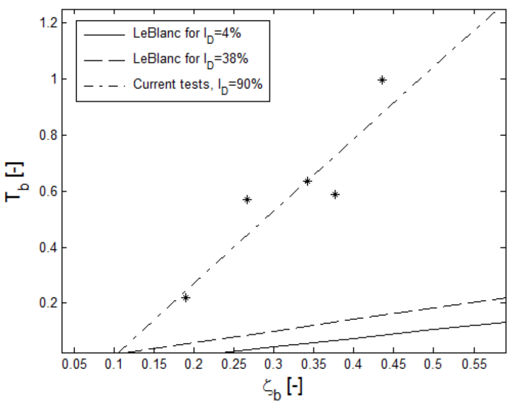

Figure 4.1: The dimensionless function T_b

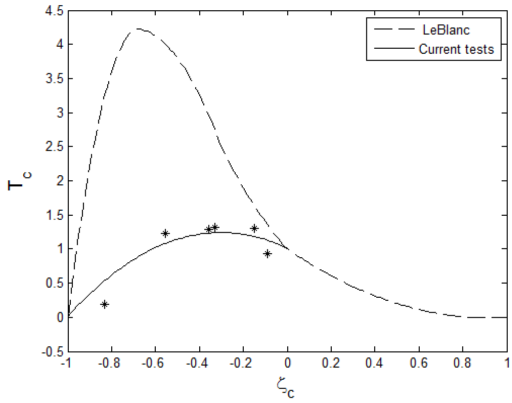

Figure 4.2: The dimensionless function T_c

The approach can be used as a preliminary design, however it requires the information of the static corresponding rotation.

The ULS for three different state of sand is found in PLAXIS. The pile of $D = 5$ m and $L = 25$ m is chosen as an example. The horizontal load is applied on the arm of $1.2 \cdot L$. The FLS is assessed for 30 % of ULS, therefore corresponding load magnitude is applied and the rotation is obtained. The results are indicated in Table 4.1.

Table 4.1: The static rotation corresponding to 30 % of ULS

I_D [%]	Static rotation [^{o}]
5	0.446
40	0.603
85	0.837

EXAMPLE

The load characteristics of ζ_c = -0.9 is chosen and the number of cycles is predicted to be 10^7. The pile is embedded in dense sand. The accumulated rotation , $\Delta\theta(N)$, can be calculated as following:

$$\Delta\theta(N) = T_b \cdot T_c \cdot N^n \cdot \theta_s =$$
$$0.56 \cdot 0.4 \cdot (10^7)^{0.14} \cdot 0.837 = 1.79^o$$

The most often the tolerable criteria for the permanent rotation is set to be 0.2^o, so the obtained value exceeds this limit. However, in this case all cycles are working in the same direction, and as the multi directional loading is rather expected, the permanent rotation would be smaller. Nevertheless, when ζ_c is set to be $\approx -0.4 \div -0.6$ the accumulated rotation would be much larger.

5 Conclusion

A number of simulations for the laterally loaded monopiles embedded in drained sand have been performed. Different pile geometries and model properties have been used in order to analyze the changes in the ultimate soil resistance. Currently, the most often used approach for the design of offshore monopile is the p-y curve approach. The relation between the pile lateral deformation and the soil resistance is based inter alia on the ultimate soil capacity. According to the standards, only the pile diameter and the soil properties have the influence on the value of the ultimate resistance. Moreover, the p-y curve was formed for a slender pile. Currently the large diameter piles are used in the offshore sector.

The results of PLAXIS simulations confirm that there is a difference in the deformation pattern between the slender and the rigid pile. The former behave flexible under the lateral loads, whereas the latter show a more stiff response. The results of different simulations reveal that the ultimate moment capacity is dependent not only on the pile diameter and soil properties, as it is stated in DNV [2011] and API [2005]. The length and the load eccentricity was found to influence the bearing resistance as well. However, the pile diameter and the change in the soil density are found to be the most significant, wheres the load eccentricity is considered the least contributing. Nevertheless, when the deformation of the pile for applied 30 % of ULS are inspected, the load eccentricity was found to be more meaningfull than the length of the pile. This is explained with the changes in the initial stiffness when changning the load eccentricity.
A method for designing the offshore monopile should be improved, so that all the parameters influencing the pile displacements will be included.

Also the cyclic response for the monopile should be accompanied by the new calculation approach. The proposition given by LeBlanc *et al.* [2010] should be still investigated for its validation and confirm by the full-scale results.

References

Abbas, Jasim M, Chik, Zamri Hj, & Taha, Mohd Raihan. 2008. Single Pile Simulation and Analysis Subjected to Lateral Load. *Electronic Journal of Geotechnical Engineering*, **13-E**, 1–15.

Achmus, M., Kuo, Y., & Abdel-Rahman, K. 2009. Behavior of monopile foundations under cyclic lateral load. *Computers and Geotechnics*, **36**, 725–735.

API, American Petroleum Insitute. 2005. *Recommended practice for planning, designing and constructing fixed offshore platform*. Downloaded: 10-10-2013.

Augustesen, A.H., Brødbæk, K.T., Møller, M., Sørensen, S.P.H., Ibsen, L.B., Pedersen, T.S., & Andersen, L. 2009. Numerical Modelling of Large-Diameter Steel Piles at Horns Rev. *Proceedings of the Twelfth International Conference on Civil, Structural and Environmental Engineering Computing*, **Paper 239**.

Brinkgreve, R.B.J., Engin, E., & Swolfs, W.M. 2012. *Manual for PLAXIS 3D 2012*. Downloadet: 02-05-2014.

DNV, Det Norske Veritas. 2011. *Design of Offshore Wind Turbine Structures*. Downloaded: 10-10-2013.

Lada, A., Gres, S., Nicolai, G., & Ibsen, L. Bo. 2014. Response of a stiff monopile for a long-term cyclic loading. *Department of Civil Engineering, Aalborg University*, **part of a Master thesis**.

LeBlanc, C., Houlsby, G.T., & Byrne, B.W. 2010. Response of stiff piles in sand to long-term cyclic lateral loading. *Geotechnique 60*, **No.2**, 79–90.

Lesny, K., Paikowsky, S.G., & Gurbuz, A. 2007. Scale effects in lateral load response of large diameter monopiles. *Contemporary Issues in Deep Foundations, Geotechnical Special Publication*, **158**.

Lunne, T., Robertson, P.K., & Powell, J.J.M. 2007. *Cone penetration testing in geotechnical practice*. Handbook, nos. ISBN: 0–419–23750–X. E & FN SPON - an Imprint of Routledge.

Onofrei, M.G., & Ibsen, L.B. 2010. Numerical analysis of lateral deflection for monopiles in drained sand. *Department of Cuvil Engineering, Aalborg University*.

Conclusions 4

The main part of the thesis is a research work dedicated to the design of the monopile foundations for the offshore wind turbine. Three independent scientific papers have been prepared and included in the report. The research work can be divided into three parts of which the outputs are included in those papers. The main interest was put on the following issues:

1. The study of the literature and the current state of art related to the subject
2. The small-scale tests of the rigid monopile subjected to the long-term cyclic loading
3. The numerical simulations for a laterally loaded monopile

For each of the issues the main aim is focusing on the evaluation of the pile response. The overall conclusions are described in the following sections.

Current design standards and the state of art

The most often used standards recommend the use of the p-y curve approach for the design of the offshore wind turbines. The method was derived from a few full-scale tests on the slender piles. Even though the use of the method was validated by some other researchers, currently this approach is doubtfull, as most of the monopiles used in the offshore sector are characterized by a larger pile diameter resulting in the much smaller slender ratio. The pattern of the behaviour is assessed differently for the slender and the stiff piles. In many papers this is confirmed by showing that the p-y curve approach overestimates the pile displacement for the stiff piles. Also the initial stiffness given by the p-y curve is uncertain, as it is only based on the soil parameters. The stiffness describe the relation between the pile and soil and therefore it should be related to the parameters of the pile as wel.
The assumptions for the cyclic loading conditions used in the p-y curve approach were undermined in many works. The standards assume the degradation of the ultimate soil resistance. Different researches reveal that the changes in the soil capacity due to the cyclic loads are profitable. Additionally, the changes in the cyclic stiffness were confirmed in some of the researches.

Laboratory results

The small-scale tests were performed for a rigid pile embedded in saturated, dense sand in order to simulate the offshore conditions. The number of cycles and the loading magnitude was chosen according to FLS, where the number of cycles is predicted to be 10^7 with the

load of 30 % of ULS. The load cycles were applied with the frequency corresponding to the offshore conditions, f = 0.1 Hz. Therefore, the initiation of all cycles would be too time consuming and therefore the number of cycles $5 \cdot 10^5$ is chosen. As the results show the stabilization and a good fit to the chosen function long before this number is achieved, the choice is assumed to be sufficient for assessing the long-term conditions.
The experimental work reveals many difficulties with tests, as the rig is really sensitive to external and internal factors. The data must be carefully analyzed.

The results of laboratory tests have been used for analyzing the accumulated rotation and the change in stiffness as an effect of the long-term cyclic loading. The approach proposed by Leblanc et al. [2010] was used and modified for a dense state of sand. The exponential increase with the number of cycle was found to be the best fit for the results of accumulated rotation, whereas the logarithmic increase with the number of cycles was revealed to be the best fit for the results of the change in stiffness. The state of sand used in Leblanc et al. [2010] research was assessed as loose and medium-dense. The results for the dense sand indicate the same shape of dimensionless functions used in the calculations. Generally the more acucmulated rotation and more increase in stiffness are found for the denser sand.
The test results show that the most of rotation is accumulated when the cyclic conditions are between one-way and two-way loading. However, the results of the change in stiffness do not show the same trend. Nevertheless, the biggest increase of the stiffness is observed in the first couple cycles for all of the tests. The accumulated rotation is also much bigger in the first couple cycles, whereas the increment is more stable and smaller for the larger number of cycles. The change in the initial stiffness cause the smaller accumulation of rotation in the later stage of the cyclic loading, as the soil becomes stronger. Therefore, it is concluded that the accumulation of rotation is dependent on the soil stiffness, however, it is not an exclusive factor affecting the rotation.

Each cyclic test was followed by a post-cyclic static test and its results are used for the investigation of the change in the ultimate resistance. The results reveal the increase in the post-cyclic resistance. The value of the ultimate resistance was found to be dependent on the loading magnitude and on the loading direction. The ultimate resistance increase more, where the bigger load amplitude is applied on the pile-soil system. It is also concluded that the increase is significant for the one-way loading cycles and for the tests where almost two-way loading conditions are used. For the tests with the value of ζ_c between 0 and -1 this increase is much smaller.
The tests with varying number of cycles were performed in order to assess the influence of the number of cycles on the ultimate capacity and the total change in stiffness. A logarithmic increasing dependency was revealed. Again, the connection between the bearing capacity and the stiffness is confirmed. The change in stiffness are crucial for the design, because the incorrect prediction of the stiffness for the structure can lead to the resonance between the eigenfrequency of the structure and the frequencies of working loads. Such a phenomena will cause excessive vibration and an improper wind operation.

The results obtained from the laboratory tests require validation with another tests and also confirmation by the results of full-scale turbines. Both, the accumulated rotation and the change in stiffness are extremely important for the design of the offshore wind turbines, regulating the proper conditions for the most effective energy production. Especially the formulation for the change in stiffness must be investigated, as there is no relation found for the dimensionless parameter included in the equation for dense sand.

Results from PLAXIS

The results obtained from the finite element analysis shows the differences between the slender and the stiff pile subjected to the lateral loading conditions. For large diameter pile used nowadays the prediction of a more rigid response was confirmed. It is concluded that the rigid behaviour is more favorable in the offshore conditions as it provides less deformation. As the pile is deformed at the bottom, the resulting shear stress might increase the soil resistance.

The results of different simulations reveal that not only a pile diameter influences the ultimate capacity, as it is stated in DNV [2011]. The pile length and the load eccentricity was found to influence the bearing capacity as well. However, the pile diameter is found to be the most contributing. Nevertheless, all of the parameters that influence the results, should be included in the design in order to give an accurate prediction and to provide a less expansive solution.

Bibliography

Abbas, J., Chik, Z., and Taha, M. (2008). Single pile simulation and analysis subjected to lateral load. *Electronic Journal of Geotechnical Engineering*, 13-E:pages 1–15.

API (2005). *American Petroleum Insitute. Recommended practice for planning, designing and constructing fixed offshore platform.* Downloadet: 27-02-2013.

Augustesen, A., Brødbæk, K., Møller, M., Sørensen, S., Ibsen, L., Pedersen, T., and Andersen, L. (2009). Numerical modelling of large-diameter steel piles at horns rev. *Proceedings of the Twelfth International Conference on Civil, Structural and Environmental Engineering Computing*, Paper 239.

Benz, T. (2007). *Small-Strain Stiffness of Soils and its Numerical Consequences. Institute of Geotechnics at Stuttgart University, Germany. ISBN 978-3-921837-55-9.*

Brinkgreve, R., Engin, E., and Swolfs, W. (2012). *Manual for PLAXIS 3D 2012.* Downloadet: 02-05-2014.

Brødbæk, K., Møller, M., Sørensen, S., and Augustesen, A. (2009). Review of p-y relationships in cohesionless soil. *Department of Civil Engineering Water and Soil, Aalborg University*, DCE technical Report No.57.

DNV (1992). *Det Norske Veritas. Foundations - Classification notes.* Downloadet: 11-02-2013.

DNV (2011). *Det Norske Veritas. Design of Offshore Wind Turbine Structures.* Downloadet: 11-02-2013.

EWEA (2013). Wind in power, 2012 european statistics.

Fan, C. and Long, J. (2005). Assessment of existing methods for predicting soil response of laterally loaded piles in sand. *Computers and Geotechnics*, 32:pages 274–289.

Ibsen, L. B., Hanson, M., Hjort, T., and Thaarup, M. (2009). Mc - parameter calibration for baskarp sand no. *Department of Civil Engineering, University of Aalborg.*

Kulhawy, F. and Mayne, P. (1990). *Manual on estimating soil properties for foundation design.* Downloadet: 26-04-2014.

LeBlanc, C. (2009). *Design of Offshore Wind Turbine Support Structures.* PhD Thesis - DCE Thesis No.18. Department of Civil Engineering, Faculty of Engineering, Aalborg University.

Leblanc, C., Houlsby, G., and Byrne, B. (2010). Response of stiff piles in sand to long-term cyclic lateral loading. *Geotechnique 60*, No.2:pages 79–90.

Lunne, T., Robertson, P., and Powell, J. (2007). *Cone penetration testing in geotechnical practice.* E & FN SPON - an Imprint of Routledge. ISBN: 0-419-23750-X.

Miceli, F. (2012). *http://www.windfarmbop.com.* Downloadet: 11-01-2014.

O'Neill, M. and Murchinson, J. (1983). An evaluation of p-y relationships in sand. *A report to the American Petroleum Institute.*

Reese, L., Cox, W., and Koop, F. (1974). Analysis of laterally loaded piles in sand. *Proceeding of the Sixth Annual Offshore Technology Conference, Houston, Texas*, paper no. OTC 2080:pages 473–484.

Sørensen, S. P. H. (2012). Soil-structure interaction or non-slender, large-diameter offshore monopiles. phd thesis. river publishers. isbn: 978-87-92982-29-2.

Thomsen, K. (2012). *http://kirt-thomsen.com/.* Downloadet: 12-01-2014.

The p-y curve A

The approach of the p-y curves comes from the differential equation of the pile, equation (A.1), from which the pile deformation and the pile stress can be obtained for each depth [DNV, 2011].

$$EI \cdot \frac{d^4y}{dx^4} + Q_A \cdot \frac{d^2y}{dx^2} - p(y) + q = 0 \tag{A.1}$$

with

$$EI \cdot \frac{d^3y}{dx^3} + Q_A \cdot \frac{dy}{dx} = Q_L \text{ and } EI \cdot \frac{d^2y}{dx^2} = M \tag{A.2}$$

where

EI	The flexural rigidity of the pile [kNm^2]
y	The lateral displacement of the pile [m]
x	The position along the pile axis [m]
Q_A	The axial force [kN]
Q_L	The lateral force [kN]
$p(y)$	The lateral soil reaction [kN/m^2]
q	A distributed load along the pile [kN/m]
M	The bendning moment[kNm]

The initial stiffness can be obtained from the differentiation of the p-y curve expression, equation (A.3).

$$\begin{aligned} E^*_{py,init} &= \frac{\partial}{\partial x}\left[A \cdot p_u \cdot tanh\left(\frac{k \cdot x}{A \cdot p_u} \cdot y\right)\right]_{y=0} \\ E^*_{py,init} &= k \cdot x \end{aligned} \tag{A.3}$$

There is a linear dependency between the initial stiffness of a p-y curve and a depth.

The value of the initial modulus of subgrade reaction can be read from the graph presented in Figure A.1.

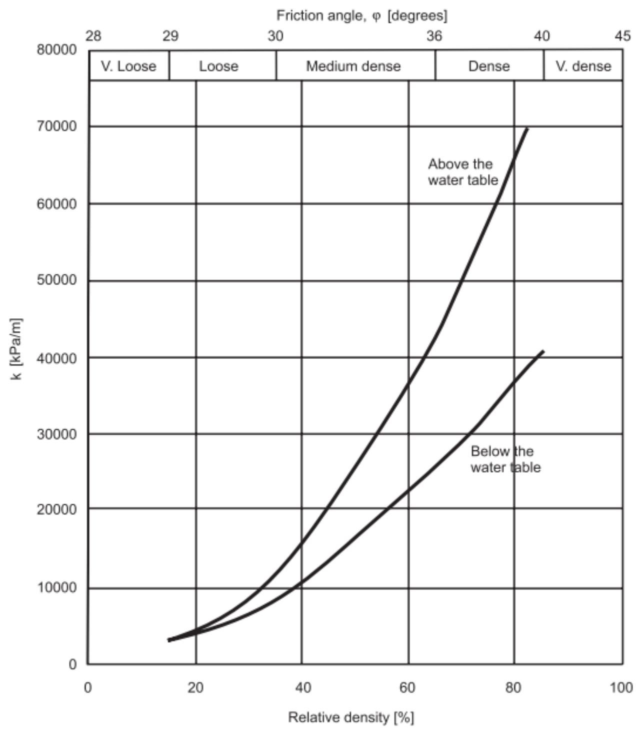

Figure A.1. An initial modulus of subgrate reaction, k [API, 2005]

For cohesionless soil the ultimate lateral resistance varies with the depth, which can be calculated using equation (A.4) for shallow depths and equation (A.5) for greater depth. The greater depth is considered from the depth, when the value of the ultimate resistance for a given height is equal for both equations.

$$p_{us} = (C_1 \cdot x + C_2 \cdot D) \cdot \gamma \cdot x \tag{A.4}$$

$$p_{ud} = C_3 \cdot D \cdot \gamma \cdot x \tag{A.5}$$

where

γ	An effective unit weight of soil [kN/m^3]
C_1,C_2,C_3	Coefficients based on the value of effective friction angle [-]
D	A pile diameter [m]

The factor accounting for the loading conditions can be obtained as following:

$$A = \begin{cases} \left(3 - 0.8 \cdot \frac{x}{D}\right) \geq 0.9, & \text{for static loading} \\ 0.9, & \text{for cyclic loading} \end{cases}$$

The coefficients used in the calculation of the ultimate soil resistance can be obtained from the graph on Figure A.2.

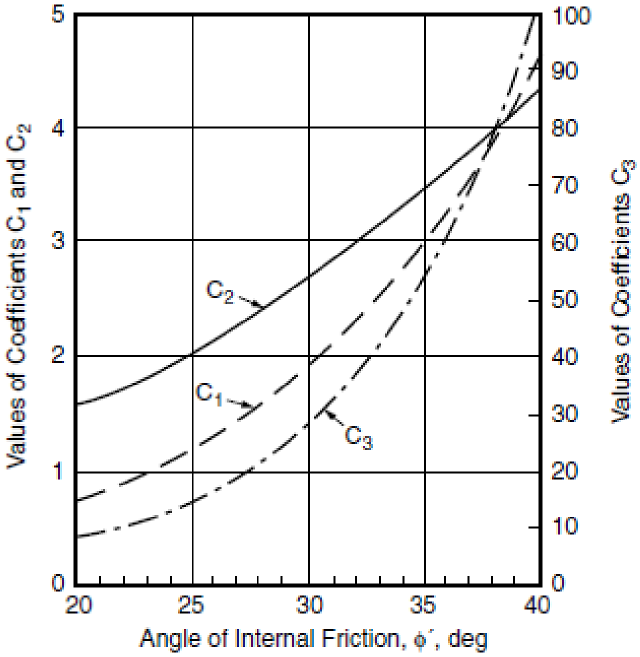

Figure A.2. Coefficient C_1, C_2 and C_3

When the knowledge about the loading condition is available the response of the soil-pile system can be obtained. The deflection can be estimated by the integration of the p-y formulation over the length of a pile.

If there are favorable condition for the scour, it must be taken into consideration, as the scour decreases the total soil resistance. However, the scour calculation and its protection is beyond the project's content and it is not analyzed.

Limitation of the p-y curve approach

There are many limitations concerning the p-y curve approach [Brødbæk et al., 2009]. The formulation of the p-y curves is based on full-scale tests performed at Mustang Island in 1966 described by Cox et al. (1974). The expression for the p-y curve for piles embedded in sand was first derived by Reese et al. [1974] and then reformulated by O'Neill and Murchinson [1983]. The final expression was adapted in current standards. However, the piles tested at Mustang Island were flexible, with a slenderness ratio $L/D = 34.4$. Currently, a large diameter piles are used for the offshore wind turbine. Their behaviour under a lateral load is described as a stiff. Therefore, the expression of the p-y curve might not be valid anymore. The criteria for a pile behaviour are presented in the companion article in section 3.1 on page 11.

Another important aspect is due to the fact that only a small attention is put on the stiffness of the p-y curve, that is only depended on the soil properties. As it describes the interaction between the pile and soil, the construction of the p-y curve is very doubtful. Other assumptions of the approach are questionable. One of them is the Winkler approach assuming the uncoupled springs, what indicates that soil continuity is not considered. Also the contribution of shearing that appears in soil in the p-y curve is not clear. The uncoupled system of the springs assumes that the layers are independent on each others and shearing between them is omitted. However, the p-y curve expression is based on full-scale tests, so the shearing could be indirectly included.

There are some assumptions concerning the ultimate soil resistance, like a disregard of the friction between the pile and soil and a negligence of the soil dilatancy. What is more, as the piles used nowadays are stiff and behave rigid, the assumption that there is no deflection below the point of rotation made for deriving the p-y curve is not valid. Additionally, as there is a deflection at the pile toe, an increased lateral resistance can be expected from the shearing stresses at the bottom. Figure A.3 presents the rigid pile behaviour. [Brødbæk et al., 2009]

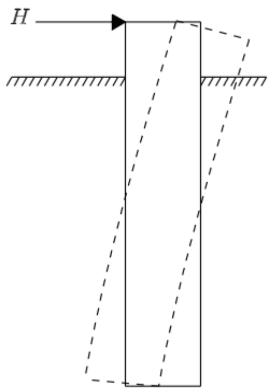

Figure A.3. The rigid pile behaviour [Brødbæk et al., 2009]

Laboratory manual B

Title:

The monopile foundation subjected to cyclic lateral loading - Laboratory manual

Authors:

Gres S.and Lada A.

Number of pages:

18

The monopile foundation subjected to cyclic lateral loading - Laboratory manual

Szymon Gres
Aleksandra Lada

2014-01-23

Table of content:

Preface

Provided manual describes the standard procedure for conducting the cyclic lateral loading test on monopile foundation at the Geotechnical Engineering laboratory at Aalborg University. Described procedure provides general information for performing the cyclic lateral loading test and determining the post-cyclic bearing capacity, and should be properly adjusted for any other purpose. The general condition to be respected in every test is to conduct each test with the same pattern in order to obtain comparable results.

Provided procedure was found to be successful for performed tests.

1. Introduction

<u>Person working in the laboratory must obey following rules:</u>

- <u>Always wear safety shoes,</u>
- <u>Working in the laboratory requires two people present,</u>
- <u>During the vibration ALWAYS use:</u>
  - ✓ <u>ear muffs</u>
  - ✓ <u>safety glows</u>
  - ✓ <u>safety strap.</u>

Each test should be proceeded by filling the paper version of the test report. After completing the test every detail regarding the test parameters or change in the procedure should be written in the "comments" section.

Three different types of test are performed: static, cyclic and post-cyclic test. The procedure of static test is not described in following manual, as it follows the procedure for post-cyclic test.

Tools used for conducted test:

- Electric screwdriver,
- Keys: 2 x 13, 17, 18, 2x19,
- Nimbus keys,
- Hydraulic motor,
- Power supply,
- Electric panel,
- Static, cyclic motor,
- Hydraulic shaft, Installation shaft,
- Electric wires,
- 2 x wooden blocks,
- 4 x Bar clamps,
- 2 x steel bars,
- Weights,
- Data acquisition system, SPIDER 8,

Equipment used for conducted test:

- Aluminum pile,
- Tower with load cells,
- Tower base,
- Pile contact head,
- Pile installation head,
- Penetration limiter,
- Rod vibrator,
- CPT device with contact head,

Used software:

- Catman (real time measurements: CPT, cyclic test, static test)
- Starter (cyclic test characteristics)

Figure 1.1 Cyclic motor, weight hanger and hinged lever

Figure 1.2 Static motor

Figure 1.3 Hydraulic motor

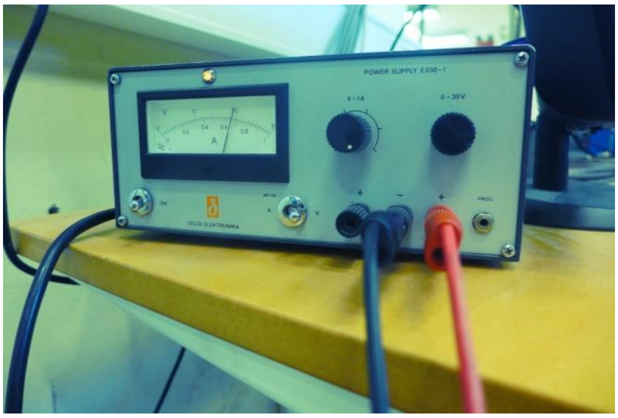

Figure 1.4 Power supply

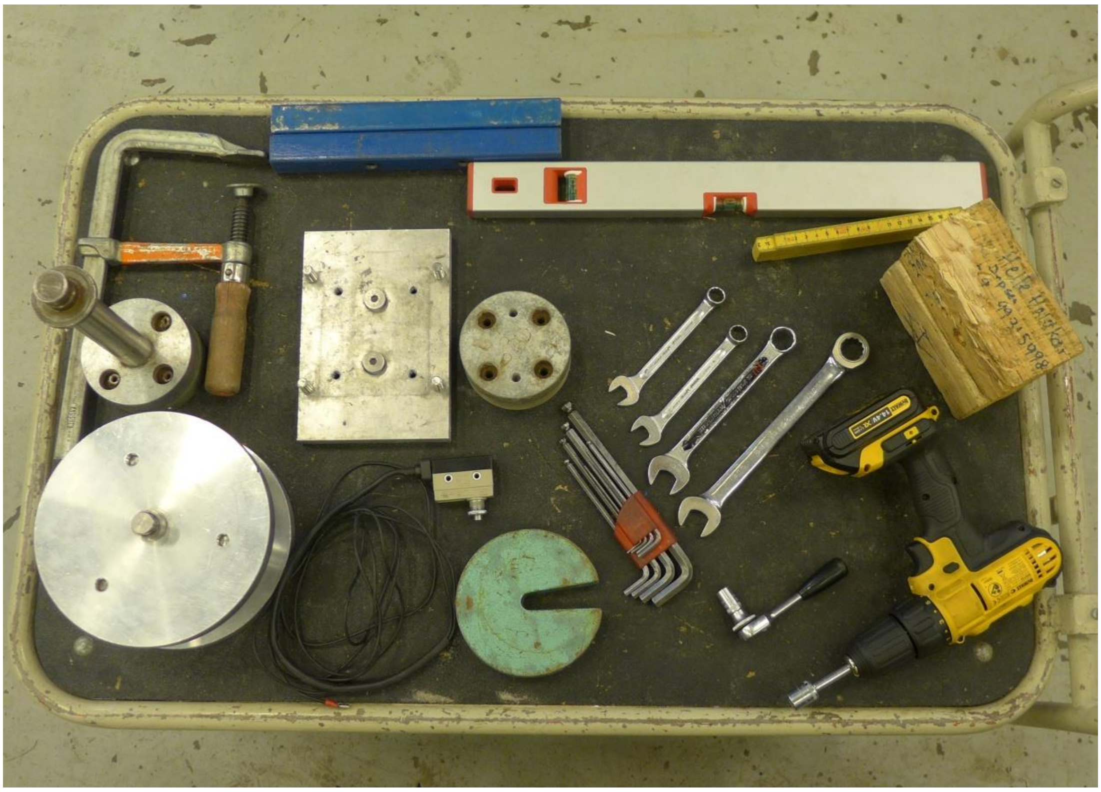

Figure 1.5 Tools and parts for conducting the experiment

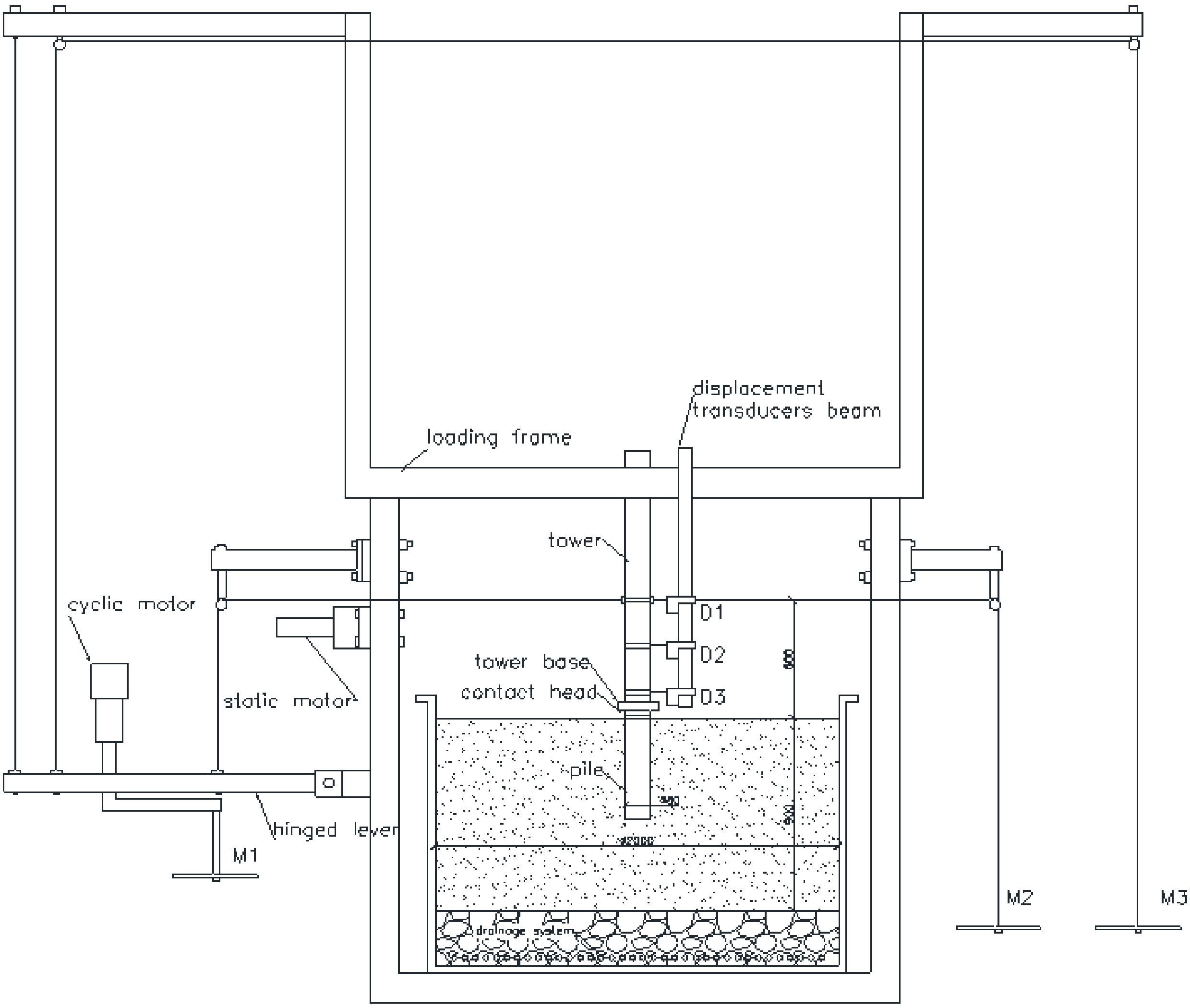

Figure 1.6 Loading rig with major components

2. Preparation of the yellow sand box

In order to prepare the appropriate soil condition in yellow rig the following procedure should be applied:

a) **Apply the water gradient**

The water gradient is applied in order to achieve loose state of sand.

Procedure:

- Make sure if the main water container is full and close all the valves connecting the main water supply to water tank. The main water container is situated in the back of lab.
- Open a blue valve at the left bottom of the rig in order to start the water flow. Water gradient height should reach the third red mark on the plastic tube. The head pressure between this line and soil in the yellow tank gives the hydraulic gradient, i=0.9. BE CAREFULL AS THE WATER MIGHT RISE FAST AND GOES OUT OF PLASTIC TUBE.
- Stop the water flow when the water level would reach around 7cm above the soil surface.

Figure 2.1 Water gradient limit

Figure 2.2 Water valves

b) Vibrate the soil

Procedure:

- Put the aluminum bar on two sockets placed in the inner perimeter of the rig.
- Place two wooden plates on the top edge of rig and bar. The joint between plates must be clamped.
- Use the rod vibrator to penetrate and densify the soil. The most convenient vibration pattern is to vibrate successively every second hole in each of wooden plates when moving forwards. On the turn each hole which was not vibrated yet should be vibrated in the same pattern as before. DO NOT force the downward movement of the rod to ensure that sand would be properly densyfied. Penetration of the soil should be stopped when the red mark on the rod is reached. DO NOT force the upward movement of the rod to not loosen the sand. The vibration process should be always performed with the constant speed. Remember to use appropriate protection gloves, earmuffs and safety strap,
- After vibrating, remove first wooden plate and aluminum bar. Lift up the second wooden plate and move it a little backwards (the edge of the plate should be placed on the aluminum bar),
- Next, some of the water should be removed. Place a thin aluminum plate on the soil surface close to the left edge of the rig and put the end of a hose on it. Stabilize the hose with round-shaped weight. Clean the other end of a hose and suck the air from it. The water should start flowing. Allow the water to flow to the drain grid, situated near the equipment on the left side. Stop the water flow when the water level in the rig would reach the half of the yellow element height within the container.

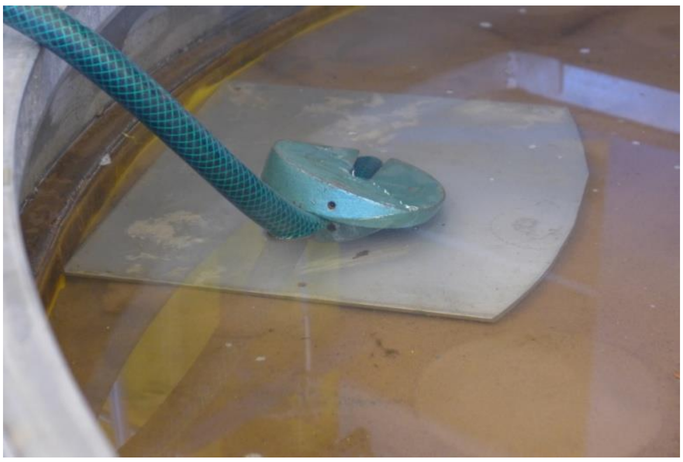

Figure 2.3 Removing the water from the rig

c) **Level the soil surface**

Procedure:

- Mount the hydraulic cables from the motor to jacks on top of hydraulic piston.
- Plug in the wires (red and black) from hydraulic motor to power supply. Order of plugging is important- wires connected to jacks with the same color- motor moving upwards, else (different colors), motor moving downwards.
- Place the hydraulic piston in the center of the steel frame above the rig.
- Mount the aluminum leveler on the bottom of the vertical part of the piston. Check if the leveler is in horizontal position.
- Lower the leveler until it touches the soil surface. Slowly rotate the leveler until the soil surface will be horizontal. This part might seem to be long , however it is extremely important for the test accuracy that the level will be horizontal and installed pile will not be initially rotated.
- Unplug and change the colors of the wires connected to power supply and start to raise the leveler.
- Unmount the leveler.

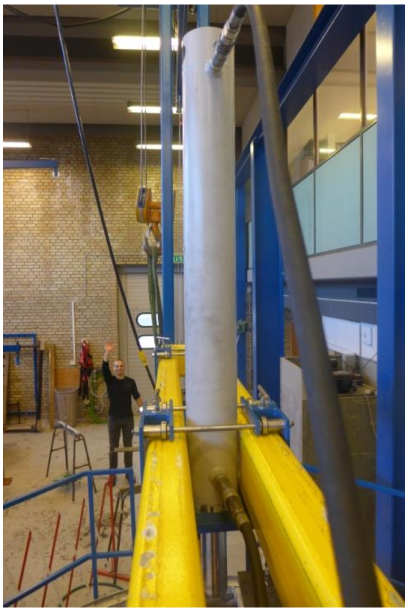

Figure 2.4 Hydraulic piston

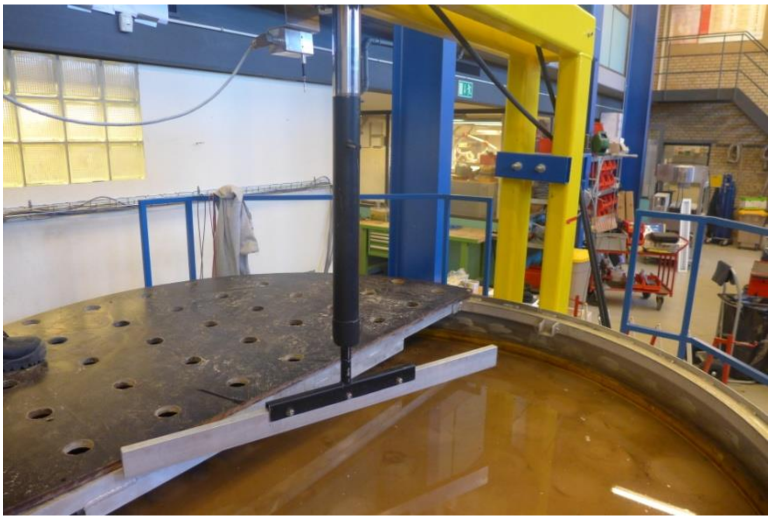

Figure 2.5 Soil leveler

d) Perform the cone penetration test (CPT)

Preperation:

- Mount the contact head to bottom part of the hydraulic piston.
- Install CPT device by tightening three screws to contact head and mount corresponding electrical cables to control panel.
- Fix the displacement transducer wire to CPT device. Mind to connect it to the first socket in order for the wire to be vertical.
- Plug in the wires from the motor to the power supply, mind the order of plugging. Power level in the supply should be set on 20V.
- Perform CPT in three different points in the soil in order to check if the soil conditions are uniform. CPT positions are described in Figure D1.

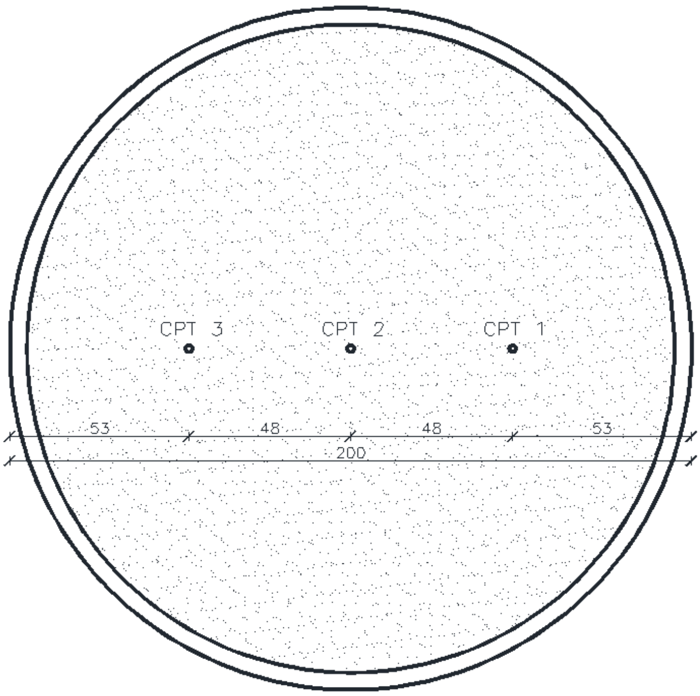

Figure 2.6 Sandbox with CPT positions

Test procedure:

- Turn on data acquisition system, Spider 8, by pressing green button on the amplifier.
- Lower the cone to the water surface by using control device from the motor. Start the “CATMAN” measurements.
- Set up the export options in general settings.
- When started online measurements, reset recorded data in “CATMAN” by pressing “Zero all active channels”.
- Start real time measurements by pressing “Run acquisition”.

- Penetrate the soil until the top of the red mark will reach soil surface (approximately 40cm).
- Stop measurements by pressing “Stop measurement” in “CATMAN”.
- Repeat test procedure for positions 2 and 3.
- When test procedure is completed turn off “CATMAN”.
- Turn off the power supply and motor. Dismantle the electric and hydraulic cables.

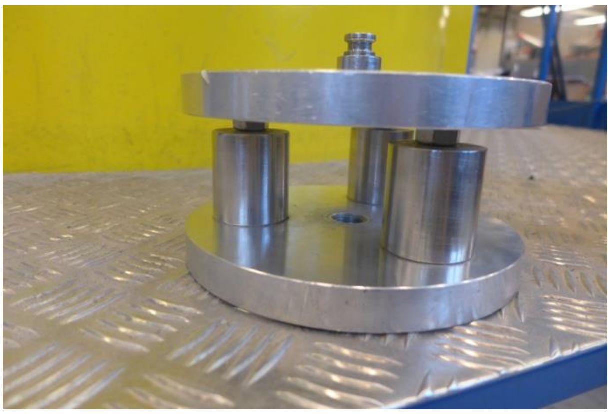

Figure 2.7 CPT head

Figure 2.8 CPT device

The “CATMAN” detailed procedure is presented on figures below:

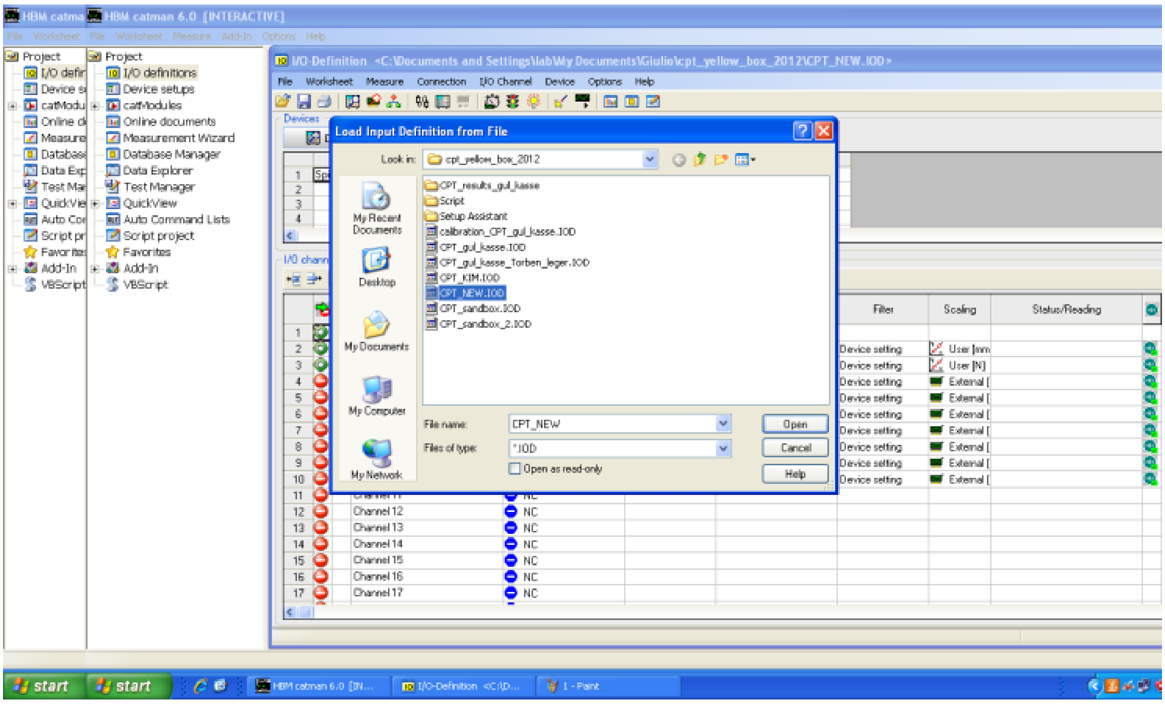

Figure 2.9 Open a IO definitions from given path

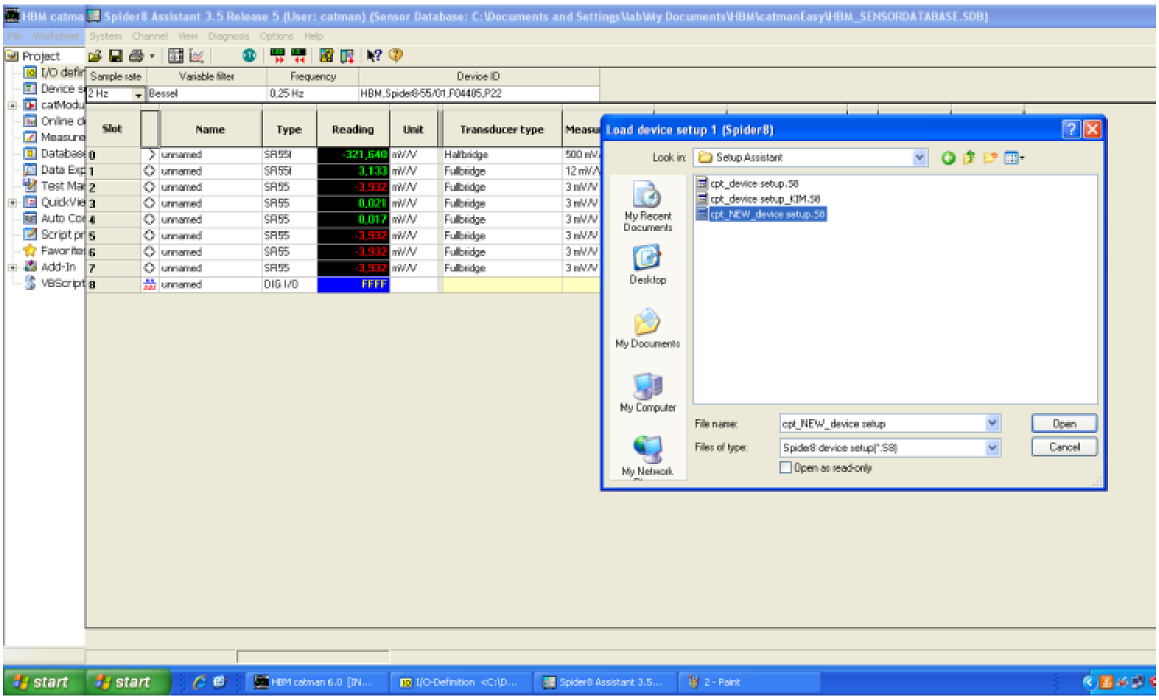

Figure 2.10 In setup assistant load the device setup

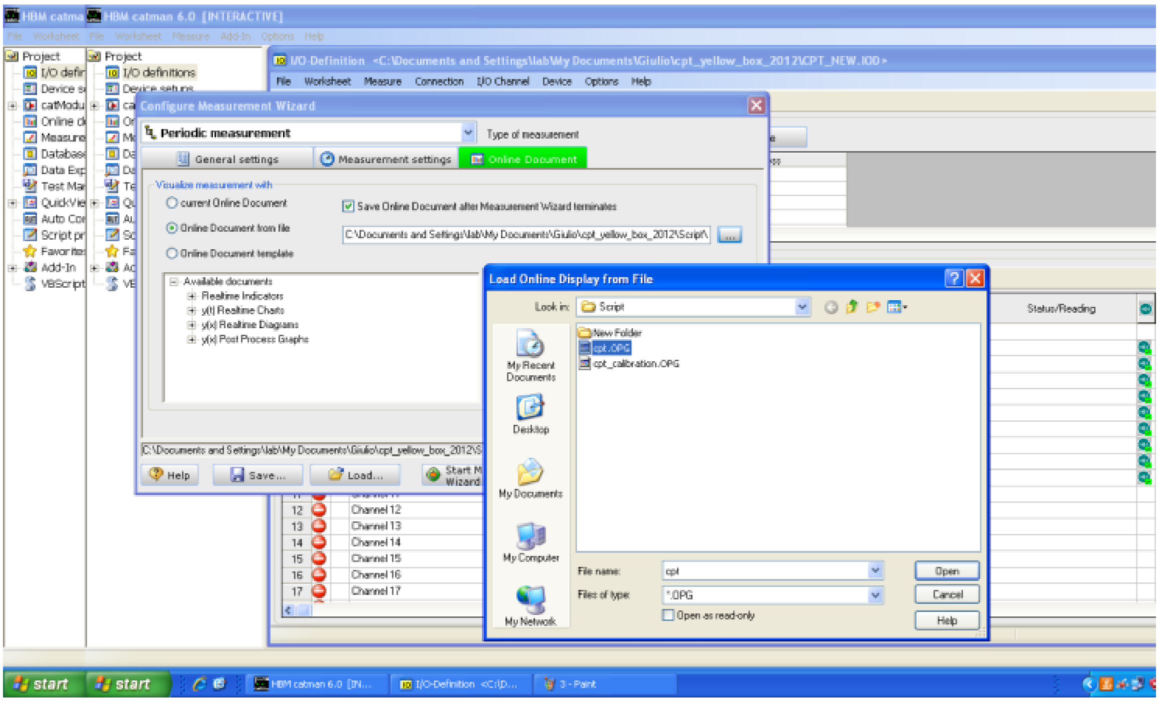

Figure 2.11 Set up the CPT calibration in Online Document

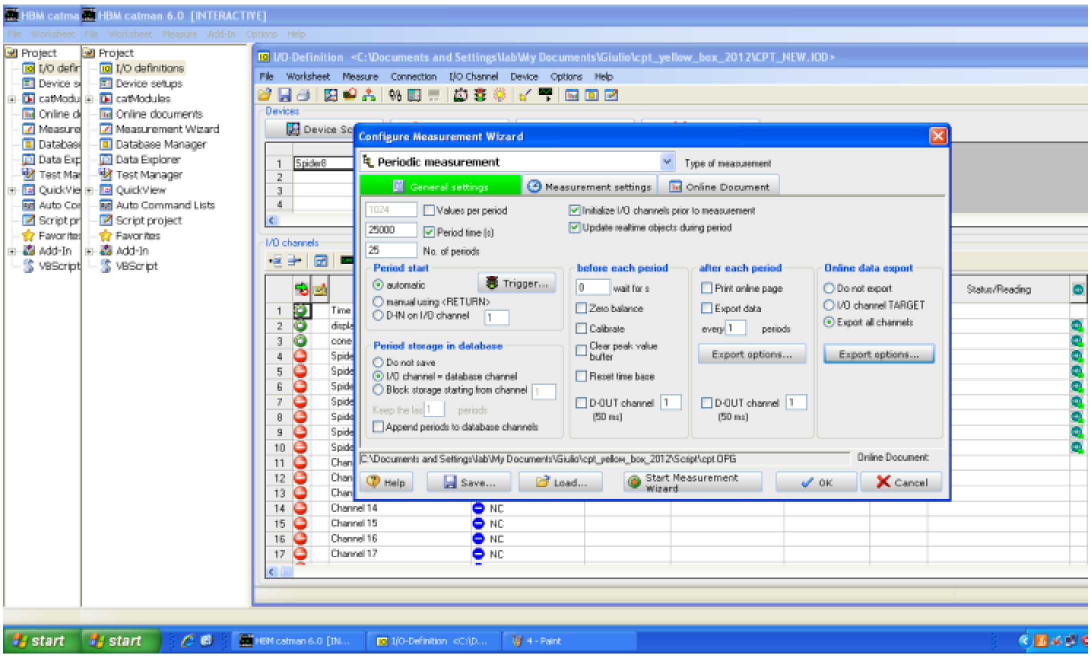

Figure 2.12 Start measurements wizard

For all performed tests, the data should be recorded in different files. The output files contain: time, displacement and cone resistance in each column respectively. These parameters should be used to calculate soil current parameters. CPT procedure should be performed before each static and cyclic test in order to investigate whether soil conditions are valid.

3. Monopile installation

The monopile foundation is driven into the soil by using installation shaft rotating with low velocity. The installation procedure is as follows:

a) **Mount steel cage blocking rotational movement of the pile**

Procedure:

- Unmount 4 nuts from the screws placed in the bottom part of the installation device.
- Mount the steel blue cage to the previously mentioned screws by using 4 nuts.

b) **Pile installation**

Procedure:

- Mount the pile to the installation head with using four bolts placed in the head. Check if the central bolt is removed from the pile, if not, remove it.

Figure 3.1 The blocking cage

- Mount the pile with installation head to the shaft by using three screws. Unmount one screw in order to manipulate the pile position.
- To control the maximum penetration depth, vertical sign has been made on the pile surface. Be sure the sign is visible during the installation.
- Mount the device in the central point of the steel frame.

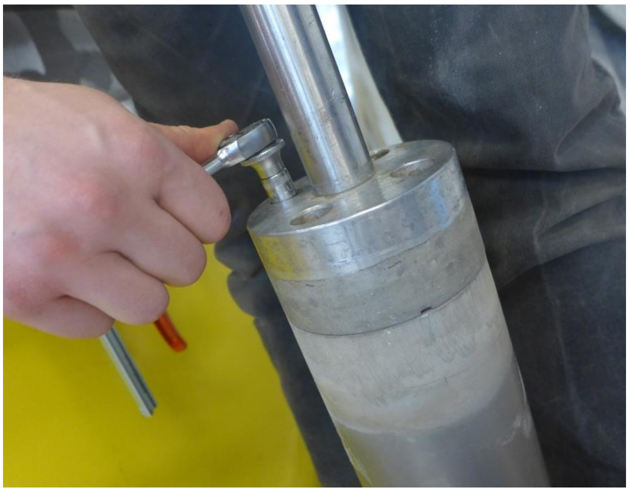

Figure 3.2 Pile installation head

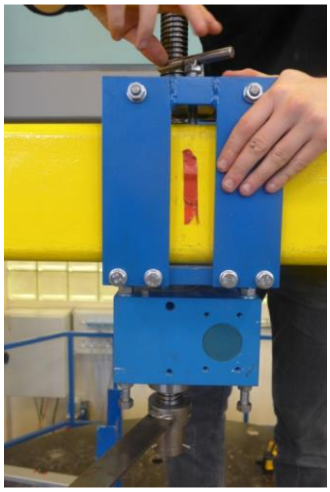

Figure 3.3 Position for pile installing

- Place the shaft arm to the right side of the blue frame in order to block the rotational movement of the pile.
- Mount the penetration limiter to the hole in the shaft arm.
- <u>The most crucial aspect of the pile installation is to maintain pile vertical and horizontal position while driving into the soil. Check it by using spirit level and properly adjust it. Than fix the installation head to the shaft,</u>
- Screw the bolt to cylindrical sleeve located in installation device. Drive the pile 2cm into the soil with using the screwdriver, maintaining low rotational velocity.
- Unscrew the bolt from the sleeve and mount the static motor in order to push pile into the soil.
- Plug in the wires from the motor and penetration limiter to power supply, mind the order of plugging. Power level in the supply should be set on 20V.
- Turn on the power supply to start pile installation. Approximate time of installation is 5h.

- Place two wooden blocks on the blue frame in order to stop pile penetration before it reaches maximum depth.

Figure 3.4 Penetration limiter

Figure 3.5 Wooden blocks activating the limiter

- When installation is stopped, take off the wooden blocks and closely observe when the vertical sign on the pile surface will reach the soil.
- Turn off and switch the wires connected to power supply.
- Unmount the pile from the shaft,
- Turn on the power supply in order to elevate the shaft from the installation head. Remember to switch the plugs, so the direction is changed to pulling.
- After that, turn off the power supply, unmount the static motor and, on its place, screw the bolt into the sleeve. Unplug the wires connected to power supply and penetration limiter. Unmount penetration limiter.
- Elevate the shaft using the screwdriver.

Before each test, static or cyclic, aluminum tower must be installed on the monopile in order to transmit the external forces acting on the pile (horizontal force and moment). Following forces are induced by the system of weights or static motor, pulling the cable fixed to the tower on selected height. Following steps describe the tower installation procedure:

- Unmount the installation head from the pile.
- Screw the central bolt to the pile head.
- Fix the rounded contact head to the pile head.
- Mount the tower base plate to the contact piece.
- Install the tower by putting it on the base and fixing the screws.
- Mount the beam with displacement transducers by fixing it to the loading frame on the right side from tower. Check the vertical position of the beam with spirit level.

- Connect the wires from displacement transducers with the tower in order to measure the displacements of pile head. Mind that the wires should be parallel to each other. Mind also the distance of displacement transducers to the pile in relation to the test type. The wires are of limited length. When static test is performed, the transducers should be as close to the tower as possible, as during the test the pile is only pulled through the left side. For cyclic tests, the distance should be fitted concerning the type of loading: one or two-way loading. The wires should be able to measure the displacement in both sides.

4. Cyclic test

The cyclic test procedure stars with setting up the recording system. Procedure for launching real time measurements in "CATMAN" is following:

- Turn on 'Spider8',
- Start 'CATMAN',
- Open I/O definitions,
- Load the Input/Output file from the following folder: 'C:\MyDocuments\Giulio\yellow_rig_2012\.IOD',
- Click the button "Configure device (all channels)" (cf. Figure I3).
- Load amplifier setup from the following file:' C:\MyDocuments\Giulio\yellow_rig_2012\.S8',
- Check whether the correct signals are broadcasted (marked in green if broadcasted),
- Close the setup assistant window,
- Click the button "Configure Measurement Wizard" (cf. Figure I3),
- In the General settings, click the button "Export options..." from the "Online data export" menu,
- Select the following File base name: 'C:\MyDocuments\Giulio\yellow_rig_2012\ Results_2012',
- Create a new folder inside the folder of the corresponding test and name it "Cyclic_Test_Number",
- Press "OK" in the "Options for Online Data Export" window,

- From the “Configure Measurement Wizard” window, click the button “Online Document” and select the following file: ‘C:\MyDocuments\Giulio\yellow_rig_2012\Script\.OPG’,
- From the “Configure Measurement Wizard” window, click the button “Start Measurement Wizard”.

After the procedure is completed, the installing of loading equipment is begun:

- Block the tower by putting 2 bars on each side of the tower and fixed them by bar clamps to the rig frame.
- Fix the two loading wires to the load cells connected to the tower on both sides, make sure if the cables are correctly placed in the blocks.
- Disconnect the safety wire from the end of hinged lever.
- Before launching the cyclic motor check its movement by rotating the weight hanger for one cycle by hand.
- Launch the “STARTER” program and set up all prerequisite settings with following procedure:

  — Start ‘Starter’,

  — Connect the cyclic motor to a program by clicking : Connect device in the “File” menu,

  — Press the “Open project” button and open the default file,

  — Open the “Project” window and select “Connect to target system”,

  — Double click on “S110_CU305_DP” from the Starter main window,

  — Double click on “SERVO_02” from the Starter main window,

  — Select “Commissioning”,

  — Select “Control panel”,

  — Select “Assume control priority!”,

  — From the “Assume control priority” window, set 1000 ms and press “Accept”,

  — Press “Enables”,

  — Set 150 round per minute (rpm),

  — Restore the “Starter” window.

- Simultaneously put the calculated weights on corresponding hangers.
- Unmount the bar clamps and take of the bars blocking the tower. Simultaneously launch the cyclic motor. The side where smaller weight is attached should be unblocked at first.

During the test, use of any programs or functions apart from "STARTER" might stop the measurements. For that reason disconnect the internet cable and turn of all the automatic updates, system scans, etc. In the case of stopping the test, do not turn off the "CATMAN" measurements but try to restart the test from "STARTER" level. The test should be stopped after reaching target number of cycles, by turning off the cyclic motor and quitting the "STARTER". "CATMAN" measurements should be kept on in case of conducting the post-cyclic test. If not, turn off all the measurements and dismantle equipment used for cyclic test.

5. Post-cyclic test

The post-cyclic test is performed with use of the static motor. The eccentricity of loading is fixed and equals 60cm. In case when the motor is lower than 60cm (red marks on loading frame) it should be elevated to required height, with the use of overhead travelling crane. The "CATMAN" software should remain open from cyclic test. Note that by any circumstances do not zero the results in program. The measurements are started by pressing "Start Measurement Wizard".

The test is should be stopped when the failure of soil is observed. In dense sand it is clearly visible by the decreasing loading moment.

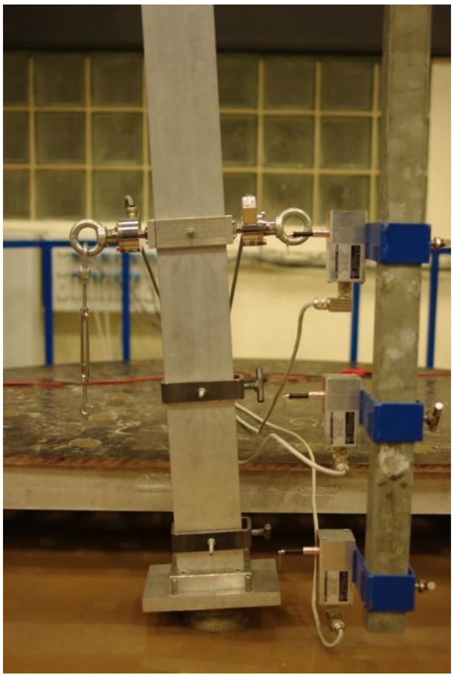

Figure 5.1 The pile with tower after post-cyclic test

Figure 5.2 The displacement of the pile

6. Dismantle phase

The uninstallation scheme after a post-cyclic test is following:

- Remove the loading cable fixed to the tower.
- Unmount the displacement transducers wires from the tower.
- Remove the steel frame with the displacement transducers from the loading frame.
- Unscrew the tower from the base, and remove it.
- Unmount the tower base and the contact head from the top of the pile.
- Unscrew the central bolt from the piles head.
- Mount the installation head to the top of the pile, do not tighten the screws. The connection between the head and the pile should allow water to freely move between.
- Use the screw driver and the installation motor to lift the pile from the soil,
- Unmount the pile from the installation motor.

After the uninstallation in the place of the pile there is a small hole in the soil. Level it by hand in order not to spend much time leveling in with leveler afterwards.

The mini CPT C

The mini cone penetration test, CPT, is performed before each test, immediately after the soil preparation. The target relative density of sand is 80-90%, what indicates a dense state. Measurements are made for three localisation, as it is indicated in the laboratory manual in appendix B. The mini cone is inserted into the soil for the deepth of around 500 mm. The velocity of cone penetration is 5 mm/s. During the penetration three measurements are recorded: time, t [s], depth, d [mm], and the cone resistance, q_c [N]. The exemplary results for the cone resistance are given in Figure C.1.

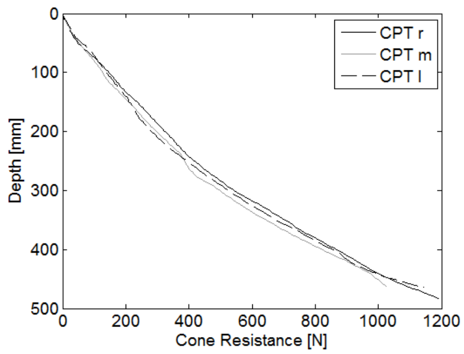

Figure C.1. The results of cone resistance

The results of CPT-s for three localization are close to each others. It can be concluded that the sand compaction is equal in the major part of the container. This indicates that the vibration of sand gives similar conditions, and therefore, the results from different tests are comparable.

The soil parameters are calculated based on CPT results and the drained triaxial tests results of Aalborg University Sand No. 1, see Table C.1.

Table C.1. Material properties of Aalborg University Sand No. 1

d_s	e_{max}	e_{min}	d_{50}	$U = d_{50}/d_{100}$
$[g/cm^3]$	$[-]$	$[-]$	$[mm]$	$[-]$
2.64	0.858	0.549	0.14	1.78

The symbol notification used in the table are as following:

d_s	Specific grain density
e_{max}	Maximum void ratio
e_{min}	Minimum void ratio
d_{50}	Particle size for 50% quantile
U	Uniformity coefficient

For assessing the relative soil density,I_D, following equations are used. Those equations were derived for Aalborg University Sand No. 1, [Ibsen et al., 2009].

$$\gamma = \frac{d_s + e \cdot S_w}{1+e} \cdot \gamma_w \tag{C.1}$$

$$\sigma'_{v0} = (\gamma - \gamma_w) \cdot d \tag{C.2}$$

$$I_D = 5.14 \cdot \left(\frac{\sigma'_{v0}}{q_c^{0.75}} \right)^{-0.42} \tag{C.3}$$

$$I_D = \frac{e_{max} - e}{e_{max} - emin} \tag{C.4}$$

where

γ	The soil unit weight [kN/m^3]
γ_w	The unit weight of water [kN/m^3]
e	The void ratio [-]
S_w	The degree of saturation ($S_w = 1$) [-]
σ'_{v0}	The effective vertical stress acting on soil [kN/m^2]

Bigger fluctuations of a relative density were noticed for the initial depths of soil. They might be influenced by the presence of the soil surface. Therefore, the mean values of I_D are obtained, when the first 150 mm is not included. The exemplary results of a relative density are given in Figure C.2.

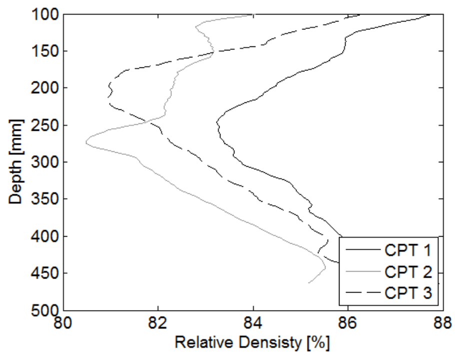

Figure C.2. The results of a relative density

The triaxial tests were performed for different confining pressure, σ'_3, varies between 5kPa to 800kPa. The results of a number of tests were used to derive the equations for the strength parameters of the sand.
For estimation of the equation for the friction angle, φ, the modified Schmertmann

expression was used as the sand is considered as dense. After fitting the expression to the triaxial tests results the equation (C.5) was obtained. No cohesion was assumed.

$$\varphi = 0.152 \cdot I_D + 27.39 \cdot \sigma_3'^{-0.2807} + 23.2 \tag{C.5}$$

The dilatacy angle, ψ, can be obtained from equation (C.6), which was found by fitting the triaxial tests data.

$$\psi = 0.195 \cdot I_D + 14.86 \cdot \sigma_3'^{-0.09764} - 9.946 \tag{C.6}$$

For deriving the parameters for mini CPT the confining pressure of 5 kPa is used. The mean values of parameters obtained from three localization is used as a representative value.

Laboratory tests D

The characterization of the pile used in tests can be seen in Table D.1. Additionally, the information concerning the tower that simulates the turbine is given. The scale is set to be 1:50. The weights of the tower and additional parts correspond to the vertical load of around 8 MN in the full-scale.

Table D.1. Characteristic values for the pile and the tower

The embedded length, L	500 mm
The pile diameter, D	100 mm
The pile thickness, t	5 mm
The self-weight of the pile, m_{pile}	2.22 kg
The self-weight of the tower, m_{tower}	6.58 kg
The self-weight of the transition piece	1.59 kg
The self-weight of the connection part	1.08 kg

Two different kind of tests have been performed: the displacement control static tests and the load control cyclic tests.
The aim of the static tests is to find the ultimate resistance for the soil-pile system, M_R. The aim of the cyclic tests is to analyze the accumulated rotation of the pile and the change in stiffness for the pile-soil system as an effect of the cyclic lateral load. After each cyclic test the post-cyclic static test is performed in order to inspect the change in the ultimate capacity.

The cyclic tests are characterized by the load characteristic parameters used by Leblanc et al. [2010]. ζ_b describes the loading magnitude and ζ_c describes the loading direction. They can be obtained from equations (D.1) and (D.2), where M_{max} and M_{min} are the mean maximum and the mean minimum moments that appear during a test.

$$\zeta_b = \frac{M_{max}}{M_R} \tag{D.1}$$

$$\zeta_c = \frac{M_{min}}{M_{max}} \tag{D.2}$$

As the dimensions of the rig are known, the maximum and minimum loads that are expected during the cyclic loading can be obtained from equations (D.3) and (D.4).

$$F_{max} = 3 \cdot m_1 g - m_2 g \tag{D.3}$$

$$F_{min} = m_1 g - m_2 g \tag{D.4}$$

The maximum and the minimum moment working on the pile is obtained by multiplying the force by the load eccentricity. In Table D.2 the predicted load characteristics and the measured load characteristics for some tests are presented. The total mass must be included, therefore the mass of hangers is added to the mass m_1 and m_2 that are put on them. The hanger 1 weights 2.1 kg and the hanger 2 weights 3.8 kg.

Table D.2. Predicted and real values of load characteristics

m_1 $[kg]$	m_2 $[kg]$	$\zeta_{b,predicted}$ $[-]$	$\zeta_{c,predicted}$ $[-]$	$\zeta_{b,real}$ $[-]$	$\zeta_{c,real}$ $[-]$
19	20	0.676	-0.007	0.514	-0.111
13	20	0.370	-0.405	0.284	-0.415
9	10	0.334	-0.138	0.251	-0.187

The target values are never reached. The loss is caused by the friction of the mechanical system and the lever tilting of the cyclic side of the rig. The problem concerns especially the maximum moment, as the maximum force is induced mostly by the cyclic side.

The function of accumulated rotation and the change of stiffness due to the cyclic loading is given in equations (D.5) and (D.6) and the method for determination of those values can be seen in Figure D.1.

$$\frac{\Delta\theta(N)}{\theta_s} = \frac{\theta_N - \theta_0}{\theta_s} = T_b \cdot T_c \cdot N^n \tag{D.5}$$

$$k_N = k_0 + A_k \cdot ln(N) \tag{D.6}$$

where

$$k_0 = K_b \cdot K_c \tag{D.7}$$

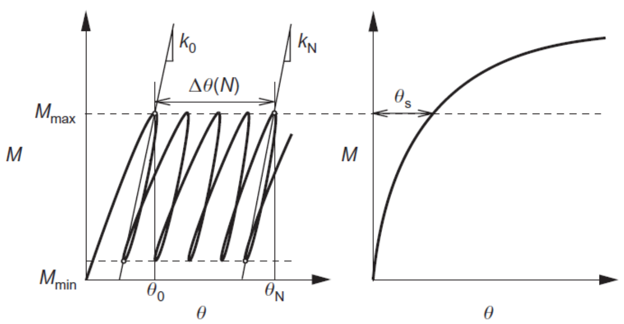

Figure D.1. Method for determination of stiffness and accumulated rotation: cyclic test (on the left) and static test (on the rigth) [Leblanc et al., 2010]

The aimed number of cycles in almost all tests was set to 50 000 in order to simulate long-term cyclic loading. Only for tests number 63-64 and 66-70 the aimed number of cycles is changing and the results of those tests are used for investigation of the stiffness and the post-cyclic resistance changes in the dependence on the number of cycles.

D.1 Test journal

The detailed description of performed tests is given later in this section. Only the tests performed in the period between September 2013 and June 2014 are included. The overview of all tests is given in the electronic appendix. The journal includes all the static and the cyclic tests accompanied with the results of the post-cyclic test. The tests are named with letter 's' for the static and 'c' for the cyclic and the subsequent numbers. Tests that failed or are not used in the analysis are not included.

The static tests are described as following:

1. **Test information:**
   - date
2. **CPT data:**
   - graphs that present the cone resistance and the relative density changes with depth
   - a table with soil parameters for all three localizations accompanied with the mean value of each parameter
3. **Test results:**
   - a graph presenting the moment capacity with marked ultimate moment capacity
   - a table with the ultimate moment capacity for the system, M_R
   - comments

The cyclic tests are described as following:

1. **Test information:**
   - date
   - loading conditions
   - values of predicted ζ_b and ζ_c
2. **CPT data:**
   - the same as for static test
3. **Test results:**
   - a table with basic values from the test:
     - the load characteristics, ζ_b and ζ_c
     - the number of cycles, N
     - the accumulated rotation after N cycles, $\Delta\theta(N)$
     - the unloading rotational stiffness after 1the st cycle, $k_{0,unload}$
     - and after the last cycle, $k_{N,unload}$

- graphs showing the results
  - the number of cycles vs. the moment on the seabed, M
  - the number of cycles vs. $\Delta\theta(N)$
  - the number of cycles vs. $k_{unload}(N)$
- comments

4. **Parameters from LeBlanc approach:**
   - a table with fitting parameters for dense sand (T_b, T_c, n, A_k, K_b and K_c)
   - graphs showing the fitted function of $\Delta\theta(N)$ and $k_{unload}(N)$ in comparison to the LeBlanc fixed values of n and A_k [Leblanc et al., 2010]
   - comments

5. **Post-cyclic resistance:**
   - a graph presenting the moment capacity from static test in comparison to soil resistance obtained after cyclic test
   - a table with the value of post-cyclic resistance and the value of the resistance change

TEST S48

1. Test information:

Date: **12-09-2013**

Type of test: static test

2. CPT data:

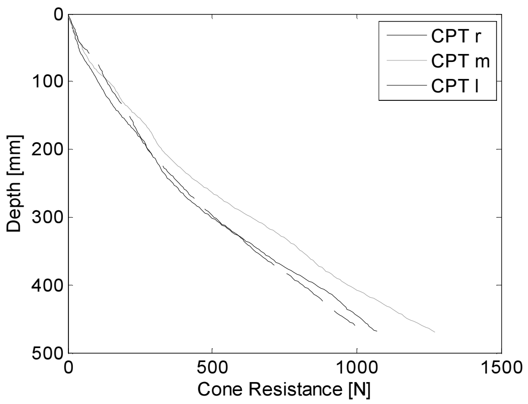

Figure 1: CPT for three localizations

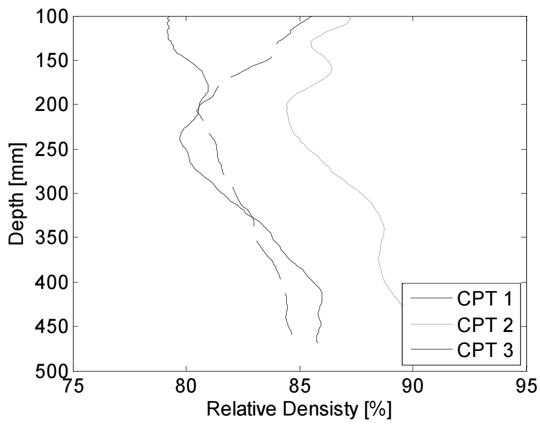

Figure 2: The relative density obtained from CPT

position	I_D [%]	φ [°]	ψ [°]	e [-]	γ' [kN/m³]
r (right)	82.23	53.14	18.78	0.702	9.46
m (middle)	87.23	53.90	19.76	0.659	9.70
l (left)	82.86	53.24	18.91	0.696	9.49
MEAN	**84.11**	**53.43**	**19.15**	**0.685**	**9.55**

3. Test results:

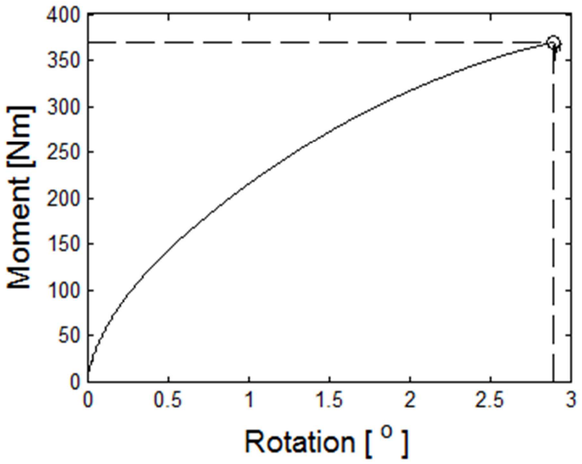

Figure 3: Ultimate soil-pile resistance

M_R [Nm]	369.15

Comments:

The results of this test are not reliable, as the pile was tilled after the installation.

The test was stopped when an immediate decrease in the force was observed. The maximum moment is then taken as the ultimate soil-pile resistance. The soil loose its capacity for rotation of 2.90°.

TEST S50

1. Test information:

Date: **30-09-2013**

Type of test: static test

2. CPT data:

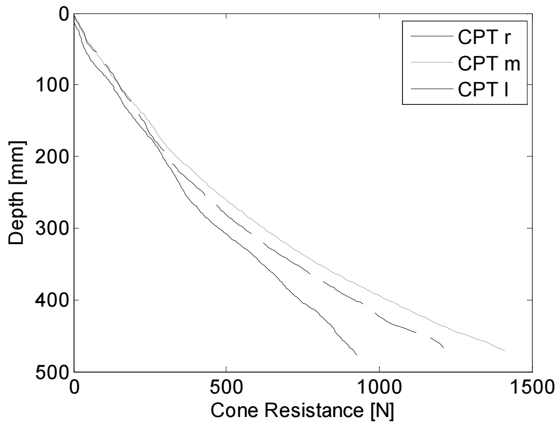

Figure 1: CPT for three localizations

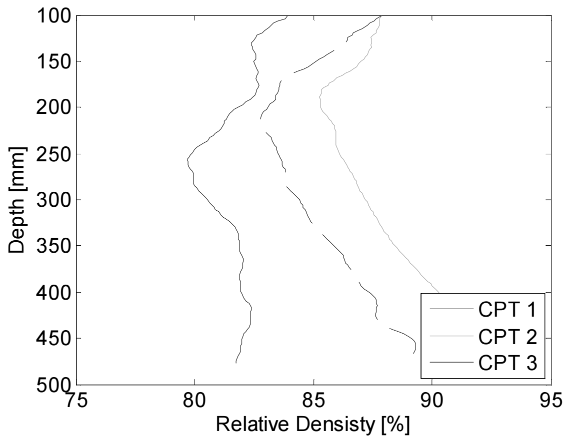

Figure 2: The relative density obtained from CPT

position	I_D [%]	φ [°]	ψ [°]	e [-]	γ' [kN/m³]
r (right)	81.70	53.06	18.69	0.706	9.43
m (middle)	88.03	54.02	19.92	0.652	9.74
l (left)	85.45	53.63	19.42	0.674	9.61
MEAN	**85.06**	**53.57**	**19.34**	**0.677**	**9.59**

3. Test results:

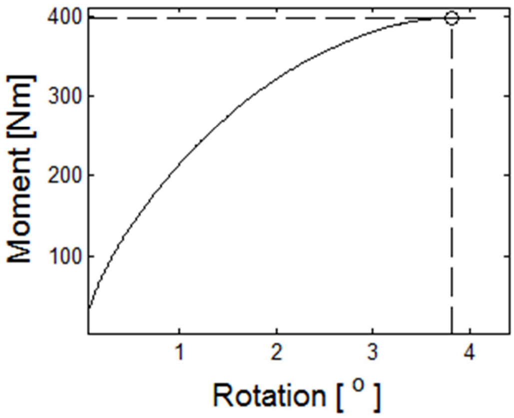

Figure 3: Ultimate soil-pile resistance

M_R [Nm]	398.62

Comments:

The test was stopped when no more increase in the force was observed. The maximum moment is then taken as the ultimate soil-pile resistance. The soil loose its capacity for rotation of 3.81°. The result of this tests are much bigger in comparison to other static tests.

TEST S51

1. Test information:

Date: **02-10-2013**

Type of test: static test

2. CPT data:

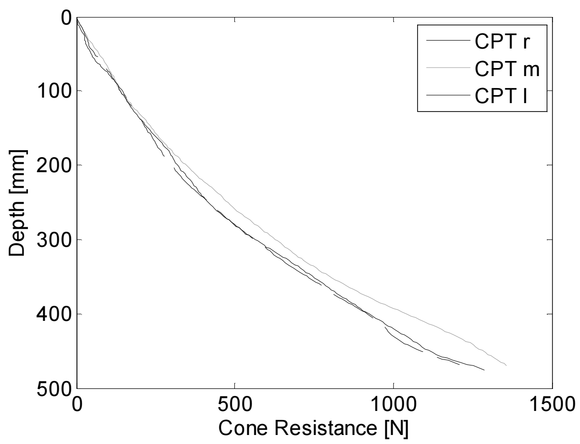

Figure 1: CPT for three localizations

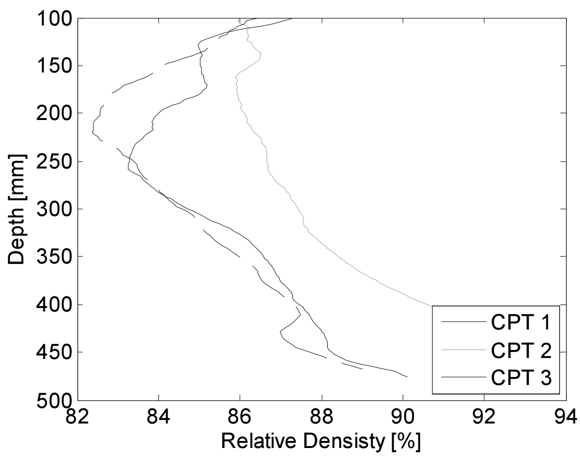

Figure 2: The relative density obtained from CPT

position	I_D [%]	φ [°]	ψ [°]	e [-]	γ' [kN/m³]
r (right)	85.77	53.68	19.48	0.671	9.62
m (middle)	88.01	54.02	19.92	0.652	9.74
l (left)	85.08	53.58	19.34	0.677	9.59
MEAN	**86.29**	**53.76**	**19.58**	**0.667**	**9.65**

3. Test results:

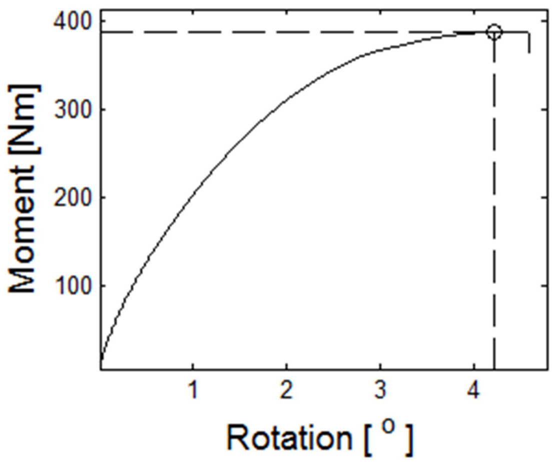

Figure 3: Ultimate soil-pile resistance

M_R [Nm]	387.98

Comments:

The test was stopped when the force started to decrease immediately. The maximum moment is then taken as the ultimate soil-pile resistance. The soil looses its capacity for rotation of 4.20°.

TEST C53

1. Test information:

Date: **17-10-2013**

Type of test: cyclic test

<table>
<tr><th colspan="2">Mass 1</th><th colspan="2">Mass 2</th><th rowspan="2">$\zeta_{b,\ predicted}$</th><th rowspan="2">$\zeta_{c,\ predicted}$</th><th rowspan="2">$N_{planned}$</th></tr>
<tr><td>hanger 1 [kg]</td><td>m1 [kg]</td><td>hanger 2 [kg]</td><td>m2 [kg]</td></tr>
<tr><td>2.1</td><td>17</td><td>3.8</td><td>28</td><td rowspan="3">0.44</td><td rowspan="3">-0.50</td><td rowspan="3">50 000</td></tr>
<tr><td colspan="4">Total mass [kg]</td></tr>
<tr><td colspan="2">19.1</td><td colspan="2">31.8</td></tr>
</table>

2. CPT data:

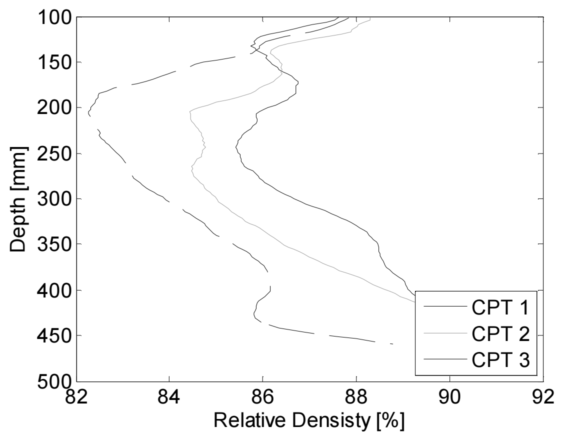

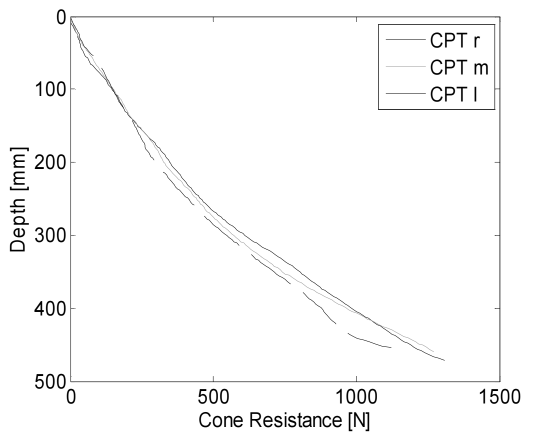

Figure 1: CPT for three localizations

Figure 2: The relative density obtained from CPT

position	I_D [%]	φ [°]	ψ [°]	e [-]	γ' [kN/m³]
r (right)	87.41	53.93	19.80	0.657	9.71
m (middle)	86.60	53.81	19.64	0.664	9.67
l (left)	84.71	53.52	19.27	0.680	9.58
MEAN	**86.24**	**53.75**	**19.57**	**0.667**	**9.65**

3. Test results:

ζ_b [-]	ζ_c [-]	N [-]	$\Delta\theta(N)$ [°]	$k_{0,unload}$	$k_{N,unload}$
0.298	-0.671	34 669	1.42	192.12	180.71

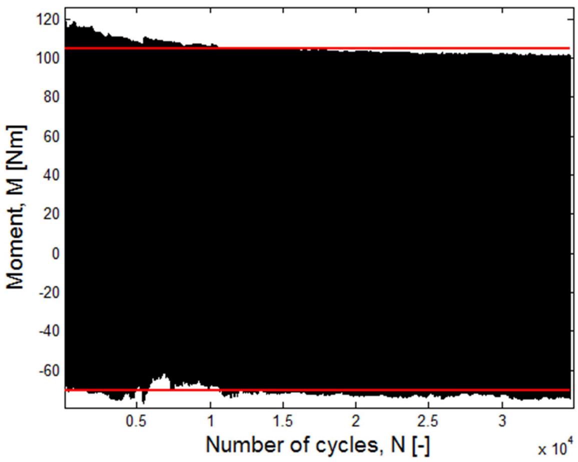

Figure 3: Test results graph – N vs. M

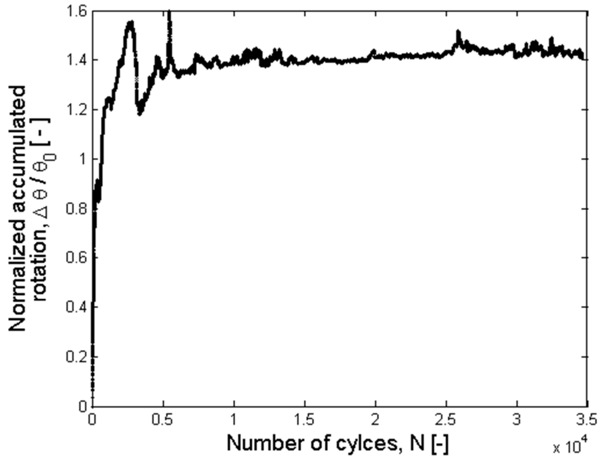

Figure 4: Test results graph – N vs. $\Delta\theta$(N)

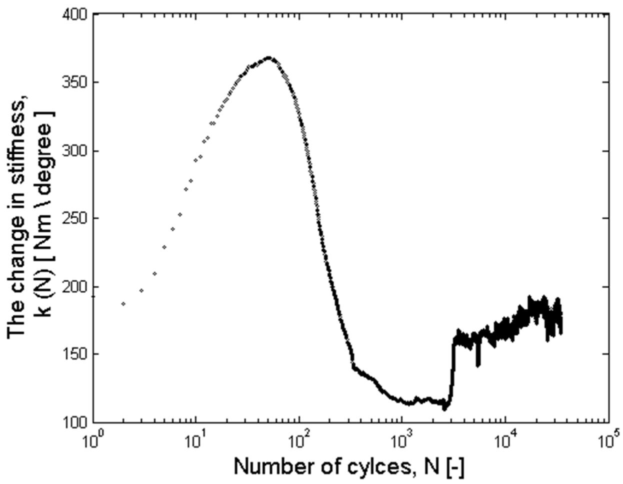

Figure 5: Test results graph – N vs. k_{unload}(N)

Comments:

During the preparation soil was disturbed more than usually, as the pile was inserted too deep and pulled back till the normal level. This might have influenced the results. From unknown reasons the rig was also not able to perform 50 000 cycles. Test was stopped earlier.

Cyclic test – C53

The most of rotation is accumulated during the first 20-40 cycles. After reaching the maximum, the sudden decrease of stiffness is observed. After around 2 x 10^3 cycles, the stiffness increases again. The final stiffness is however smaller than the initial stiffness.

4. Parameters from LeBlanc approach:

T_b [-]	T_c [-]	n [-]	A_k [-]	K_b [-]	K_c [-]
0.522	1.534	0.058	-2.12	652.115	0.295

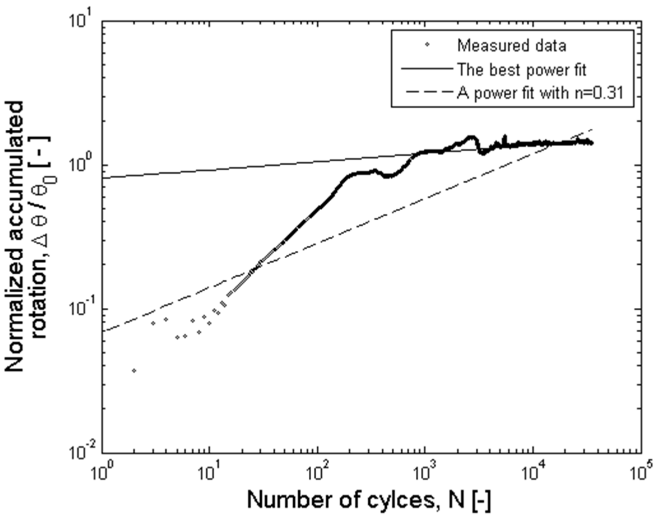

Figure 6: Fitting for Δθ(N)

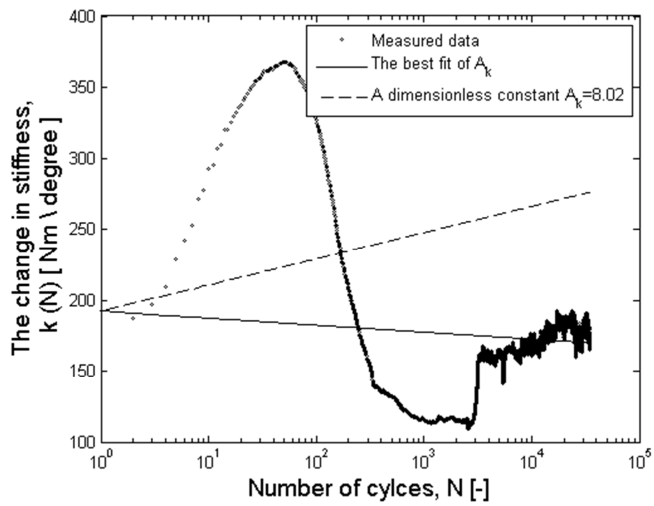

Figure 7: Fitting for k_{unload}(N)

Comments:

The fit for accumulated rotation is suitable for the larger number of cycles, but it does not fit for the results of first cycles. For the stiffness it cannot be concluded that the good fit is obtained. Even though the fitting function is close to the data for the last 1 000 of cycles, the data seems to increase, whereas the function is decreasing.

5. Post-cyclic resistance:

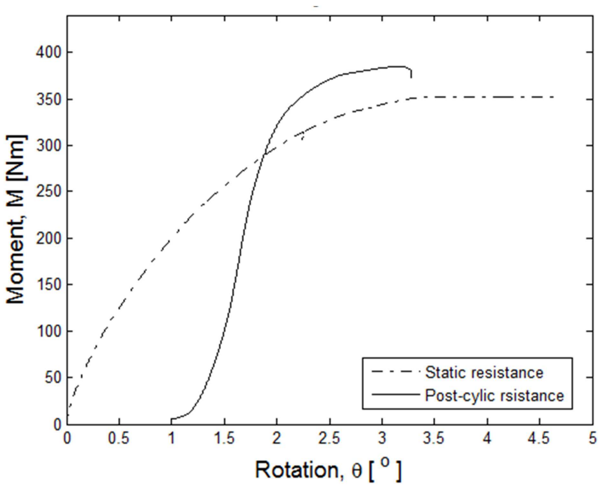

Figure 8: Ultimate soil-pile resistance

M_{PC} [Nm]	384.74
M_{PC} / M_R [-]	1.09

TEST C54

1. Test information:

Date: **24-10-2013**

Type of test: cyclic test

<table>
<tr><th colspan="2">Mass 1</th><th colspan="2">Mass 2</th><th rowspan="2">$\zeta_{b, predicted}$</th><th rowspan="2">$\zeta_{c, predicted}$</th><th rowspan="2">$N_{planned}$</th></tr>
<tr><td>hanger 1 [kg]</td><td>m1 [kg]</td><td>hanger 2 [kg]</td><td>m2 [kg]</td></tr>
<tr><td>2.1</td><td>13</td><td>3.8</td><td>20</td><td rowspan="3">0.37</td><td rowspan="3">-0.40</td><td rowspan="3">50 000</td></tr>
<tr><td colspan="4">Total mass [kg]</td></tr>
<tr><td colspan="2">15.1</td><td colspan="2">23.8</td></tr>
</table>

2. CPT data:

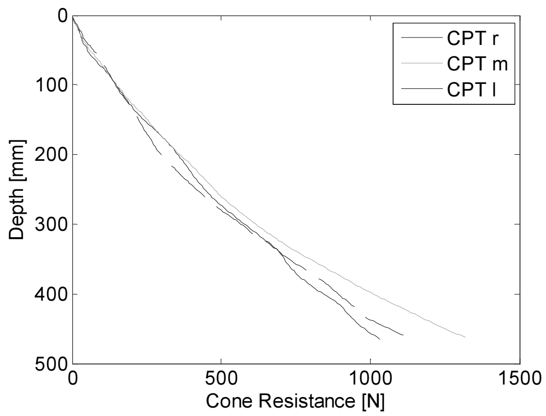

Figure 1: CPT for three localizations

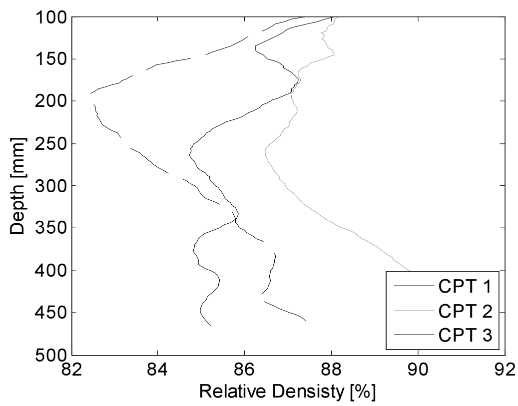

Figure 2: The relative density obtained from CPT

position	I_D [%]	φ [°]	ψ [°]	e [-]	γ' [kN/m³]
r (right)	85.72	53.67	19.47	0.672	9.63
m (middle)	88.14	54.04	19.94	0.651	9.75
l (left)	85.01	53.57	19.33	0.678	9.59
MEAN	**86.29**	**53.76**	**19.58**	**0.667**	**9.65**

3. Test results:

ζ_b [-]	ζ_c [-]	N [-]	$\Delta\theta(N)$ [°]	$k_{0,unload}$	$k_{N,load}$
0.284	-0.415	42 618	1.03	310.20	410.26

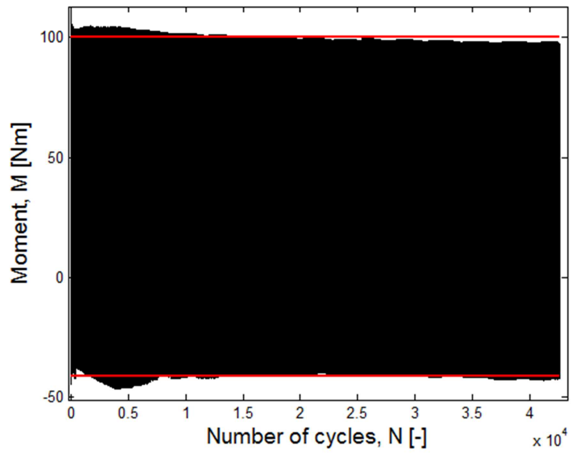

Figure 3: Test results graph – N vs. M

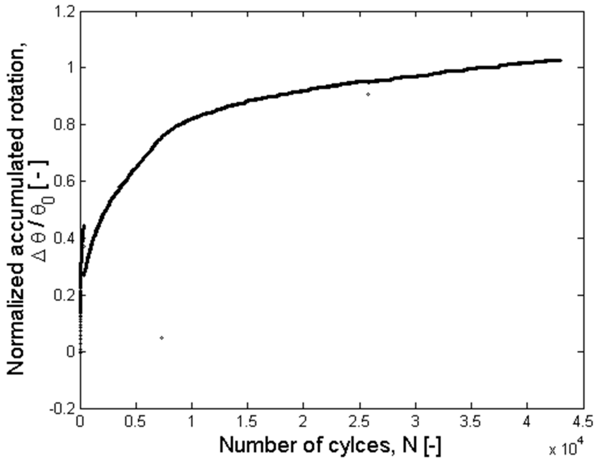

Figure 4: Test results graph – N vs. $\Delta\theta(N)$

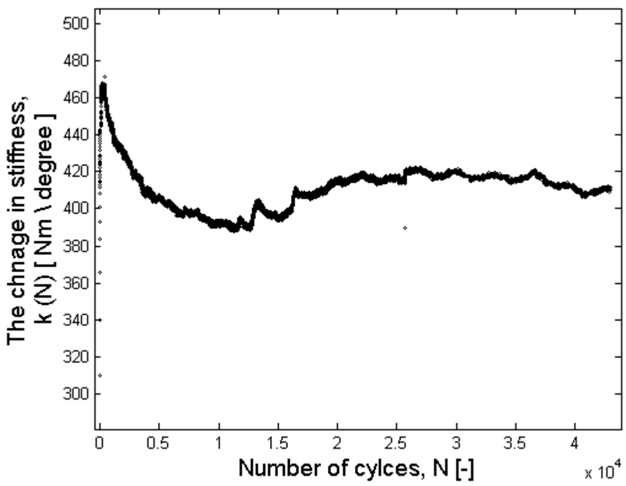

Figure 5: Test results graph – N vs. $k_{unload}(N)$

Comments:

The test was stopped and started again during the cycles, therefore a visible jump in the rotation is observed. A significant changes in the maximum and the minimum moments are observed in first cycles. The most of rotation is accumulated in first couple cycles and also the most of stiffness increase is observed for first couple cycles. However, the stiffness, after reaching the maximum, starts to decrease and again increase.

4. Parameters from LeBlanc approach:

T_b [-]	T_c [-]	n [-]	A_k [-]	K_b [-]	K_c [-]
0.486	0.219	0.216	10.316	685.547	0.452

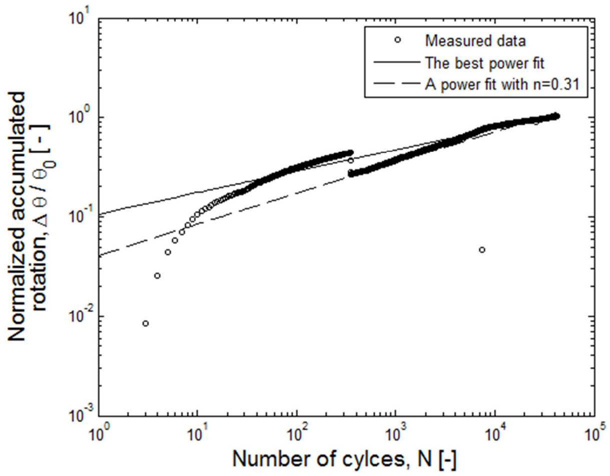

Figure 6: Fitting for Δθ(N)

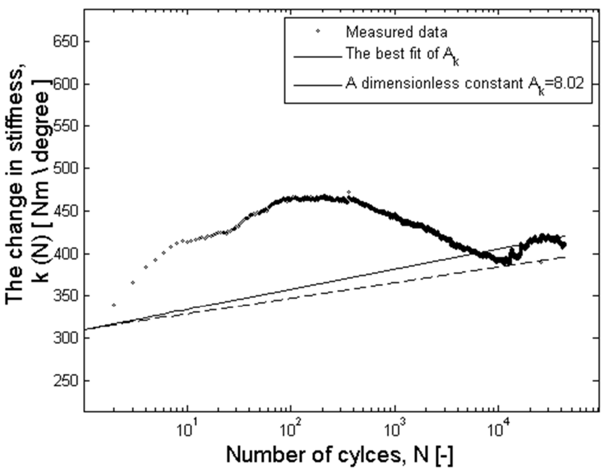

Figure 7: Fitting for k_{unload}(N)

Comments:

There is a good fit of data for the accumulated rotation in a larger number of cycles. The fit for a stiffness is not so good for small number of cycles. The stiffness increases the most in first couple cycles, however, it decreases unexpectedly later on. For larger number of cycles the fit seems to be reasonable.

5. Post-cyclic resistance:

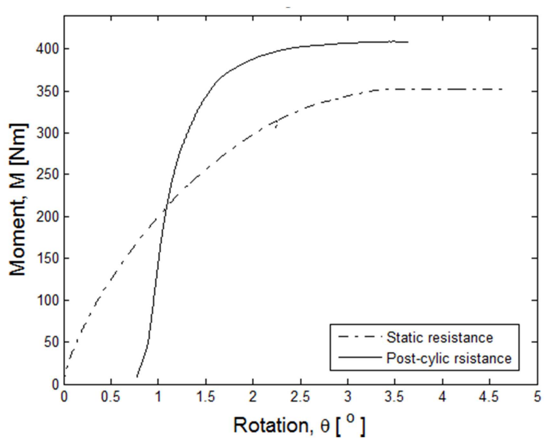

Figure 8: Ultimate soil-pile resistance

M_{PC} [Nm]	408.83
M_{PC} / M_R [-]	1.16

TEST C55

1. Test information:

Date: **31-10-2013**

Type of test: cyclic test

Mass 1		Mass 2		$\zeta_{b, predicted}$	$\zeta_{c, predicted}$	$N_{planned}$
hanger 1 [kg]	m1 [kg]	hanger 2 [kg]	m2 [kg]			
2.1	14	3.8	23	0.37	-0.50	50 000
Total mass [kg]						
16.1		26.8				

2. CPT data:

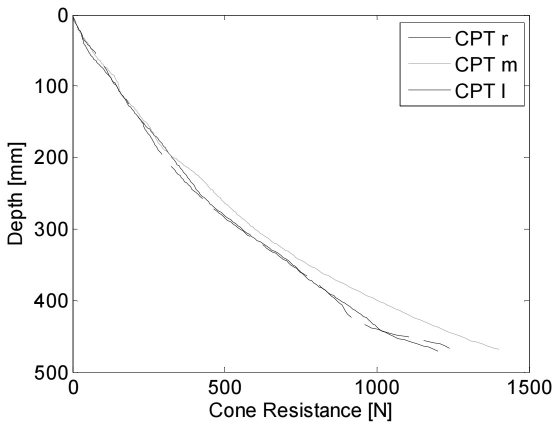

Figure 1: CPT for three localizations

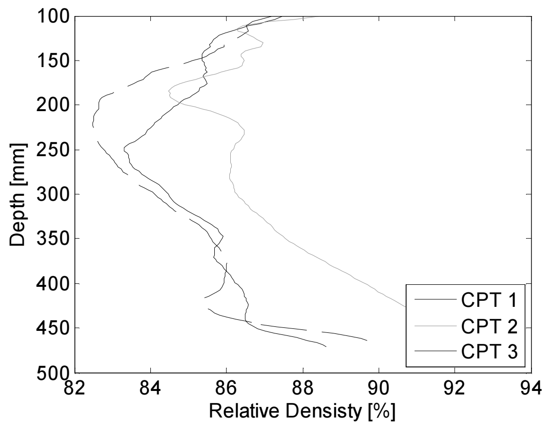

Figure 2: The relative density obtained from CPT

position	I_D [%]	φ [°]	ψ [°]	e [-]	γ' [kN/m³]
r (right)	85.40	53.62	19.41	0.674	9.61
m (middle)	87.48	53.94	19.81	0.656	9.71
l (left)	84.85	53.54	19.30	0.679	9.58
MEAN	**85.91**	**53.70**	**19.51**	**0.670**	**9.63**

3. Test results:

ζ_b [-]	ζ_c [-]	N [-]	$\Delta\theta(N)$ [°]	$k_{0,unload}$	$k_{N,load}$
0.275	-0.544	50 195	0.83	283.70	401.30

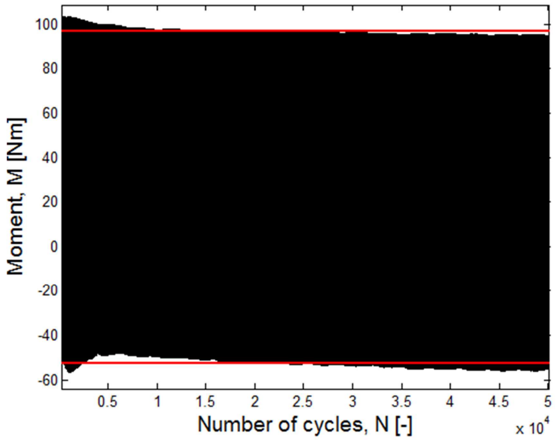

Figure 3: Test results graph – N vs. M

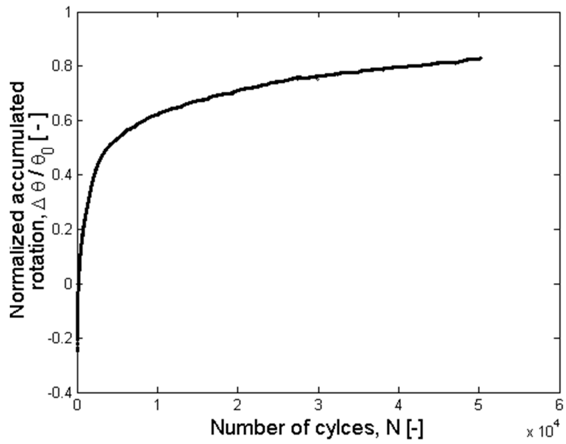

Figure 4: Test results graph – N vs. $\Delta\theta(N)$

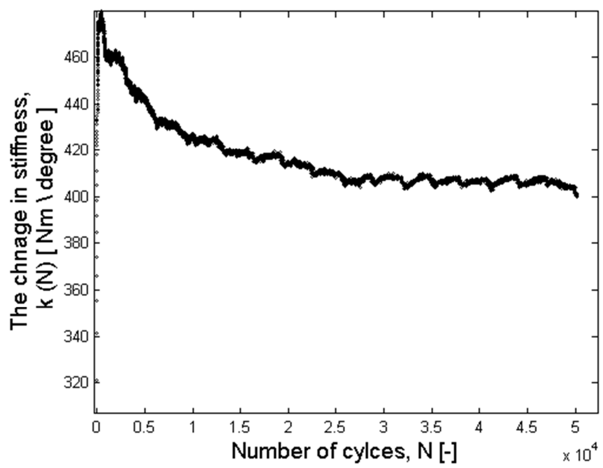

Figure 5: Test results graph – N vs. $k_{unload}(N)$

Comments:

The rotation in first cycles is negative, what can be explained by the bigger negative moment at the beginning of loading. The most of rotation is accumulated in first couple cycles. The most of stiffness growth is observed in first 10 cycles. However, the increasing tendency is not maintained, because the stiffness starts to decrease after 500 cycles. The results of the stiffness are completely different from expectations.

4. Parameters from LeBlanc approach:

T_b [-]	T_c [-]	n [-]	A_k [-]	K_b [-]	K_c [-]
0.463	0.168	0.221	13.298	708.894	0.400

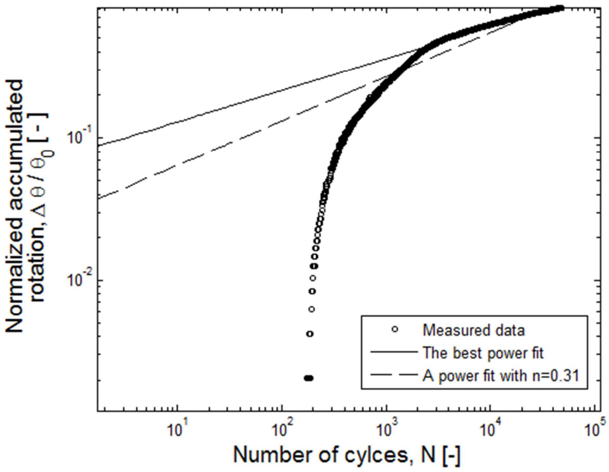

Figure 6: Fitting for Δθ(N)

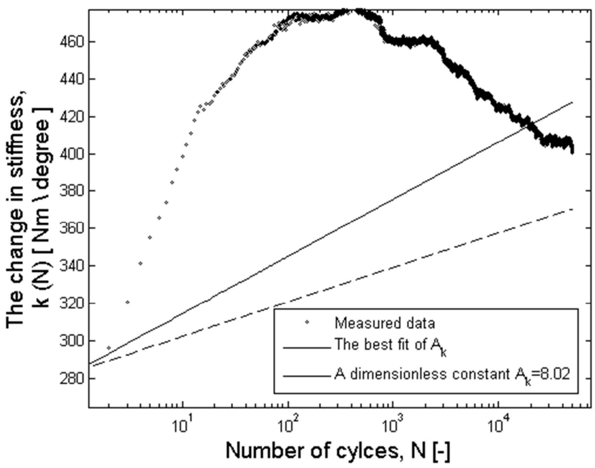

Figure 7: Fitting for k_{unload}(N)

Comments:

Even though the accumulated rotation starts with negative values, a good fit with exponential function was obtained for larger number of cycles. The stiffness is completely not in a good fit with the logarithmic function.

5. Post-cyclic resistance:

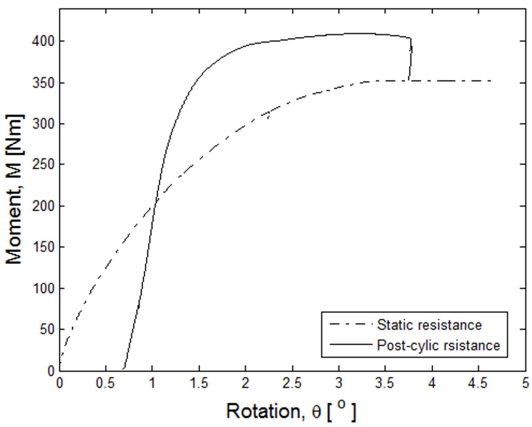

Figure 8: Ultimate soil-pile resistance

M_{PC} [Nm]	409.09
M_{PC} / M_R [-]	1.16

TEST C56

1. Test information:

Date: **08-11-2013**

Type of test: cyclic test

Mass 1		Mass 2		$\zeta_{b, predicted}$	$\zeta_{c, predicted}$	$N_{planned}$
hanger 1 [kg]	m1 [kg]	hanger 2 [kg]	m2 [kg]			
2.1	17	3.8	33	0.36	-0.86	50 000
Total mass [kg]						
19.1		36.8				

2. CPT data:

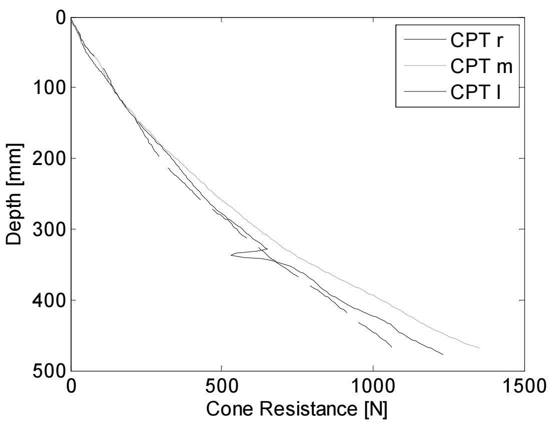

Figure 1: CPT for three localizations

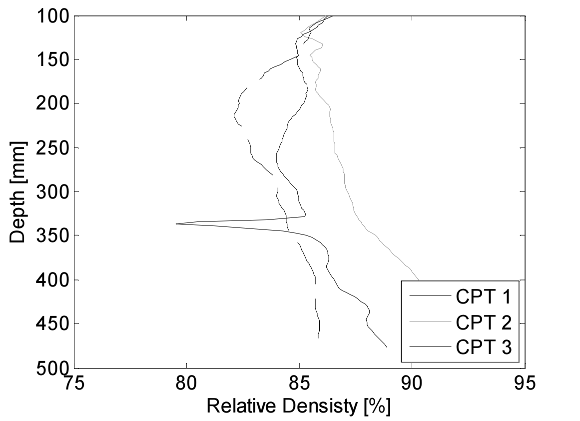

Figure 2: The relative density obtained from CPT

position	I_D [%]	φ [°]	ψ [°]	e [-]	γ' [kN/m³]
r (right)	85.55	53.65	19.44	0.673	9.62
m (middle)	87.71	53.98	19.86	0.654	9.72
l (left)	84.35	53.47	19.20	0.683	9.56
MEAN	**85.87**	**53.70**	**19.50**	**0.670**	**9.63**

3. Test results:

ζ_b [-]	ζ_c [-]	N [-]	$\Delta\theta(N)$ [°]	$k_{0,unload}$	$k_{N,load}$
0.213	-1.39	50 286	-0.737	237.317	322.164

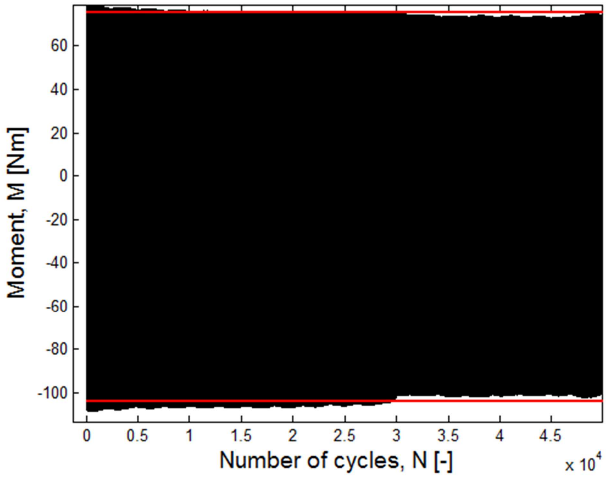

Figure 3: Test results graph – N vs. M

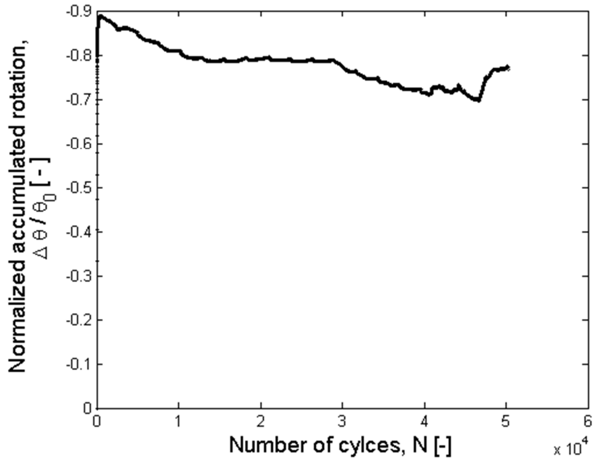

Figure 4: Test results graph – N vs. $\Delta\theta(N)$

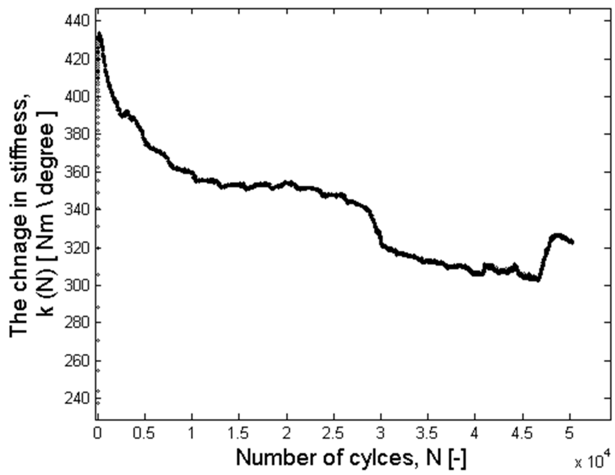

Figure 5: Test results graph – N vs. $k_{unload}(N)$

Comments:

The accumulated rotation is increasing, but the increase has place on the negative side of the rig. During the test there is a small decrease in the accumulated rotation, but it starts to increase again. The most of rotation is accumulate in first 10 cycles. The most of stiffness increase is observed also in first 10 cycles. However, the stiffness is later decreasing during the most of cycles. There is also a small increase of stiffness at the last 500 cycles.

4. Parameters from LeBlanc approach:

T_b [-]	T_c [-]	n [-]	A_k [-]	K_b [-]	K_c [-]
0.431	-2.89	-0.05	-25.78	741.798	0.320

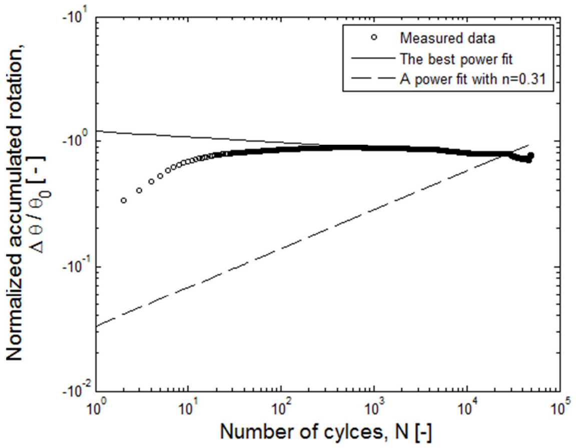

Figure 6: Fitting for $\Delta\theta(N)$

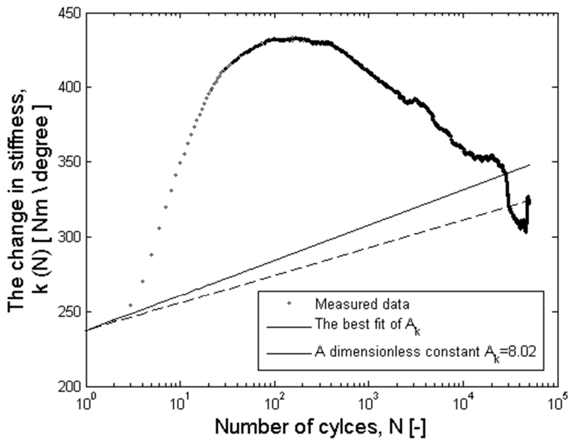

Figure 7: Fitting for $k_{unload}(N)$

Comments:

There is a quite good fit for the accumulated rotation at the larger number of cycles. The fitting for the change in stiffness is not good.

5. Post-cyclic resistance:

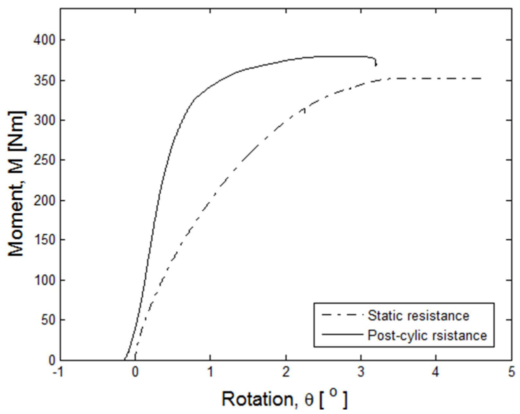

Figure 8: Ultimate soil-pile resistance

M_{PC} [Nm]	379.91
M_{PC} / M_R [-]	1.08

TEST C57

1. Test information:

Date: **16-11-2013**

Type of test: cyclic test

Mass 1		Mass 2		$\zeta_{b, predicted}$	$\zeta_{c, predicted}$	$N_{planned}$
hanger 1 [kg]	m1 [kg]	hanger 2 [kg]	m2 [kg]			
2.1	17	3.8	29	0.42	-0.56	50 000
Total mass [kg]						
19.1		32.8				

2. CPT data:

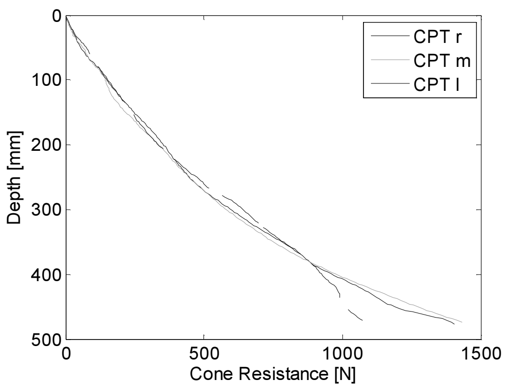

Figure 1: CPT for three localizations

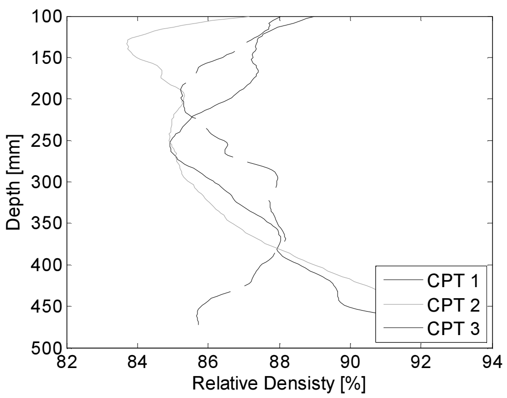

Figure 2: The relative density obtained from CPT

position	I_D [%]	φ [°]	ψ [°]	e [-]	γ' [kN/m^3]
r (right)	87.48	53.94	19.81	0.656	9.71
m (middle)	86.66	53.82	19.65	0.664	9.67
l (left)	86.83	53.84	19.69	0.662	9.68
MEAN	**86.99**	**53.87**	**19.72**	**0.661**	**9.69**

Cyclic test – C57

3. Test results:

ζ_b [-]	ζ_c [-]	N [-]	$\Delta\theta(N)$ [°]	$k_{0,unload}$	$k_{N,load}$
0.256	-0.831	50 087	0.528	271.534	414.944

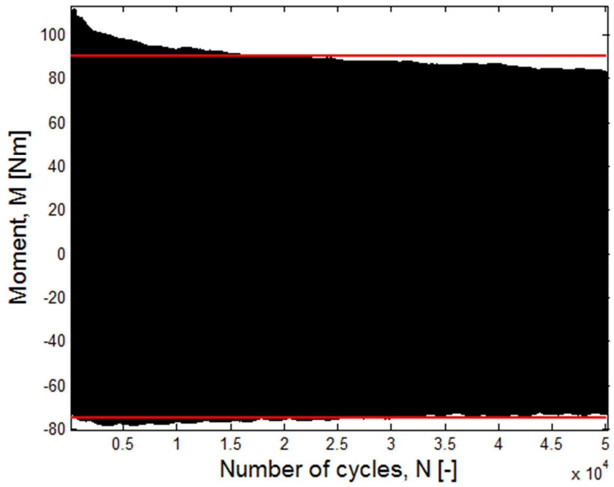

Figure 3: Test results graph – N vs. M

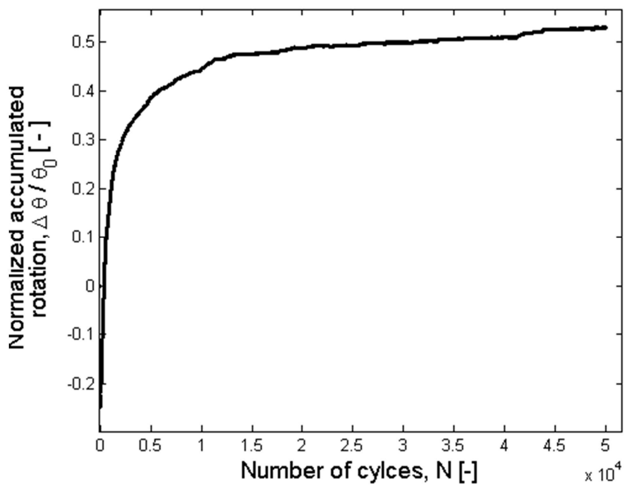

Figure 4: Test results graph – N vs. $\Delta\theta(N)$

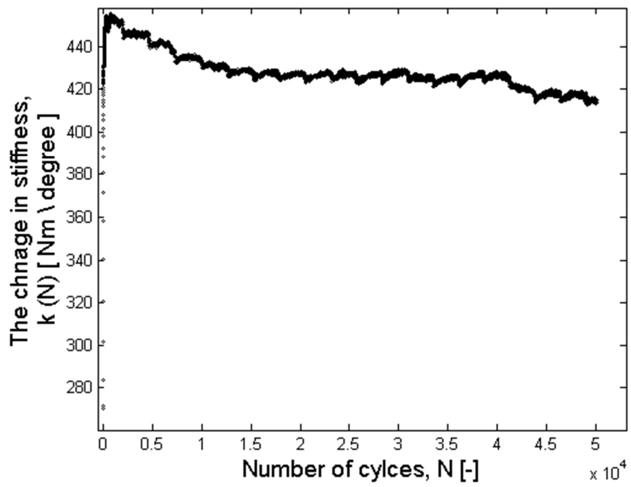

Figure 5: Test results graph – N vs. $k_{unload}(N)$

Comments:

The most of accumulated rotation is observed for first 10 cycles. The rotation is negative for first couple cycles, but it has an increasing trend. The most increase in stiffness is also observed for first 10 cycles. After reaching the maximum, the stiffness results decrease.

4. Parameters from LeBlanc approach:

T_b [-]	T_c [-]	n [-]	A_k [-]	K_b [-]	K_c [-]
0.415	0.194	0.178	15.701	763.622	0.356

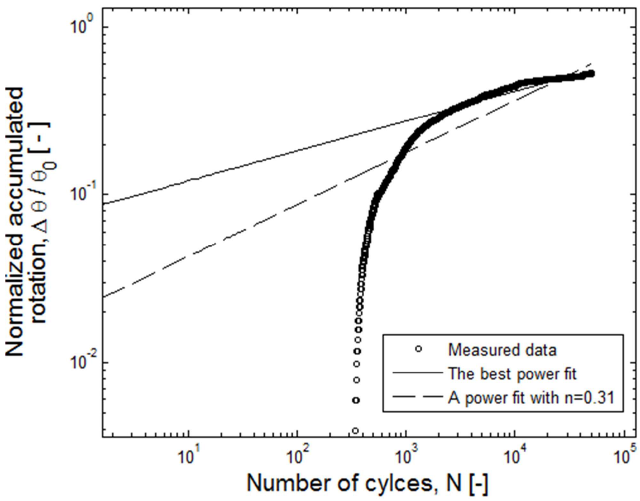

Figure 6: Fitting for $\Delta\theta(N)$

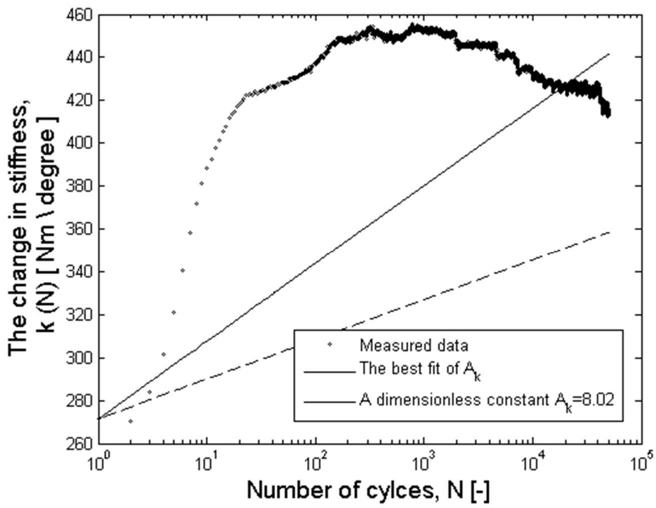

Figure 7: Fitting for $k_{unload}(N)$

Comments:

A good fit with for the accumulated rotation is observed for a larger number of cycles. There is no good fit for the stiffness results.

5. Post-cyclic resistance:

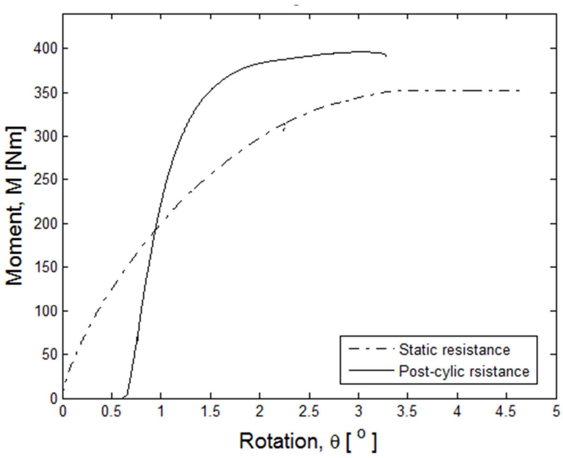

Figure 8: Ultimate soil-pile resistance

M_{PC} [Nm]	396.17
M_{PC} / M_R [-]	1.22

TEST S58

1. Test information:

Date: **28-11-2013**

Type of test: static test

2. CPT data:

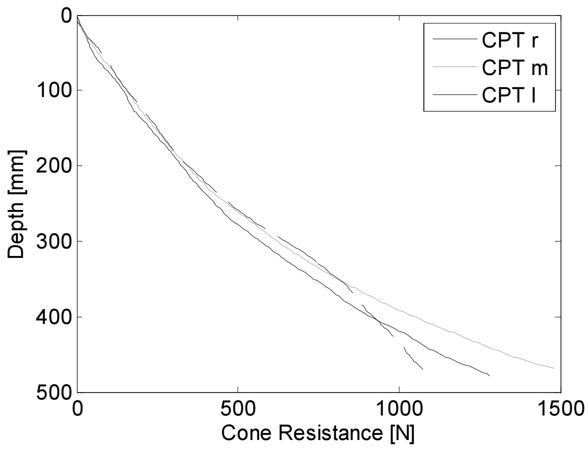

Figure 1: CPT for three localizations

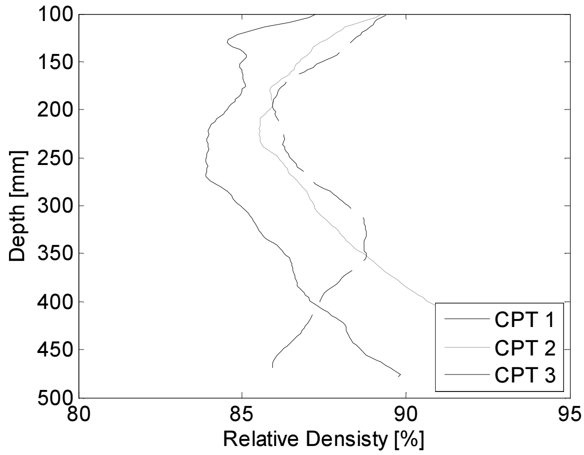

Figure 2: The relative density obtained from CPT

position	I_D [%]	φ [°]	ψ [°]	e [-]	γ' [kN/m³]
r (right)	85.85	53.69	19.49	0.670	9.63
m (middle)	88.27	54.06	19.97	0.650	9.75
l (left)	87.36	53.92	19.79	0.657	9.71
MEAN	**87.16**	**53.89**	**19.75**	**0.659**	**9.70**

3. Test results:

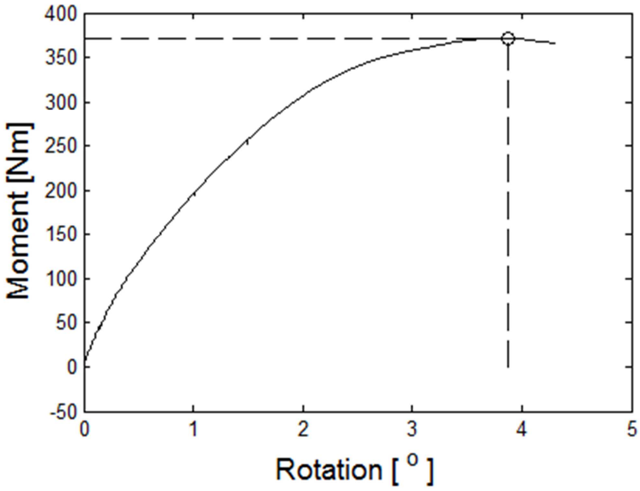

Figure 3: Ultimate soil-pile resistance

M_R [Nm]	371.71

Comments:

The test was stopped, when no more increase in the force was observed. The maximum moment is then taken as the ultimate soil-pile resistance. The soil looses its capacity for rotation of 3.87°.

TEST S59

1. Test information:

Date: **04-12-2013**

Type of test: static test

2. CPT data:

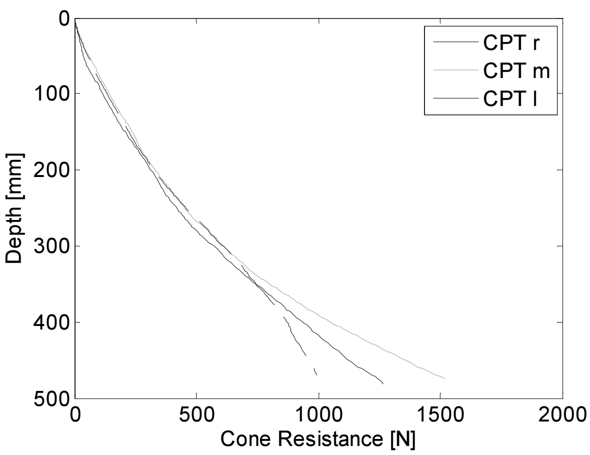

Figure 1: CPT for three localizations

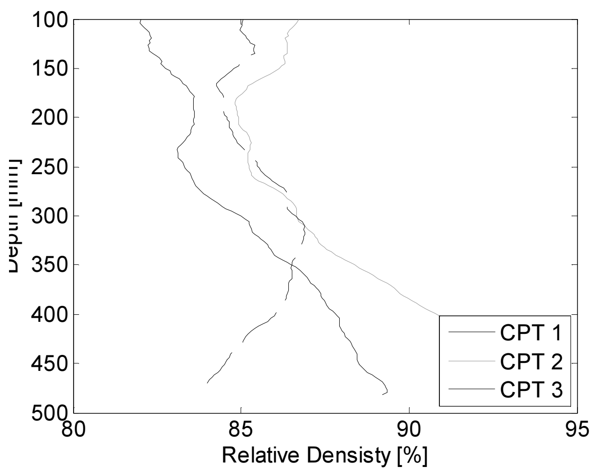

Figure 2: The relative density obtained from CPT

position	I_D [%]	φ [°]	ψ [°]	e [-]	γ' [kN/m³]
r (right)	85.22	53.60	19.37	0.676	9.60
m (middle)	87.88	54.00	19.89	0.653	9.73
l (left)	85.50	53.64	19.42	0.673	9.61
MEAN	**86.20**	**53.75**	**19.56**	**0.667**	**9.65**

3. Test results:

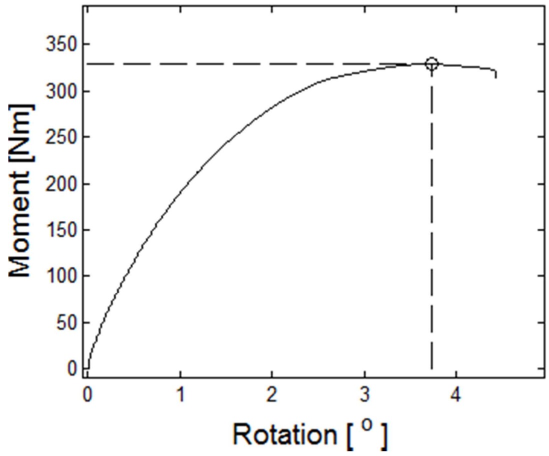

Figure 3: Ultimate soil-pile resistance

M_R [Nm]	329.40

Comments:

The test was stopped when the force started to decrease. The maximum moment is then taken as an ultimate soil-pile resistance. The soil loose its capacity for rotation of 3.73°.

The moment capacity obtained from this test is small in comparison with the other static test that were performed. The reason for that might be due to a slightly smaller compaction of the soil on the right and left side of the pile, what can be seen in CPT results.

TEST S60

1. Test information:

Date: **12-12-2013**

Type of test: static test

2. CPT data:

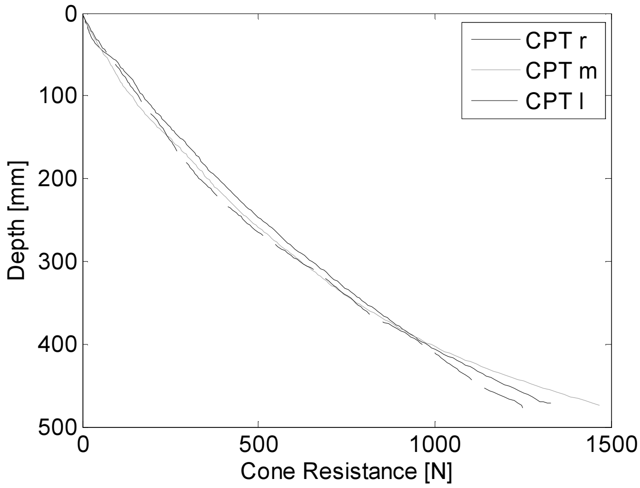

Figure 1: CPT for three localizations

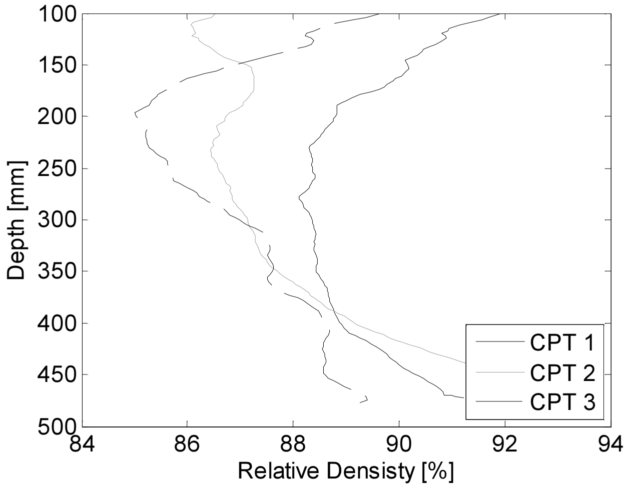

Figure 2: The relative density obtained from CPT

position	I_D [%]	φ [°]	ψ [°]	e [-]	γ' [kN/m³]
r (right)	89.23	54.21	20.15	0.641	9.80
m (middle)	87.95	54.01	19.90	0.652	9.74
l (left)	87.23	53.90	19.76	0.659	9.70
MEAN	**88.14**	**54.04**	**19.94**	**0.651**	**9.75**

3. Test results:

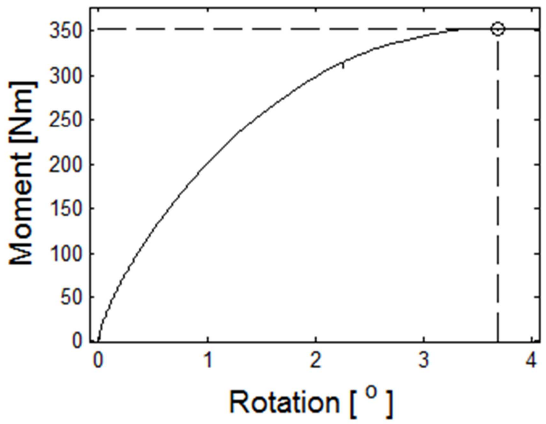

Figure 3: Ultimate soil-pile resistance

M_R [Nm]	352.78

Comments:

The test was stopped, when no more increase in force was observed. The maximum moment is then taken as an ultimate soil-pile resistance. The soil loose its capacity for rotation of 3.68°.

TEST C63

1. Test information:

Date: **14-02-2014**

Type of test: cyclic test

Mass 1		**Mass 2**		$\zeta_{b,\ predicted}$	$\zeta_{c,\ predicted}$	$N_{planned}$
hanger 1 [kg]	m1 [kg]	hanger 2 [kg]	m2 [kg]			
2.1	9	3.8	10	0.33	-0.14	50 000
Total mass [kg]						
11.1		13.8				

2. CPT data:

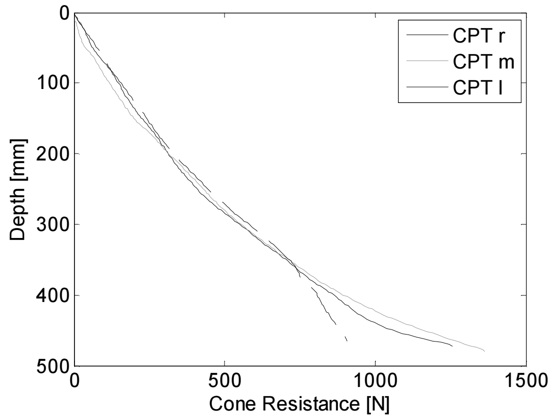

Figure 1: CPT for three localizations

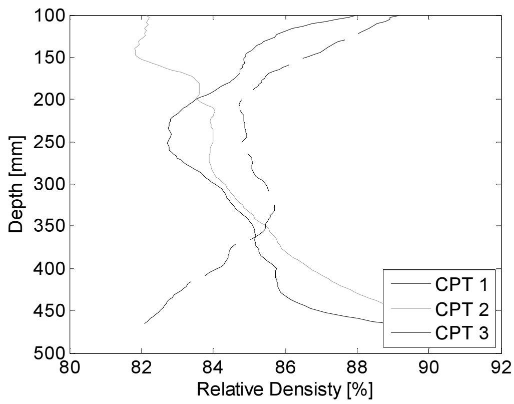

Figure 2: The relative density obtained from CPT

position	I_D [%]	φ [°]	ψ [°]	e [-]	γ' [kN/m³]
r (right)	84.89	53.55	19.31	0.679	9.58
m (middle)	85.02	53.57	19.33	0.678	9.59
l (left)	85.14	53.58	19.36	0.677	9.60
MEAN	**85.02**	**53.57**	**19.33**	**0.678**	**9.59**

Cyclic test – C63

3. Test results:

ζ_b [-]	ζ_c [-]	N [-]	$\Delta\theta(N)$ [°]	$k_{0,unload}$	$k_{N,load}$
0.251	-0.186	32442	2.679	636.549	821.453

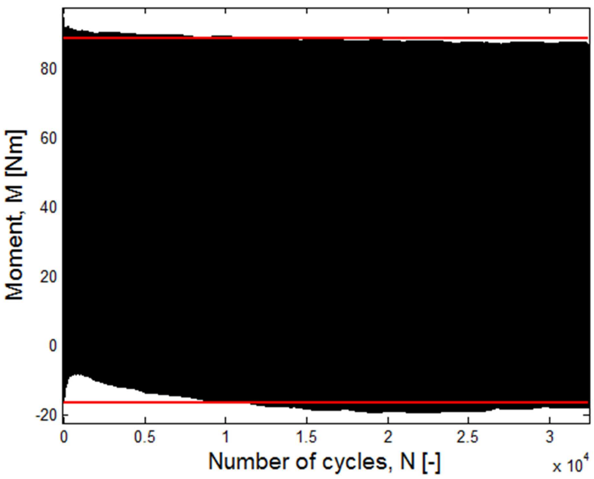

Figure 3: Test results graph – N vs. M

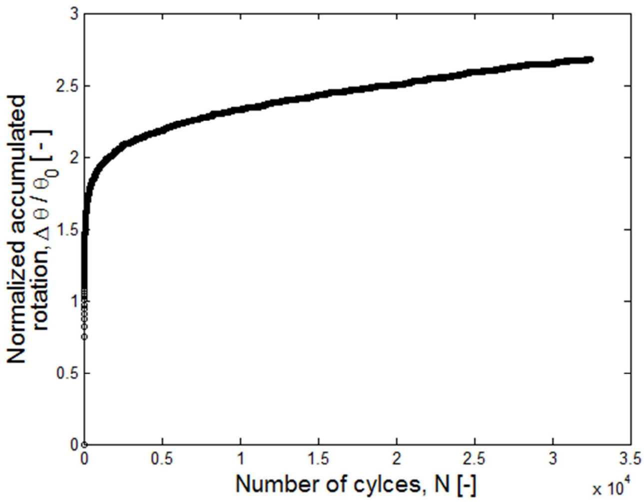

Figure 4: Test results graph – N vs. $\Delta\theta(N)$

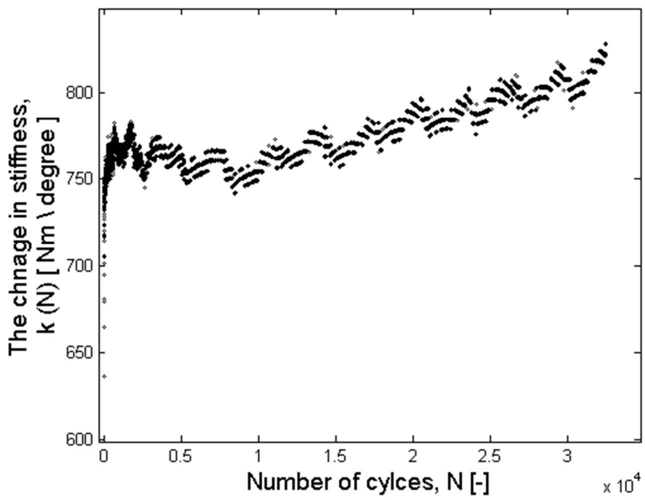

Figure 5: Test results graph – N vs. $k_{unload}(N)$

Comments:

From unknown reasons the rig was not able to perform 50 000 cycles. Test was stopped earlier. The most of the rotation accumulation and stiffness increase is found for first 10 cycles. From 10 000 of cycle a bigger, steady increase in stiffness is observed.

4. Parameters from LeBlanc approach:

T_b [-]	T_c [-]	n [-]	A_k [-]	K_b [-]	K_c [-]
0.403	2.352	0.099	14.965	778.021	0.818

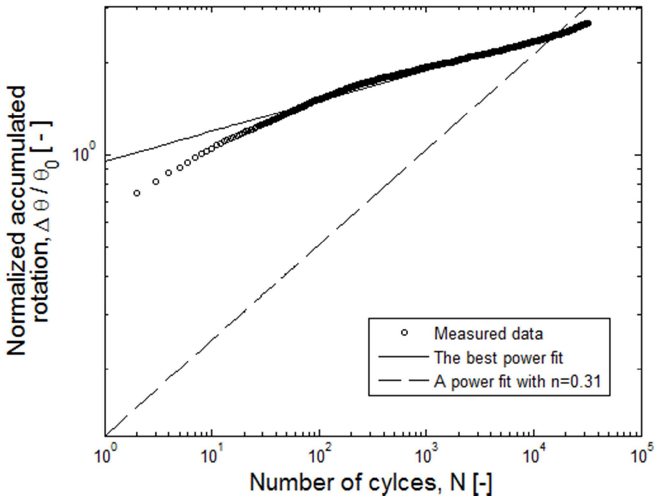

Figure 6: Fitting for $\Delta\theta(N)$

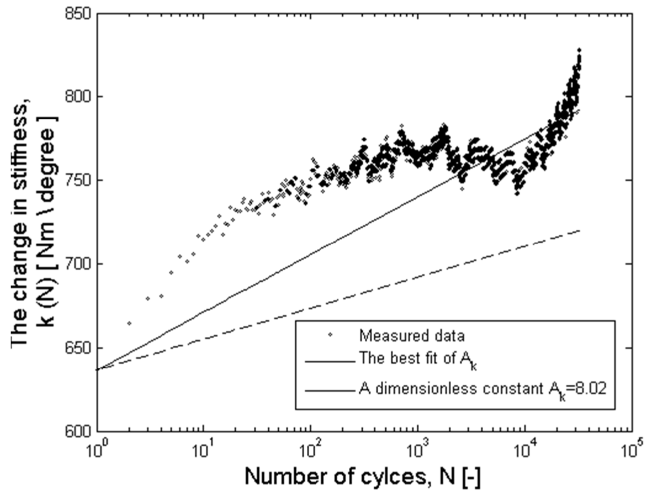

Figure 7: Fitting for $k_{unload}(N)$

Comments:

A good fit for an accumulated rotation is obtained. It can be stated that for the stiffness changes also a good fit is obtained for the larger number of data.

5. Post-cyclic resistance:

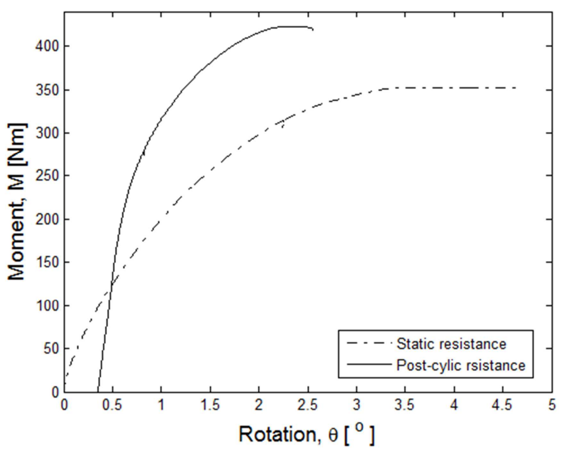

Figure 8: Ultimate soil-pile resistance

M_{PC} [Nm]	423.04
M_{PC} / M_R [-]	1.20

TEST C64

1. Test information:

Date: **27-02-2014**

Type of test: cyclic test

Mass 1		Mass 2		$\zeta_{b,\ predicted}$	$\zeta_{c,\ predicted}$	$N_{planned}$
hanger 1 [kg]	m1 [kg]	hanger 2 [kg]	m2 [kg]			
2.1	9	3.8	10	0.33	-0.14	100
Total mass [kg]						
11.1		13.8				

2. CPT data:

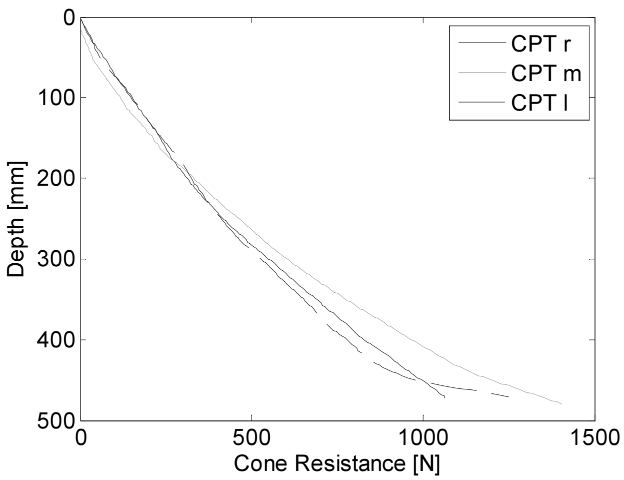

Figure 1: CPT for three localizations

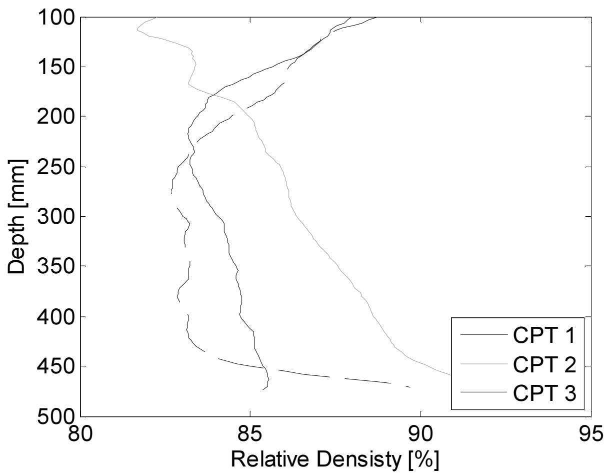

Figure 2: The relative density obtained from CPT

position	I_D [%]	φ [°]	ψ [°]	e [-]	γ' [kN/m³]
r (right)	84.66	53.51	19.26	0.681	9.57
m (middle)	86.47	53.79	19.62	0.665	9.66
l (left)	84.32	53.46	19.19	0.684	9.56
MEAN	**85.15**	**53.59**	**19.36**	**0.676**	**9.60**

3. Test results:

ζ_b [-]	ζ_c [-]	N [-]	$\Delta\theta(N)$ [°]	$k_{0,unload}$	$k_{N,load}$
0.260	-0.162	119	0.781	919.802	1062.245

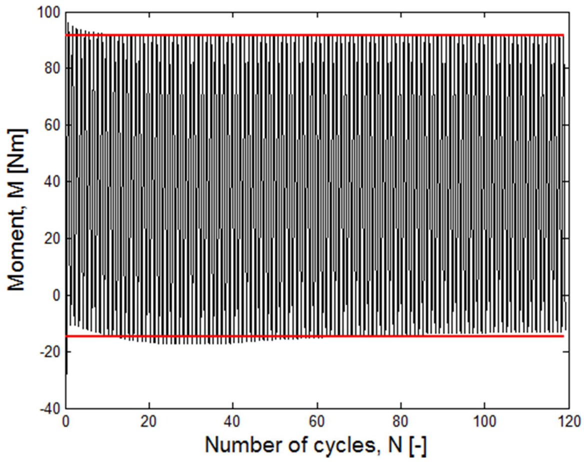

Figure 3: Test results graph – N vs. M

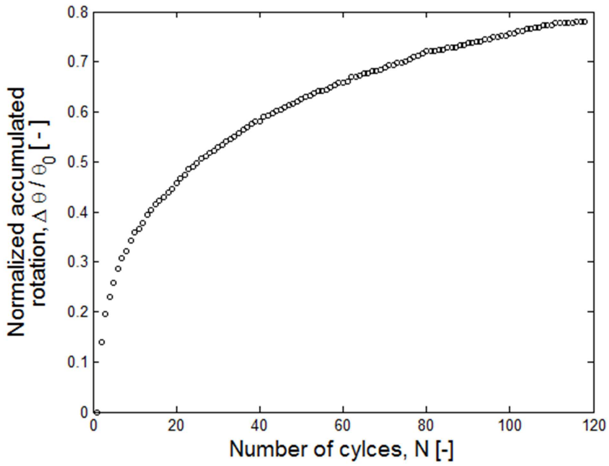

Figure 4: Test results graph – N vs. $\Delta\theta(N)$

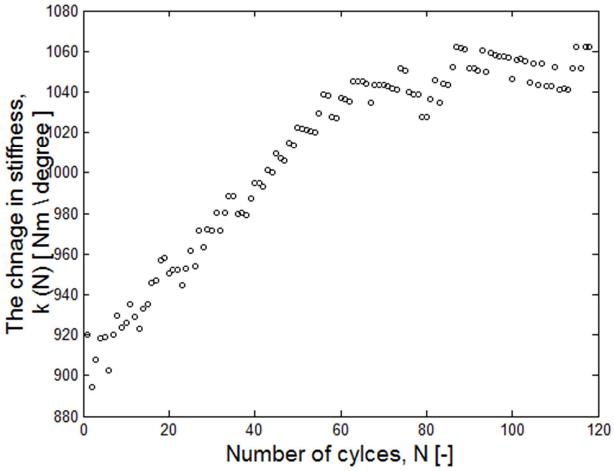

Figure 5: Test results graph – N vs. $k_{unload}(N)$

4. Parameters from LeBlanc approach:

T_b [-]	T_c [-]	n [-]	A_k [-]	K_b [-]	K_c [-]
0.425	0.400	0.327	24.972	751.74	1.224

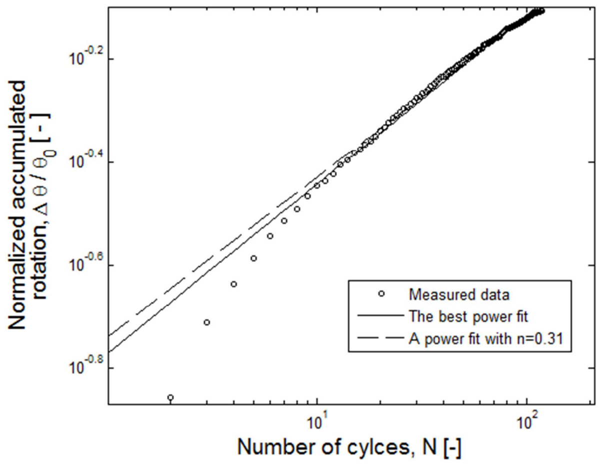

Figure 6: Fitting for $\Delta\theta(N)$

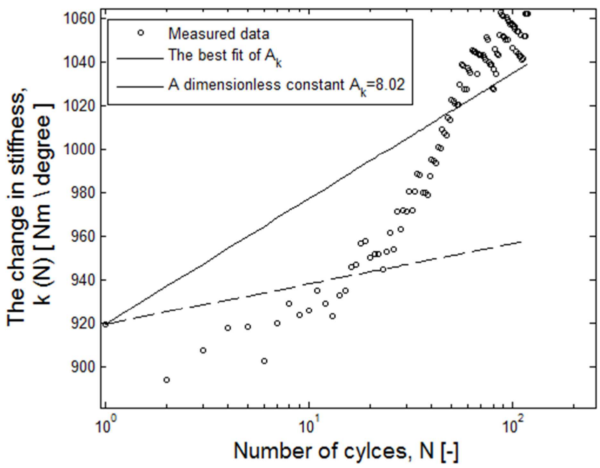

Figure 7: Fitting for $k_{unload}(N)$

Comments:

The good fit for accumulated rotation was obtained. For the stiffness it can be seen that the function fits to data for the last cycles. However, this function are intended for long-term loading, therefore there are not so relevant for 100 cycles.

5. Post-cyclic resistance:

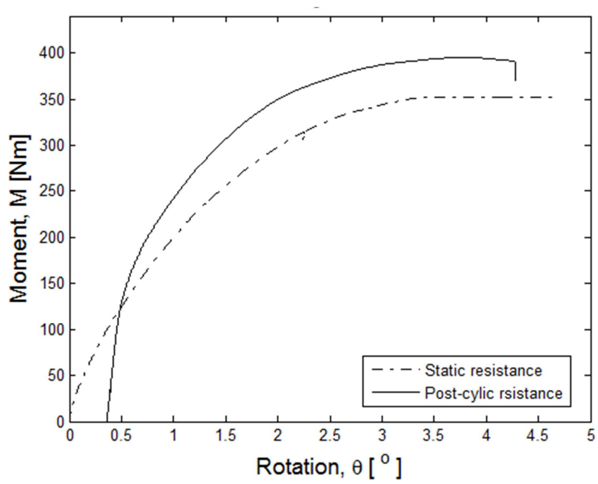

Figure 8: Ultimate soil-pile resistance

M_{PC} [Nm]	395.63
M_{PC} / M_R [-]	1.12

TEST C65

1. Test information:

Date: **17-03-2014**

Type of test: cyclic test

Mass 1		Mass 2		$\zeta_{b,\ predicted}$	$\zeta_{c,\ predicted}$	$N_{planned}$
hanger 1 [kg]	m1 [kg]	hanger 2 [kg]	m2 [kg]			
2.1	9	3.8	10	0.33	-0.14	50 000
Total mass [kg]						
11.1		13.8				

2. CPT data:

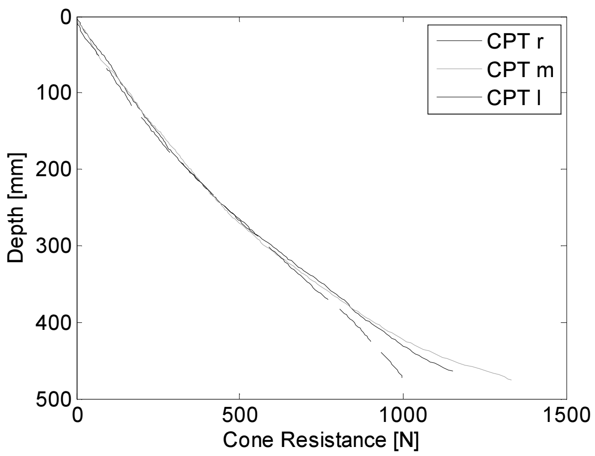

Figure 1: CPT for three localizations

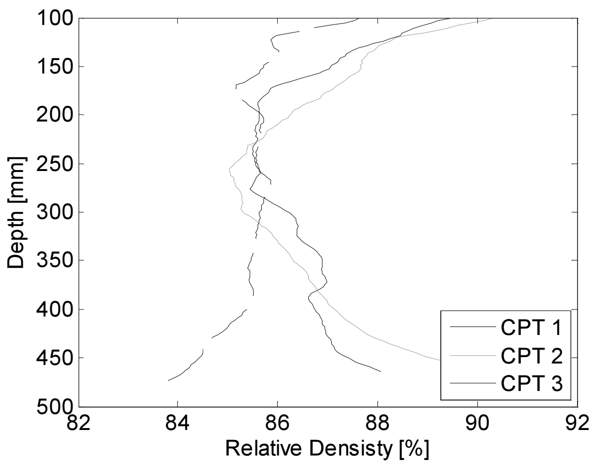

Figure 2: The relative density obtained from CPT

position	I_D [%]	φ [°]	ψ [°]	e [-]	γ' [kN/m³]
r (right)	86.59	53.81	19.64	0.664	9.67
m (middle)	86.97	53.86	19.71	0.661	9.69
l (left)	85.47	53.64	19.42	0.674	9.61
MEAN	**86.35**	**53.77**	**19.59**	**0.666**	**9.56**

3. Test results:

ζ_b [-]	ζ_c [-]	N [-]	$\Delta\theta(N)$ [°]	$k_{0,unload}$	$k_{N,load}$
0.497	0.056	2 499	1.039	357.56	668.39

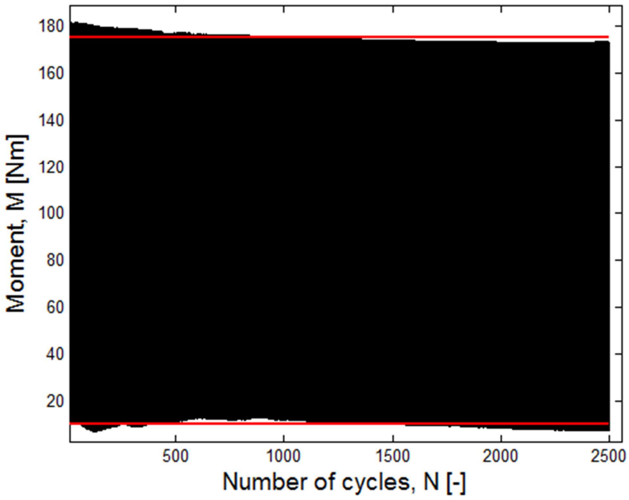

Figure 3: Test results graph – N vs. M

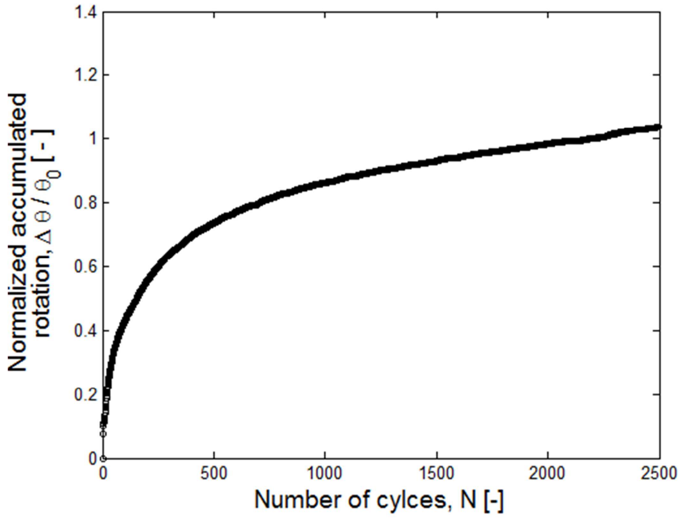

Figure 4: Test results graph – N vs. $\Delta\theta(N)$

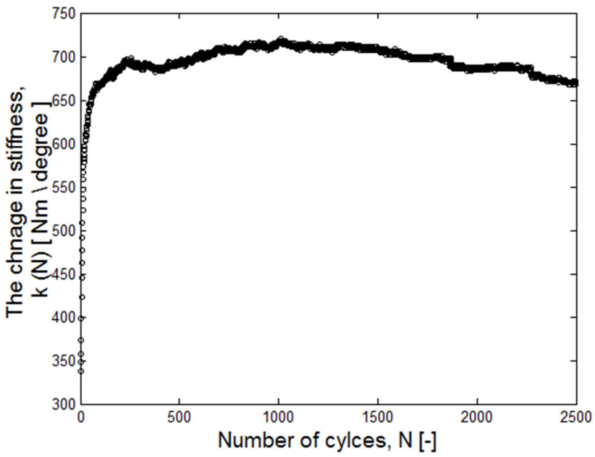

Figure 5: Test results graph – N vs. $k_{unload}(N)$

Comments:

From unknown reasons the rig was not able to perform 50 000 cycles. Test was stopped earlier. The biggest increase in accumulated rotation and the stiffness is obtained in first cycles. The small decrease can be seen for the stiffness in the last stage of cycles.

4. Parameters from LeBlanc approach:

T_b [-]	T_c [-]	n [-]	A_k [-]	K_b [-]	K_c [-]
1.037	0.150	0.244	48.472	381.076	0.938

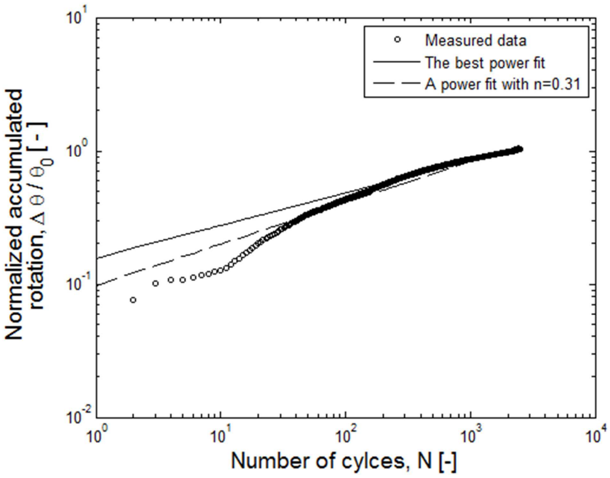

Figure 6: Fitting for $\Delta\theta(N)$

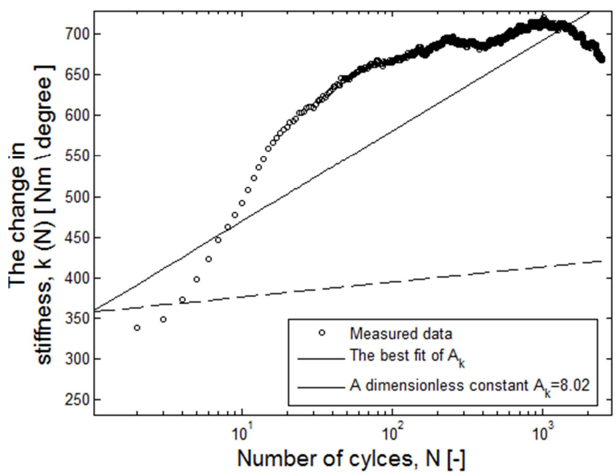

Figure 7: Fitting for $k_{unload}(N)$

Comments:

The good fit for the accumulated rotation is obtained. The fit for the stiffness is not so good.

5. Post-cyclic resistance:

A static post-cyclic test has not been performed. The rig did not performed 50 000 of cycles, so due to the time limitations the test was not performed.

TEST C66

1. Test information:

Date: **21-03-2014**

Type of test: cyclic test

Mass 1		Mass 2		$\zeta_{b,\ predicted}$	$\zeta_{c,\ predicted}$	$N_{planned}$
hanger 1 [kg]	m1 [kg]	hanger 2 [kg]	m2 [kg]			
2.1	9	3.8	10	0.33	-0.14	100
Total mass [kg]						
11.1		13.8				

2. CPT data:

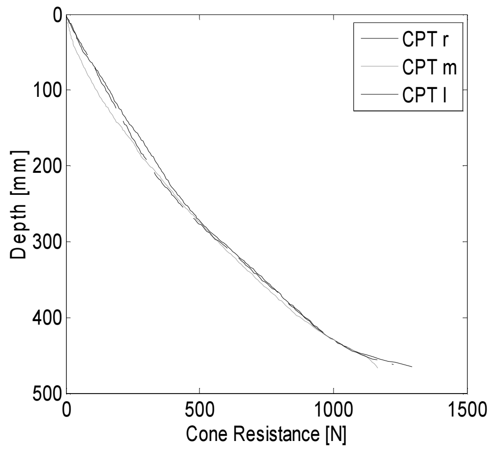

Figure 1: CPT for three localizations

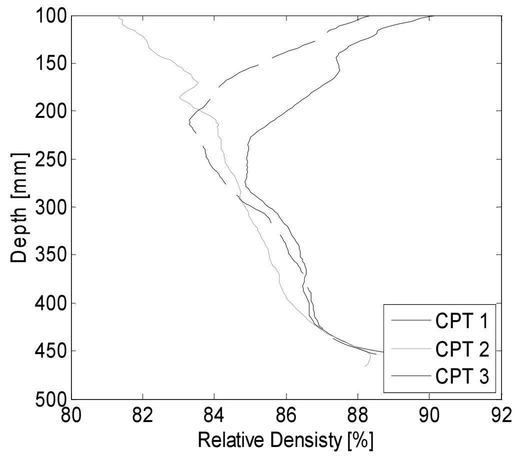

Figure 2: The relative density obtained from CPT

position	I_D [%]	φ [°]	ψ [°]	e [-]	γ' [kN/m^3]
r (right)	86.62	53.81	19.64	0.664	9.67
m (middle)	84.74	53.53	19.28	0.680	9.58
l (left)	85.61	53.66	19.45	0.673	9.62
MEAN	**85.66**	**53.66**	**19.46**	**0.672**	**9.62**

Cyclic test – C66

3. Test results:

ζ_b [-]	ζ_c [-]	N [-]	$\Delta\theta(N)$ [°]	$k_{0,unload}$	$k_{N,load}$
0.268	-0.135	101	0.619	602.978	585.163

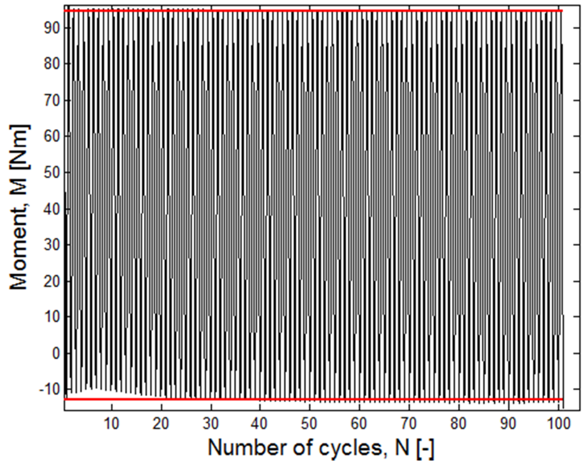

Figure 3: Test results graph – N vs. M

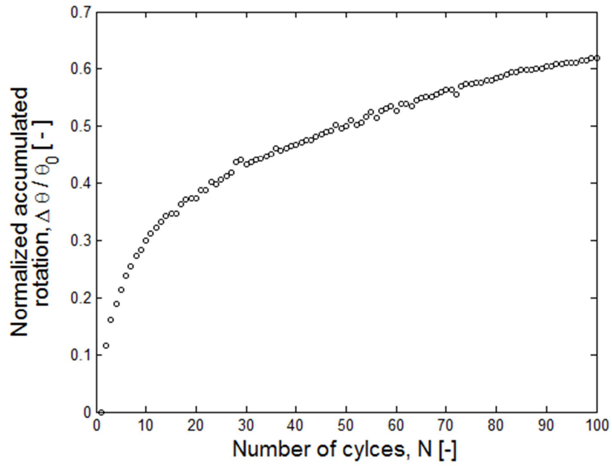

Figure 4: Test results graph – N vs. $\Delta\theta(N)$

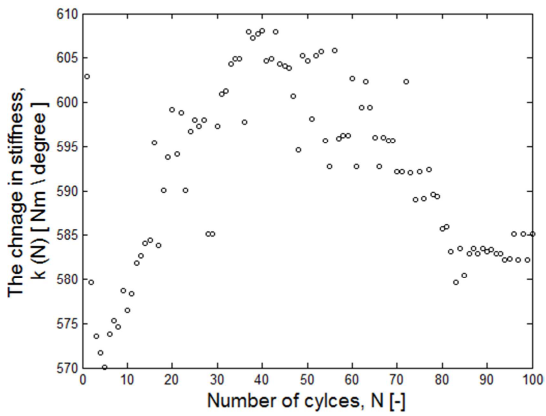

Figure 5: Test results graph – N vs. $k_{unload}(N)$

Comments:

The increasing accumulated rotation is obtained. The results of stiffness have not started to be stabilized as not enough number of cycles were applied.

4. Parameters from LeBlanc approach:

T_b [-]	T_c [-]	n [-]	A_k [-]	K_b [-]	K_c [-]
0.447	0.303	0.335	-2.674	726.952	0.829

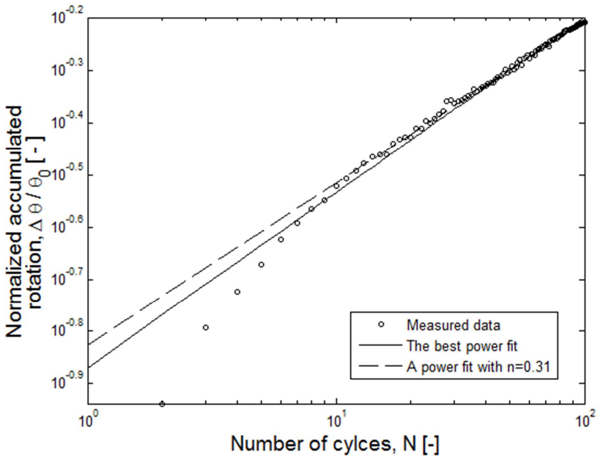

Figure 6: Fitting for $\Delta\theta(N)$

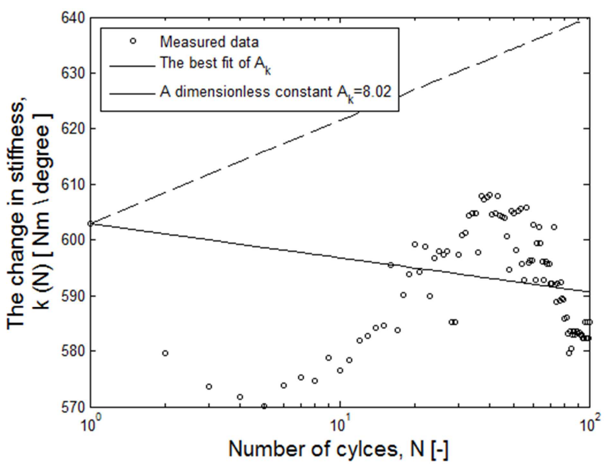

Figure 7: Fitting for $k_{unload}(N)$

Comments:

The accumulated rotation fits the function, whereas for the stiffness changes no fitting is achieved. A fitting function for the stiffness is not good.

5. Post-cyclic resistance:

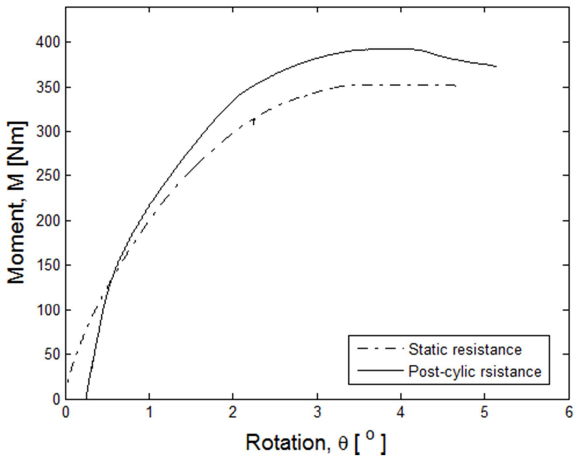

M_{PC} [Nm]	393.04
M_{PC} / M_R [-]	1.11

Figure 8: Ultimate soil-pile resistance

TEST C67

1. Test information:

Date: **27-03-2014**

Type of test: cyclic test

Mass 1		Mass 2		$\zeta_{b,\ predicted}$	$\zeta_{c,\ predicted}$	$N_{planned}$
hanger 1 [kg]	m1 [kg]	hanger 2 [kg]	m2 [kg]			
2.1	9	3.8	10	0.33	-0.14	1000
Total mass [kg]						
11.1		13.8				

2. CPT data:

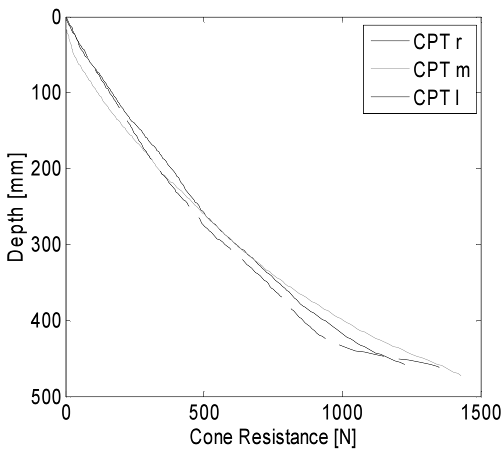

Figure 1: CPT for three localizations

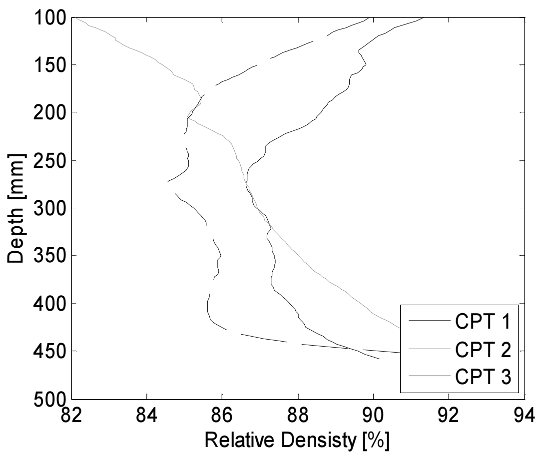

Figure 2: The relative density obtained from CPT

position	I_D [%]	φ [°]	ψ [°]	e [-]	γ' [kN/m³]
r (right)	88.17	54.05	19.95	0.651	9.75
m (middle)	87.22	53.90	19.76	0.659	9.70
l (left)	86.27	53.76	19.57	0.667	9.65
MEAN	**87.22**	**53.90**	**19.76**	**0.659**	**9.70**

3. Test results:

ζ_b [-]	ζ_c [-]	N [-]	$\Delta\theta(N)$ [°]	$k_{0,unload}$	$k_{N,load}$
0.282	-0.05	974	0.666	510.408	589.563

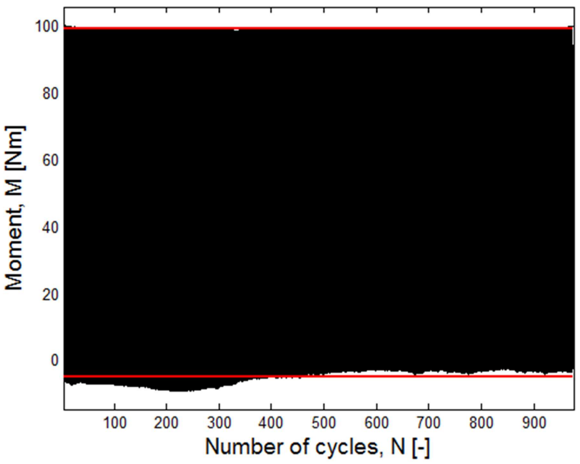

Figure 3: Test results graph – N vs. M

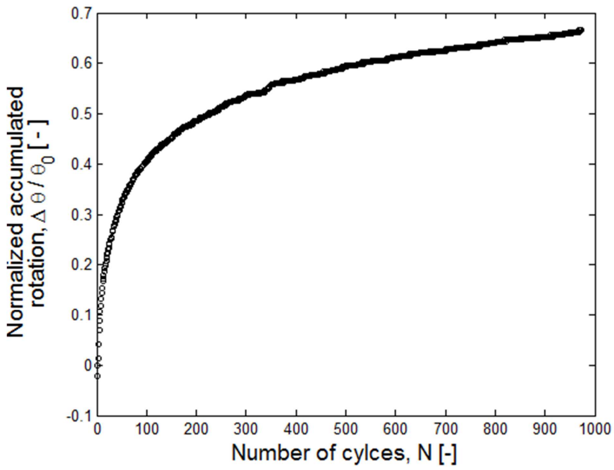

Figure 4: Test results graph – N vs. $\Delta\theta(N)$

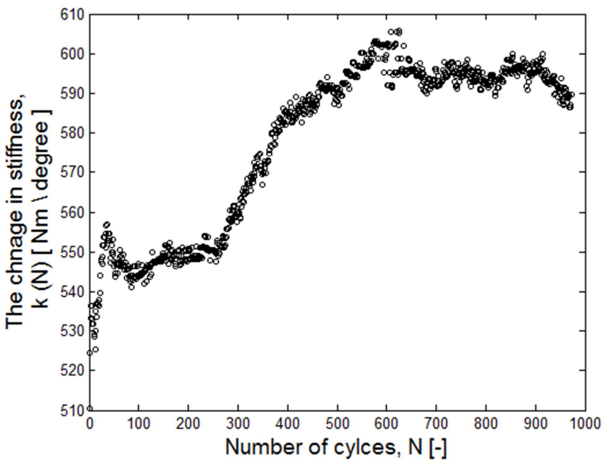

Figure 5: Test results graph – N vs. $k_{unload}(N)$

Comments:

The value of ζ_c is unexpected, as for other test with the same weights the value of ζ_c was around -0.12 - -0.13.

The most of rotation is accumulated in first couple cycles. Also the most of stiffness increase is observed for the first couple of cycles. However, there are unexpected decreases and increases in stiffness in later stage of loading.

4. Parameters from LeBlanc approach:

T_b [-]	T_c [-]	n [-]	A_k [-]	K_b [-]	K_c [-]
0.481	0.283	0.234	11.627	690.598	0.739

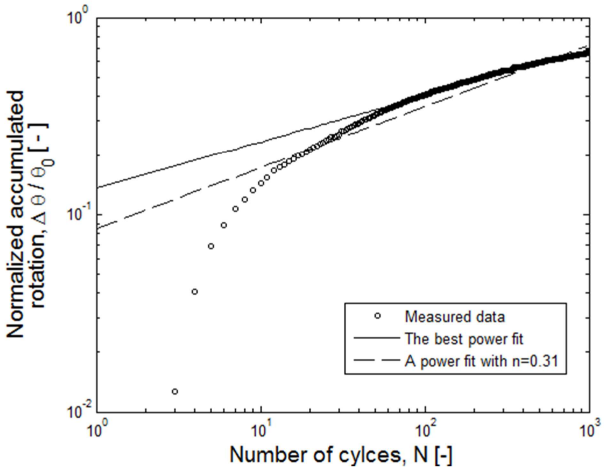

Figure 6: Fitting for $\Delta\theta(N)$

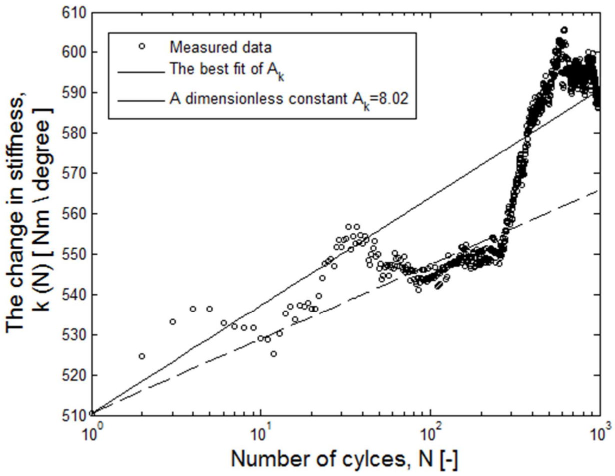

Figure 7: Fitting for $k_{unload}(N)$

Comments:

A good fit for the accumulated rotation is obtained. For the stiffness, the fit seems to follow the data in the last 200-300 cycles, therefore even a better fit would be expected if more cycles had been performed.

5. Post-cyclic resistance:

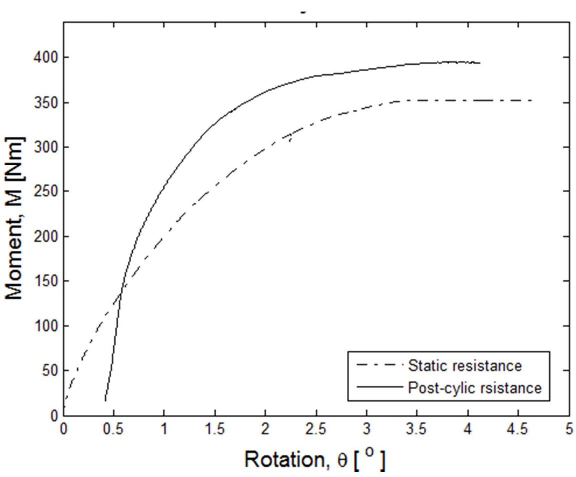

Figure 8: Ultimate soil-pile resistance

M_{PC} [Nm]	394.73
M_{PC} / M_R [-]	1.12

TEST C68

1. Test information:

Date: 07-04-2014

Type of test: cyclic test

<table>
<tr><th colspan="2">Mass 1</th><th colspan="2">Mass 2</th><th rowspan="2">$\zeta_{b,\ predicted}$</th><th rowspan="2">$\zeta_{c,\ predicted}$</th><th rowspan="2">$N_{planned}$</th></tr>
<tr><td>hanger 1 [kg]</td><td>m1 [kg]</td><td>hanger 2 [kg]</td><td>m2 [kg]</td></tr>
<tr><td>2.1</td><td>9</td><td>3.8</td><td>10</td><td rowspan="3">0.33</td><td rowspan="3">-0.14</td><td rowspan="3">10</td></tr>
<tr><td colspan="4">Total mass [kg]</td></tr>
<tr><td colspan="2">11.1</td><td colspan="2">13.8</td></tr>
</table>

2. CPT data:

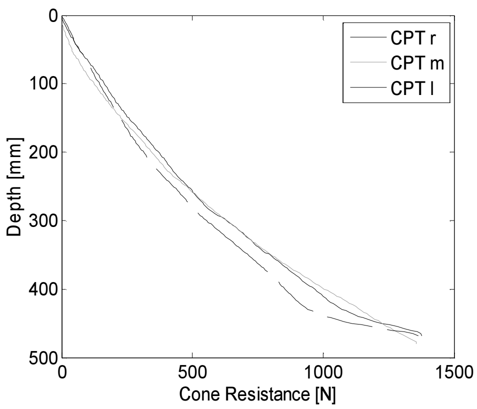

Figure 1: CPT for three localizations

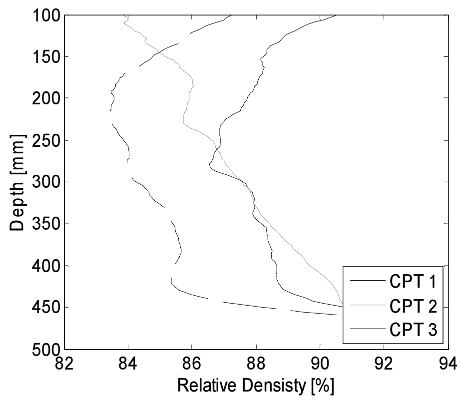

Figure 2: The relative density obtained from CPT

position	I_D [%]	φ [°]	ψ [°]	e [-]	γ' [kN/m³]
r (right)	88.30	54.06	19.97	0.649	9.75
m (middle)	87.54	53.95	19.82	0.656	9.72
l (left)	85.14	53.58	19.35	0.677	9.60
MEAN	**86.99**	**53.87**	**19.72**	**0.661**	**9.69**

3. Test results:

ζ_b [-]	ζ_c [-]	N [-]	$\Delta\theta(N)$ [°]	$k_{0,unload}$	$k_{N,load}$
0.265	-0.128	11	0.234	589.35	644.593

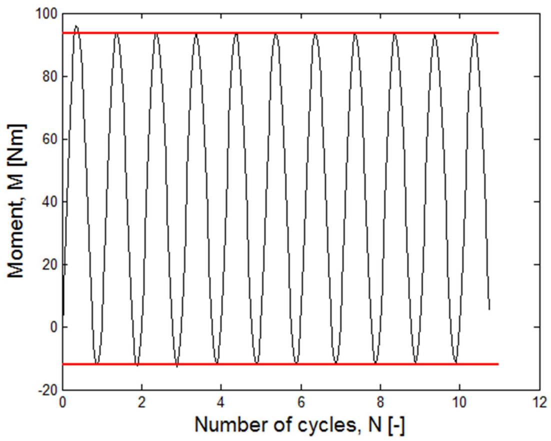

Figure 3: Test results graph – N vs. M

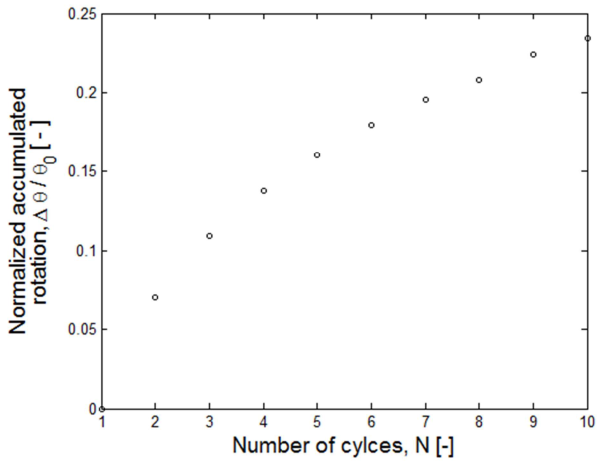

Figure 4: Test results graph – N vs. $\Delta\theta(N)$

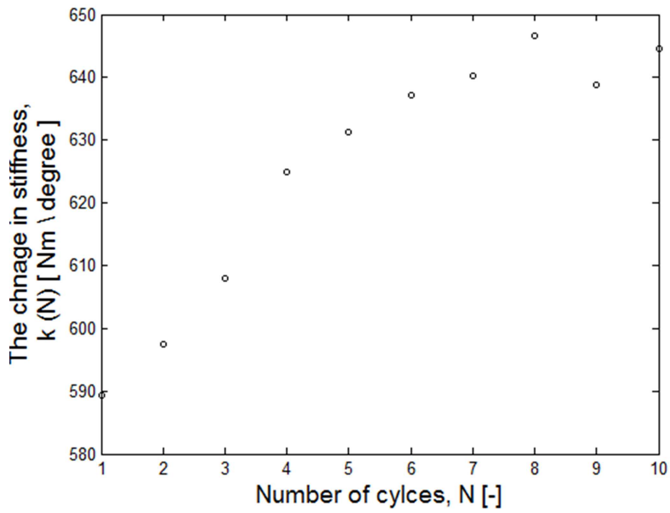

Figure 5: Test results graph – N vs. $k_{unload}(N)$

Comments:

Clearly, the rotation is accumulated the most in first cycles, as it is indicated in this test. The same conclusion can be made for the increase of the stiffness.

The fitting to the logarithmic and exponential function are not performed, as there are only few cycles and the fitting will not give any required information.

4. Post-cyclic resistance:

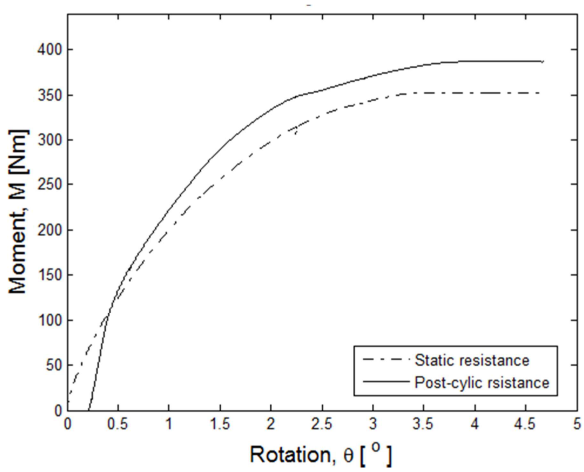

Figure 6: Ultimate soil-pile resistance

M_{PC} [Nm]	387.88
M_{PC} / M_R [-]	1.10

TEST C69

1. Test information:

Date: 10-04-2014

Type of test: cyclic test

Mass 1		Mass 2		$\zeta_{b, predicted}$	$\zeta_{c, predicted}$	$N_{planned}$
hanger 1 [kg]	m1 [kg]	hanger 2 [kg]	m2 [kg]			
2.1	9	3.8	10	0.33	-0.14	10 000
Total mass [kg]						
11.1		13.8				

2. CPT data:

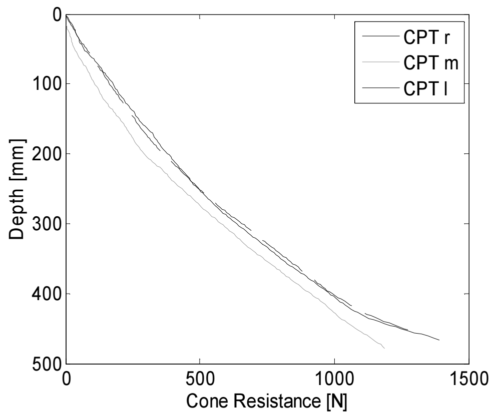

Figure 1: CPT for three localizations

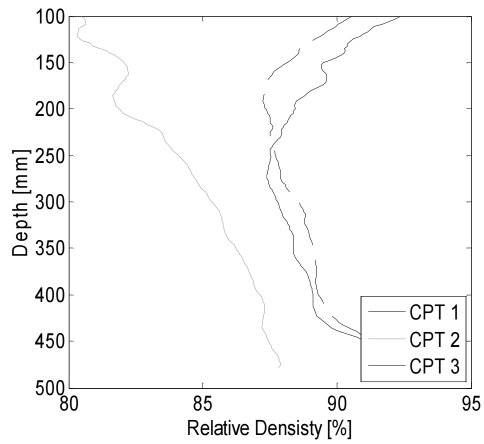

Figure 2: The relative density obtained from CPT

position	I_D [%]	φ [°]	ψ [°]	e [-]	γ' [kN/m³]
r (right)	89.02	54.17	20.11	0.643	9.79
m (middle)	84.61	53.51	19.25	0.681	9.57
l (left)	88.75	54.13	20.06	0.646	9.78
MEAN	**87.46**	**53.94**	**19.81**	**0.657**	**9.71**

3. Test results:

ζ_b [-]	ζ_c [-]	N [-]	$\Delta\theta(N)$ [°]	$k_{0,unload}$	$k_{N,load}$
0.264	-0.124	10 004	1.02	562.47	525.55

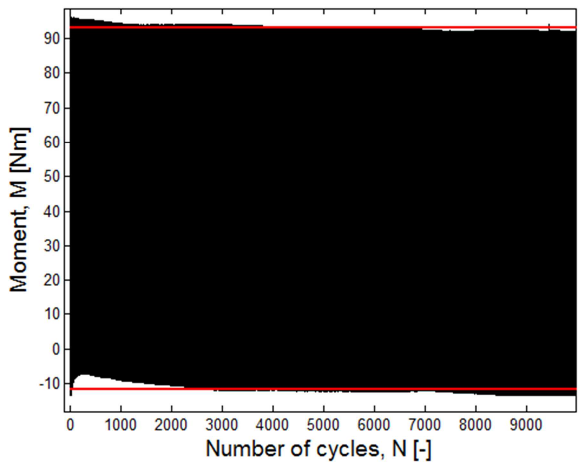

Figure 3: Test results graph – N vs. M

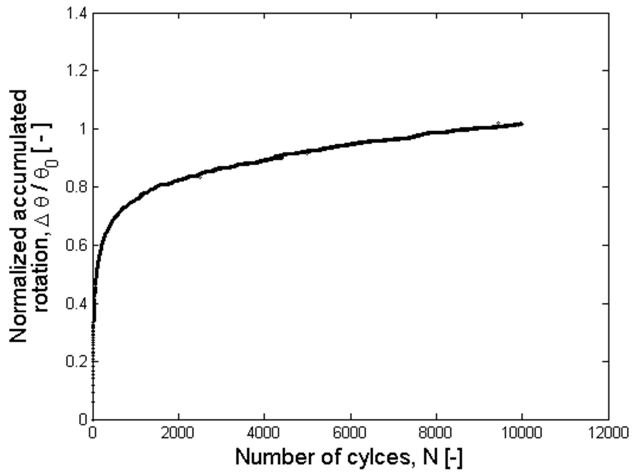

Figure 4: Test results graph – N vs. $\Delta\theta$(N)

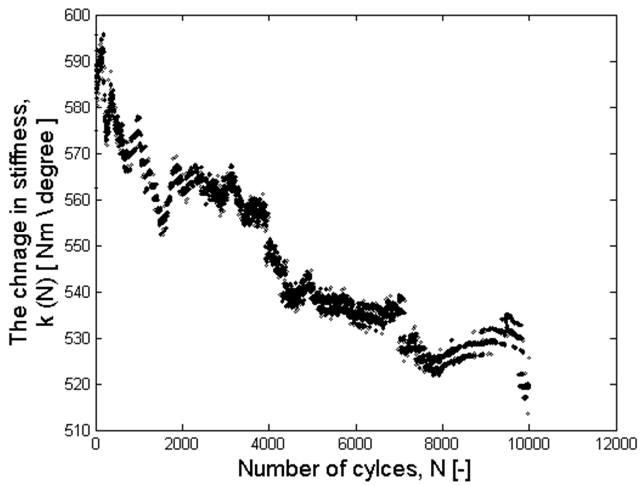

Figure 5: Test results graph – N vs. k_{unload}(N)

Comments:

Most of rotation is accumulated in first 10 cycles, when later it starts to change with a small, repetitive increment. There is only a small increase in the stiffness for its first couple cycles and after 100 cycles the stiffness starts to decrease with some fluctuations. The initial stiffness is bigger than the stiffness after 10 000 cycles.

4. Parameters from LeBlanc approach:

T_b [-]	T_c [-]	n [-]	A_k [-]	K_b [-]	K_c [-]
0.437	0.664	0.136	-2.221	737.806	0.762

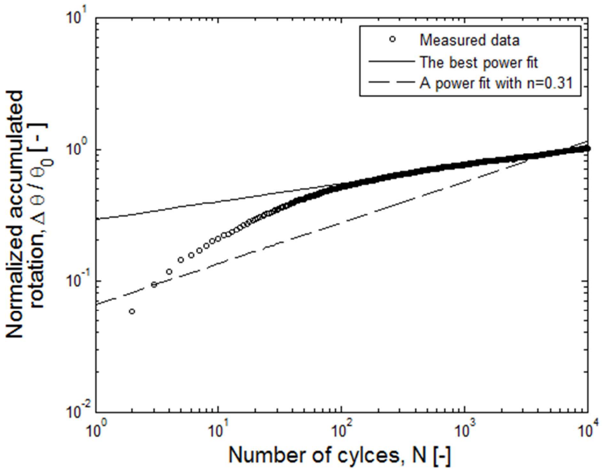

Figure 6: Fitting for Δθ(N)

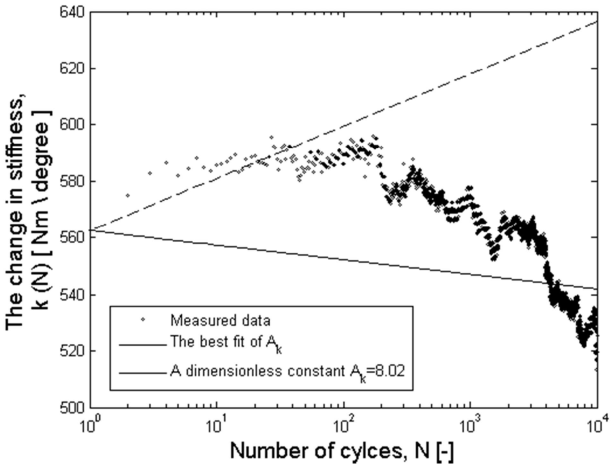

Figure 7: Fitting for k_{unload}(N)

Comments:

A good fit for the accumulated rotation is obtained. The fit for the stiffness is not in a good fit.

5. Post-cyclic resistance:

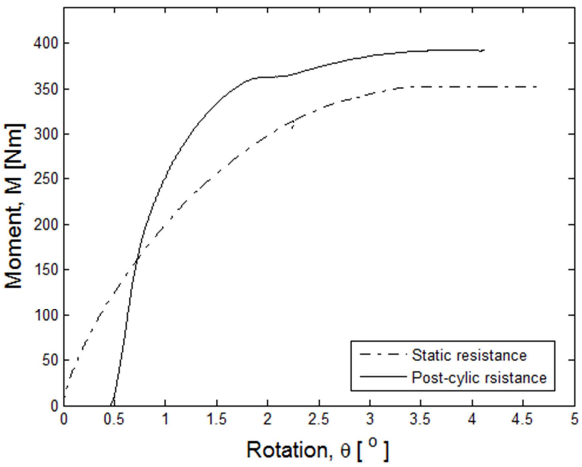

Figure 8: Ultimate soil-pile resistance

M_{PC} [Nm]	392.75
M_{PC} / M_R [-]	1.11

TEST C70

1. Test information:

Date: 07-05-2014

Type of test: cyclic test

Mass 1		Mass 2		$\zeta_{b,\ predicted}$	$\zeta_{c,\ predicted}$	$N_{planned}$
hanger 1 [kg]	m1 [kg]	hanger 2 [kg]	m2 [kg]			
2.1	9	3.8	10	0.33	-0.14	10 000
Total mass [kg]						
11.1		13.8				

2. CPT data:

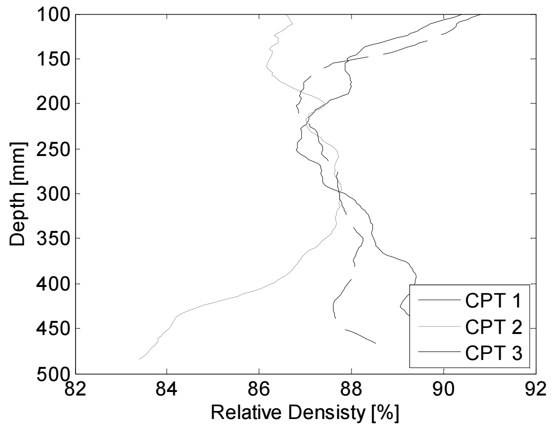

Figure 1: CPT for three localizations

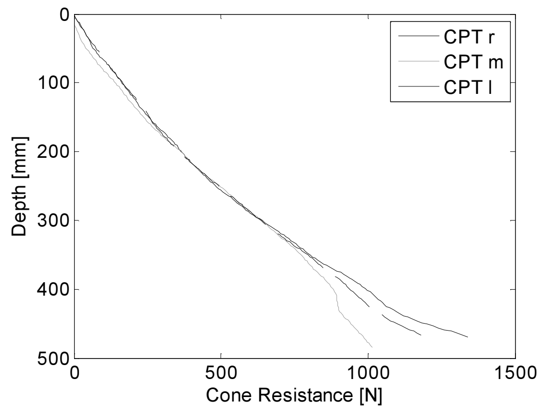

Figure 2: The relative density obtained from CPT

position	I_D [%]	φ [°]	ψ [°]	e [-]	γ' [kN/m³]
r (right)	88.42	54.08	20.00	0.648	9.76
m (middle)	86.50	53.79	19.62	0.665	9.66
l (left)	87.92	54.01	19.90	0.653	9.74
MEAN	**87.61**	**53.96**	**19.84**	**0.655**	**9.72**

3. Test results:

ζ_b [-]	ζ_c [-]	N [-]	$\Delta\theta(N)$ [°]	$k_{0,unload}$	$k_{N,load}$
0.282	-0.047	9710	1.241	516.831	537.717

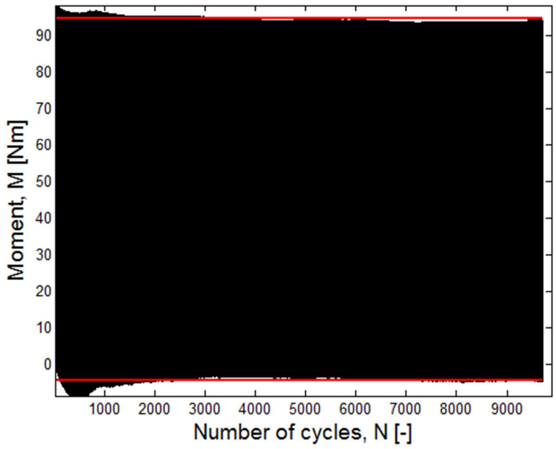

Figure 3: Test results graph – N vs. M

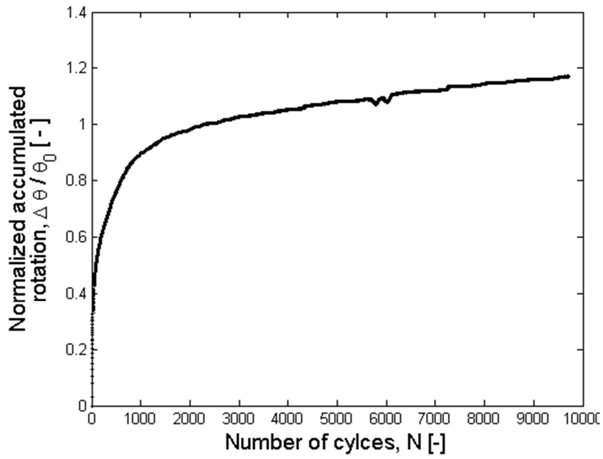

Figure 4: Test results graph – N vs. $\Delta\theta(N)$

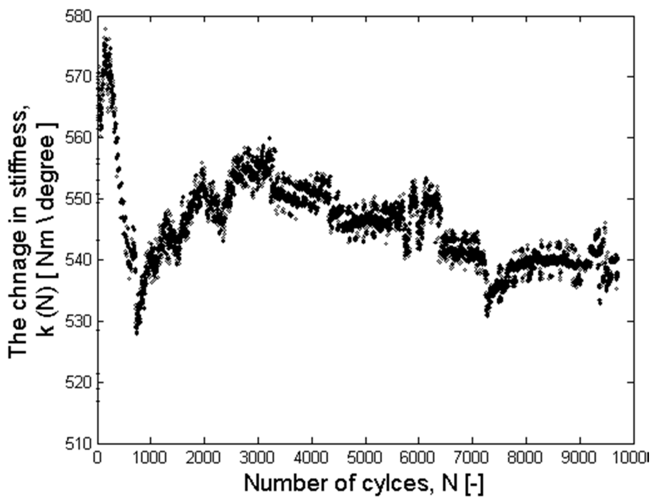

Figure 5: Test results graph – N vs. $k_{unload}(N)$

Comments:

The value of ζ_c is unexpected, as for other test with the same weights the value of ζ_c was around -0.12 - -0.13.

The most of rotation is accumulated in first couple cycles. Also the most of stiffness increase is observed for the first couple of cycles. However, for increasing number of cycles there are decreases and increases in the stiffness.

4. Parameters from LeBlanc approach:

T_b [-]	T_c [-]	n [-]	A_k [-]	K_b [-]	K_c [-]
0.446	0.813	0.136	3.434	516.831	537.717

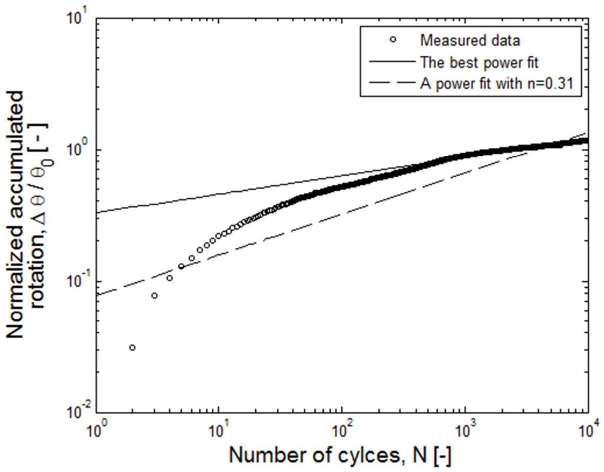

Figure 6: Fitting for $\Delta\theta(N)$

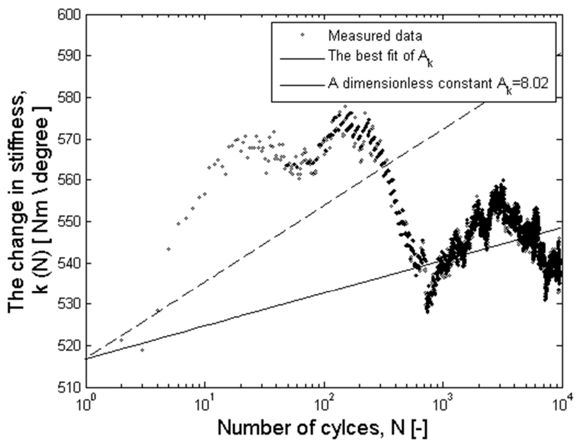

Figure 7: Fitting for $k_{unload}(N)$

Comments:

A good fit for the accumulated rotation is obtained. The fit for stiffness is not in the good fit. However, in the last stage the values are not far from the fitting function.

5. Post-cyclic resistance:

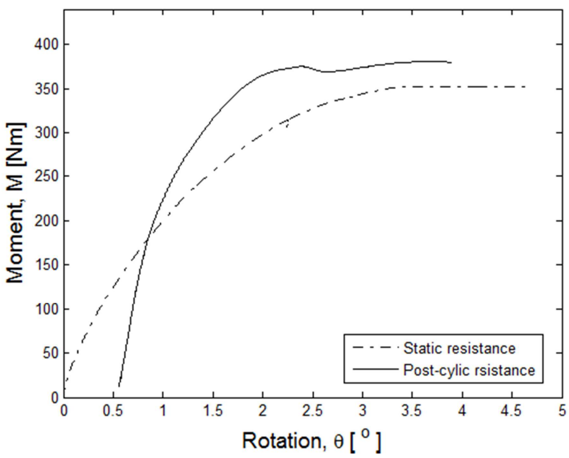

Figure 8: Ultimate soil-pile resistance

M_{PC} [Nm]	394.73
M_{PC} / M_R [-]	1.12

TEST C72

1. Test information:

Date: 14-05-2014

Type of test: cyclic test

<table>
<tr><th colspan="2">Mass 1</th><th colspan="2">Mass 2</th><th rowspan="2">$\zeta_{b, predicted}$</th><th rowspan="2">$\zeta_{c, predicted}$</th><th rowspan="2">$N_{planned}$</th></tr>
<tr><td>hanger 1 [kg]</td><td>m1 [kg]</td><td>hanger 2 [kg]</td><td>m2 [kg]</td></tr>
<tr><td>2.1</td><td>19</td><td>3.8</td><td>20</td><td rowspan="3">0.67</td><td rowspan="3">-0.07</td><td rowspan="3">50 000</td></tr>
<tr><td colspan="4">Total mass [kg]</td></tr>
<tr><td colspan="2">21.1</td><td colspan="2">23.8</td></tr>
</table>

2. CPT data:

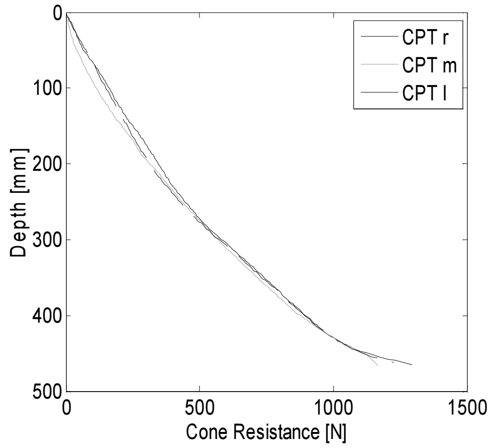

Figure 1: CPT for three localizations

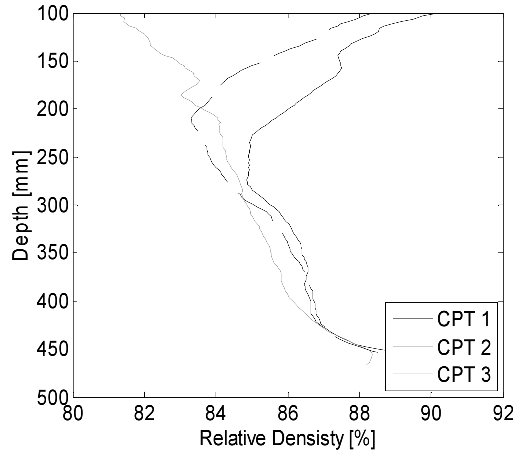

Figure 2: The relative density obtained from CPT

position	I_D [%]	φ [°]	ψ [°]	e [-]	γ' [kN/m³]
r (right)	86.62	53.81	19.64	0.664	9.67
m (middle)	84.74	53.53	19.28	0.680	9.58
l (left)	85.61	53.66	19.45	0.673	9.62
MEAN	**85.66**	**53.66**	**19.46**	**0.672**	**9.62**

Cyclic test – C72

3. Test results:

ζ_b [-]	ζ_c [-]	N [-]	$\Delta\theta(N) / \theta_s$ [°]	$k_{0,unload}$	$k_{N,load}$
0.514	-0.11	8 049	1.995	470.918	473.289

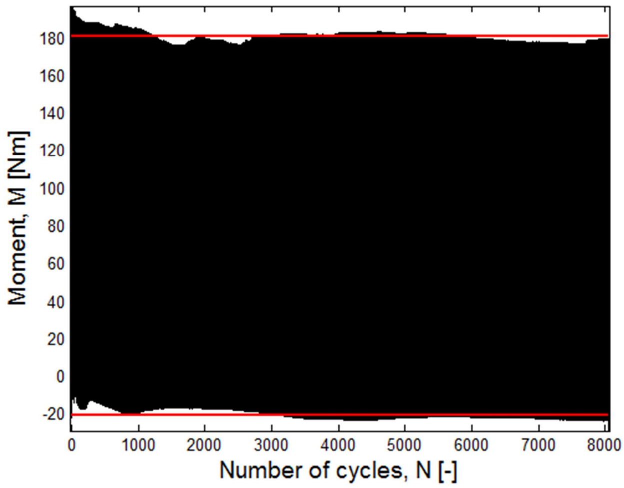

Figure 3: Test results graph – N vs. M

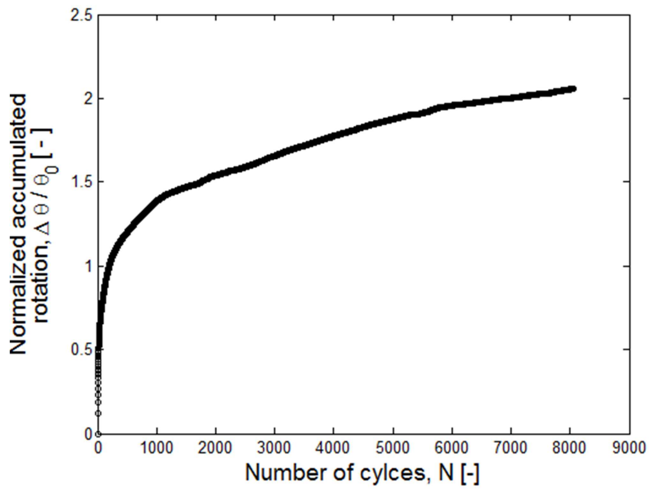

Figure 4: Test results graph – N vs. $\Delta\theta(N)/ \theta_s$

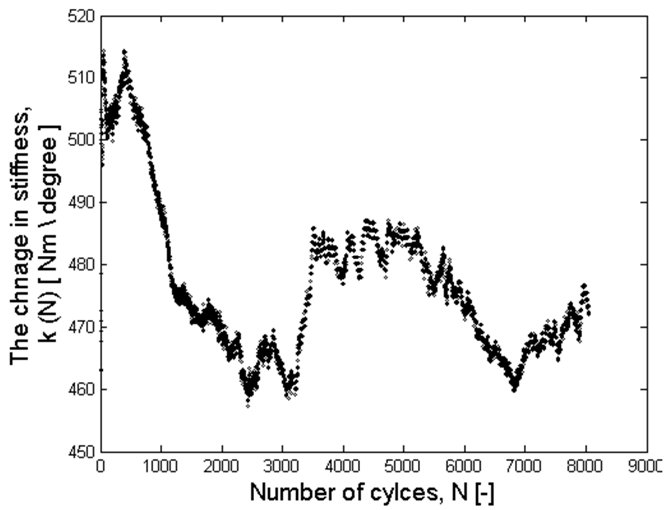

Figure 5: Test results graph – N vs. $k_{unload}(N)$

Comments:

Most of rotation is accumulated in first 10 cycles, when later it increases with a small, repetitive increment. The stiffness increases the most in first 10 cycles. After reaching the maximum value the results of stiffness are increasing and decreasing.

4. Parameters from LeBlanc approach:

T_b [-]	T_c [-]	n [-]	A_k [-]	K_b [-]	K_c [-]
1.079	0.294	0.204	0.606	368.379	1.278

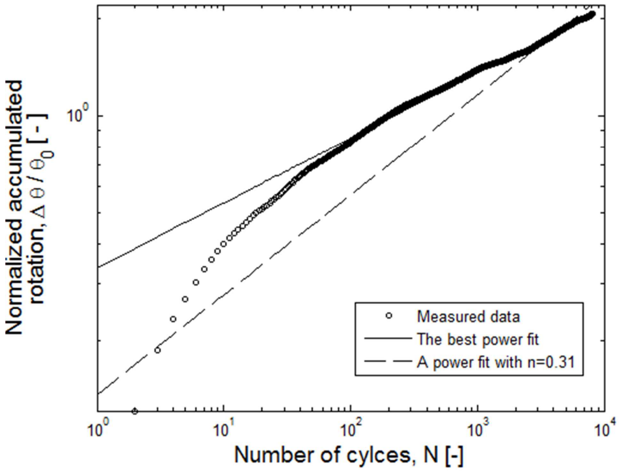

Figure 6: Fitting for Δθ(N)

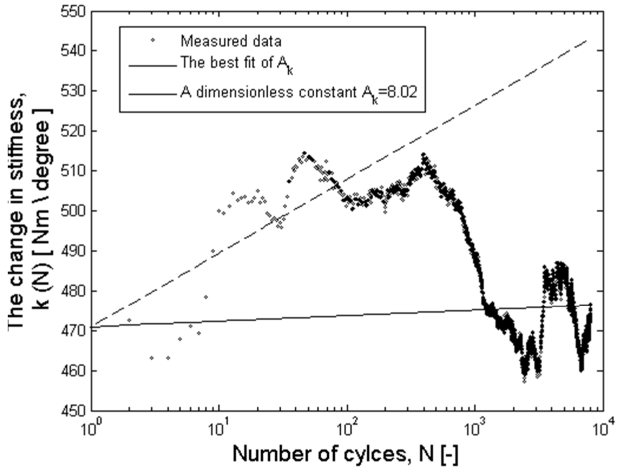

Figure 7: Fitting for k_{unload}(N)

Comments:

A good fit for the accumulated rotation results is obtained. The fit for the stiffness change is not so good, however in the last stage it starts to fluctuate around the fitting function. For more number of cycles the better fit could be obtained.

5. Post-cyclic resistance:

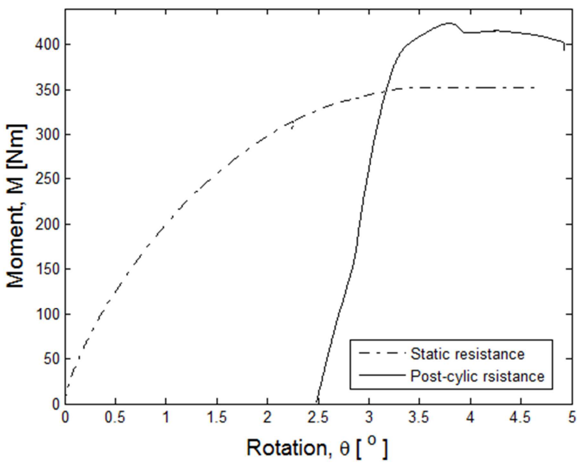

Figure 8: Ultimate soil-pile resistance

M_{PC} [Nm]	423.55
M_{PC} / M_R [-]	1.20

PLAXIS model E

Numerical calculation are done with the use of the geotechnical program PLAXIS 3D. The program has a wide range of applications, which can be used to solve different geotechnical problems. Number of simulations are performed in order to assess the following issues:

- A different pattern of the behavior for a slender and a stiff pile
- Assessment of the ultimate soil resistance
- The effects of the pile diameter and the pile length on the soil resistance
- The effects of the load eccentricity on the soil resistance

The program is not able to simulate the cyclic loading conditions. However, the results are used to assess the ULS and SLS due to mentioned differences between simulations.

Plaxis offers a number of different models that can be used to simulate the soil behaviour. The simplest model, linear elastic perfectly plastic - Mohr Coulomb model, gives the fastest response, but the limited number of parameters that are required provide only a decent approximation. More advanced model requires more soil parameters. They require more computational time and power, but the response is a much better reconstruction of the real soil behaviour.

Soil Hardening Small Strain model

In order to simulate the behaviour of monopile subjected to lateral load it is chosen to use a Soil Hardening Small Strain model. The basis for the model are taken from less advanced model - Soil Hardening. The main characteristic of a hardening plasticity is the expanding yield surface due to the plastic strains.

In the model both type of hardening, the shear hardening and the compression hardening, are used. The shear hardening models the plastic strains resulting from deviatoric loading and the compression hardening models plastic strains resulting from compression in oedometer loading and isotropic loading.
The relationship between the axial strain and the deviatoric stress is modelled as a hyperbolic dependency, based on already existing hyperbolic model (Ducan & Chang, 1970). However, some changes are introduced: theory of plasticity is used rather than theory of elasticity, soil dilatancy is included and the yield cap is introduced [Brinkgreve et al., 2012]. For the dilatancy the cut-off option can be included, so when the maximum void ratio, e_{max}, is exceeded, the dilatancy angle, ψ, is set back to zero. The yield cap is introduced in order to limit the elastic region for compression.

The plastic strain from primary deviatoric loading are controlled by the secant stiffness from standard drained triaxial tests, E_{50}, and the plastic strain from compression are controlled by the tangent stiffness for primary oedometer loading, E_{oed}. Additionally the unloading/ reloading behaviour is controlled by the unloading/reloading stiffness, E_{ur}.
The most important for the analysis is the stress dependency on the stiffness moduli, which is maintained by the power parameter, m. For Norwegian sands and silts this value was reported to be 0.5 (Janbu, 1963). The increase of the stiffness is noted with increasing pressure. [Brinkgreve et al., 2012]

The graphic representation of yield surfaces of Hardening Soil model are presented in Figure E.1 (a) in p-q plane (isotropic stress vs. deviatoric stresses) and (b) in prinipal stress space.

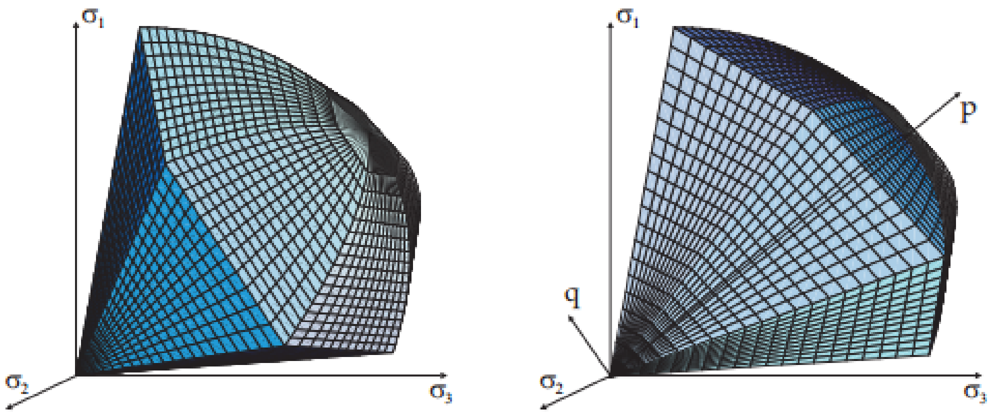

Figure E.1. Yield surfaces for Hardening soil model. Left: in principal stress space. Rigth: in p-q plane [Benz, 2007]

The relations between the reference value and the normal stiffness are given in following equations:

$$E_{50} = E_{50}^{ref} \cdot \left(\frac{c \cdot cos\varphi - \sigma_3' \cdot sin\varphi}{c \cdot cos\varphi + p^{ref} \cdot sin\varphi} \right)^m \tag{E.1}$$

$$E_{ur} = E_{ur}^{ref} \cdot \left(\frac{c \cdot cos\varphi - \sigma_3' \cdot sin\varphi}{c \cdot cos\varphi + p^{ref} \cdot sin\varphi} \right)^m \tag{E.2}$$

$$E_{oed} = E_{oed}^{ref} \cdot \left(\frac{c \cdot cos\varphi - \frac{\sigma_3'}{K_0^{nc}} \cdot sin\varphi}{c \cdot cos\varphi + p^{ref} \cdot sin\varphi} \right)^m \tag{E.3}$$

(E.4)

where:

c	(Effective) cohesion [kN/m^2]
φ	(Effective) angle of internal friction [°]
p^{ref}	The reference confining pressure (default $p^{ref} = 100$) [kPa]
σ_3'	The minor principal effective stress (negative for compression) [kPa]

The rests of parameters required for a model (the default values are recommended to be used):

ν_{ur}	Poisson's ratio for unloading-reloading (default ν_{ur}=0.2) [-]
K_0^{nc}	K_0-value for normal consolidation (default $K_0^{nc} = 1 - sin\varphi$)[-]
$\sigma_{tension}$	Tensile strength (default $\sigma_{tension} = 0$) [kN/m^2]

In the Soil Hardening with Small Strain model the non-linear decrease of stiffness for increasing strains is additionally introduced. Due to the stiffness decay, two additional parameters that control this dependency are introduced:

G_0	The initial or very small-strain shear modulus [kPa]
$\gamma_{0.7}$	The shear strain level at which the secant shear modulus, G_s, is reduced to about 70% of G_0 [-]

In both hardening models the stiffness reduction takes place due to the plastic strains. However, in more basic model the decrease is linear, whereas the decrease for more advanced model is presented in Figure E.2. The values from model are presented, accompanied with the Hardin-Drnevich relationship as the basis for this assumption. The reduction is limited by a cut-off value of shear strain due to the limits of yield surfaces. [Brinkgreve et al., 2012]

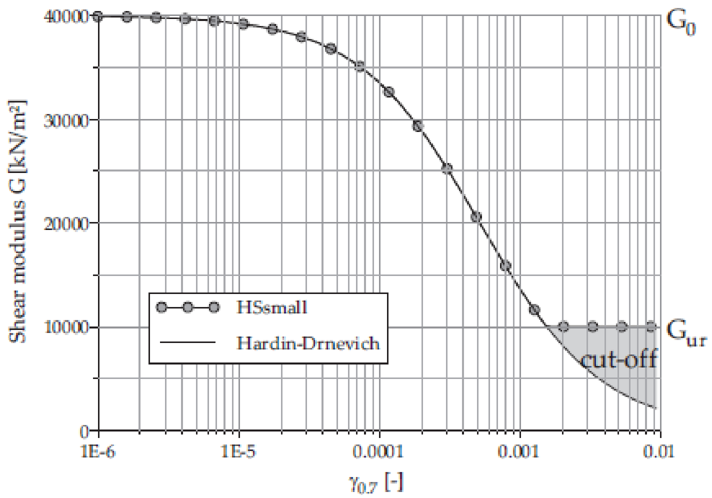

Figure E.2. The small-strain degradation curve used in Hardening Soil with Small Strain model Brinkgreve et al. [2012]

The reference value of the initial shear stiffness is obtained from equation (E.5).

$$G_0 = G_0^{ref} \cdot \left(\frac{c \cdot cos\varphi - \sigma_3' \cdot sin\varphi}{c \cdot cos\varphi + p^{ref} \cdot sin\varphi} \right)^m \qquad \text{(E.5)}$$

If the initial void ratio, e, is known, the reference initial shear stiffness can be obtained from relation given by Hardin & Black (1969), equation (E.6). The shear strain level $\gamma_{0.7}$ is obtained from equation (E.7). Both equations are recommended by [Brinkgreve et al., 2012].

$$G_0^{ref} = 33 \cdot \frac{(2.97-e)^2}{1+e} \quad \text{[MPa]} \tag{E.6}$$

$$\gamma_{0.7} = \frac{1}{9G_0} \cdot \left[2c' \cdot (1+cos(2\varphi')) - \sigma_1' \cdot (1+K_0) \cdot sin(2\varphi')\right] \tag{E.7}$$

where:

K_0	The coefficient of lateral earth pressure at rest [-]
σ_1'	The effective vertical stress [kPa]

Soil parameters

Advanced model requires a number of soil parameters that need to be calculated for a given sand state. Three states of sand are considered: dense sand, medium sand and loose sand. They are characterized by the relative density, I_D, of 85% , 40% and 5% respectively. The pre-defined sand properties of Aalborg University Sand no.1 are used, see Table C.1 on page 81. The soil unit weight is obtained with equation (C.1) at the page 82.
The values of stiffness parameters are obtained from the back calculations of the cone resistance. [Lunne et al., 2007], [Kulhawy and Mayne, 1990]

At first equation (E.8) is used in order to obtain the data for the cone resistance for each sand state.

$$I_D = \frac{1}{2.96} ln \left[\frac{\frac{q_c}{p_a}}{24.94 \cdot \left(\frac{\sigma_{v0}' \cdot \left(\frac{1+2\cdot K_0}{3}\right)}{p_a} \right)^{0.46}} \right] \tag{E.8}$$

where

q_c	The cone resistance [kPa]
p_a	The atmospheric pressure ($p_a = 100$) [kPa]
σ_{v0}'	The vertical effective stress [kPa]
K_0	The coefficient of earth pressure at rest [-]

The friction angle for each sand state is obtained from equation (E.9).

$$\varphi' = 17.6 + 11 \cdot log \left(\frac{\frac{q_t}{p_a}}{\left(\frac{\sigma_{v0}'}{p_a}\right)^{0.5}} \right) \tag{E.9}$$

The total cone resistance, q_t, for calculations is chosen to be equal to q_c.

In order to obtain the value of K_0 it is required to investigate the sand consolidation. The overconsolidation ratio, OCR, can be calculated from equation (E.10). The post consolidated soil stress, σ_{pc}, can be obtained from equation (E.11).

$$OCR = \frac{\sigma_{pc}}{\sigma'_{v0}} \tag{E.10}$$

$$\sigma_{pc} = 0.33 \cdot (q_t - \sigma_{v0})^{0.72} \tag{E.11}$$

In this equation σ_{v0} stands for the vertical normal stress. The mean OCR is found when the first 5 m of depth is disregarded. When OCR exceeds 1, the sand is considered to be overconsolidated. The value of K_0 is obtained from equation (E.12) for normally consolidated sand and from equation (E.13) for overconsolidated sand.

$$K_{0nc} = 1 - sin\varphi \tag{E.12}$$

$$K_0 = K_{0nc} \cdot OCR^{\alpha} \tag{E.13}$$

$$\alpha = sin\varphi \tag{E.14}$$

The sand is considered to be cohesionless. However, zero cohesion in PLAXIS leads to the numerical errors. Therefore c' is set to be 0.1 kPa.

The results of cone resistance are used in calculations of the oedometer stiffness: equation (E.15) for normally consolidated sand and equation (E.16) for overconsolidated sand.

$$E_{oed} = q_c \cdot 10^{1.09-0.0075 \cdot I_D} \tag{E.15}$$

$$E_{oed} = q_c \cdot 10^{1.78-0.0122 \cdot I_D} \tag{E.16}$$

where I_D is in %.

The two others required stiffness can be obtained from the following equations:

$$E_{50} = E_{oed} \cdot \frac{1 - \nu - 2\nu^2}{1 - \nu} \tag{E.17}$$

$$E_{ur} = 3 \cdot E_{50} \tag{E.18}$$

The Poisson's ratio, ν, is calculated from equation (E.19).

$$\nu = \frac{1 - sin\varphi}{2 - sin\varphi} \tag{E.19}$$

The shear modulus obtained from equation (E.20) is set as the initial shear stiffness.

$$G = 1634 \cdot q_c^{0.25} \cdot \sigma_{v0}'^{0.375} \tag{E.20}$$

The reference values of modulus are chosen as the values corresponded to the effective vertical stress of 100 kPa. In some cases the program does not accept the given parameters and recommends to change some of the values for a given proposition. In such cases, the proposed parameters are used.

The monopile model

The monopile is designed in plaxis as a circular tube with applied plate. The pile is extended, so that the load can be applied on the arm, providing the desire moment on the seabed. At the top the tube is closed with a plate, so that the vertical load can be applied as a surface load. A steel material of characteristics presented in Table E.1 is chosen for a monopile representation. For the extended part, the material of a small unit weight and a large stiffness is chosen, so that the additional part will not effect the soil-pile interaction.

Table E.1. Properties of materials

	γ $[kN/m^3]$	E $[GPa]$	ν $[-]$	t $[m]$
Pile	77.09	210	0.3	0.06
Extension	1	10e9	0.3	0.06

As the main model the monopile with diameter $D = 5$ m and embedded length $L = 25$ m is chosen. In order to inspect the soil-pile ultimate resistance different pile geometries are used. The main model of the pile is presented in Figure E.3, where the pile is marked in dark blue color and the extension in light blue.

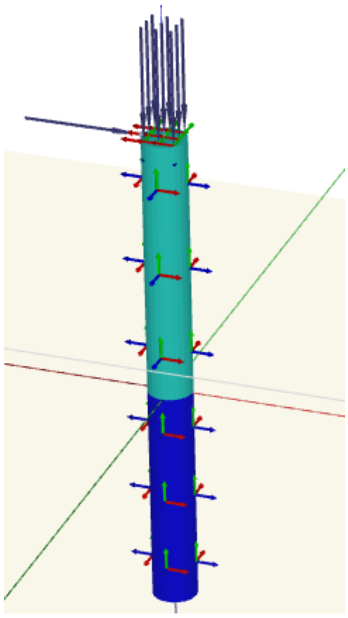

Figure E.3. The monopile model in plaxis

Between the structure and the surrounding soil the interface is created. The interface has the soil properties, however, they are reduced by the chosen factor, R_{inter}. For cohesionless soil this factor can be obtained based on the friction angle and the angle of soil friction on the pile wall, δ. [DNV, 1992] proposes value of $\delta = 30°$, $\delta = 25°$ and $\delta = 20°$ for dense, medium dense and loose sand respectively.

The factor can be then obtained from equation (E.21).

$$R_{inter} = \frac{tan\delta}{tan\varphi} \tag{E.21}$$

Model boundaries and mesh

The boundaries of the model must be chosen correctly, so the results will not be influenced by them. On the other hand, the bigger is the model, the more time-consuming are the calculations. The first guess on the boundary was made from recommendations of Abbas et al. [2008]. The width and the length of model was set to be $40D$, where D is a pile diameter and the depth of model was set to be $L+20D$, where L is the embedded length of the pile. The boundaries were decreased in order to reduce the calculation time. However, the differences in the results were significant, indicating that the boundaries have some effects on the stress state. Therefore, the first chosen dimensions are used for all simulations. Not only the appropriate boundaries of model, but also the element type and sufficient mesh provide an adequate condition for a finite element analysis. In PLAXIS the types of elements are prescribed, so there is no option for choosing them. For using model there are three different elements used: the soil elements, the plate elements and the interface elements. [Brinkgreve et al., 2012]

The soil is discretized into 10-noded tetrahedral elements. The 3D elements consists of 4 Gauss points for stress/strain calculations. Each node has three degrees of freedom, which are related to translation in three direction (u_x, u_y and u_z). The quadratic shape functions are used.

The plate is discretized into 2D triangular elements with 6 nodes and with 3 Gauss points. The linear shape functions simulate the plate behaviour. Each node has 6 degree of freedom, where apart of translation, also the rotation is included (ϕ_x, ϕ_y and ϕ_z).

The interface joint the soil with the plate and therefore, it is discretized into elements that have pairs of nodes instead of single nodes. The distance between two nodes in pair is equal to zero. However, each node has 3 degrees of freedom, so differential displacement between the two nodes in pair is possible. Each element has 3 Gauss points.

The soil element and the plate element are presented in Figure E.4.

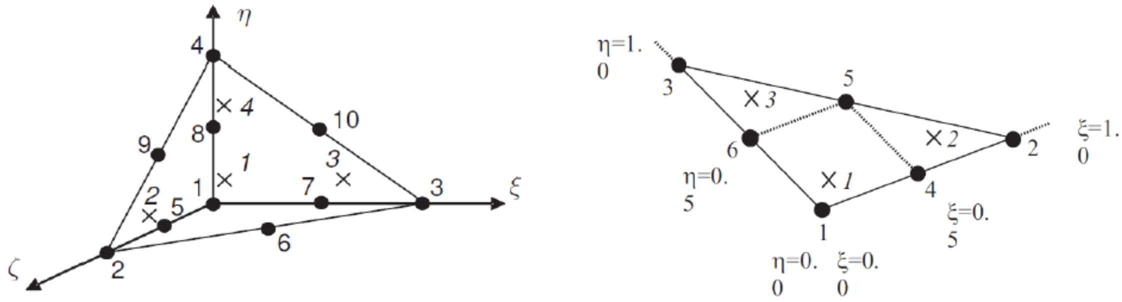

Figure E.4. The soil element (on the left) and the plate element (on the left), with nodes and Gauss points [Brinkgreve et al., 2012]

The mesh in PLAXIS can be controlled by choosing the overall mesh and also by choosing the FinenessFactor for each part of model: soil volume or plate. The FinenessFactor set to 0.5 reduces the size of the elements for a half. The ovearll mesh can be very coarse, coarse, medium, fine and very fine, where each has set the relative element size factor. The overall mesh is chosen as a coarse, as the results far from pile are not considered in the ULS calculations. The soil near the pile is refined. Due to that two soil volumes are extracted for refining, see Figure E.5. The soil situated the closest to the pile is always more refined that the soil situated little bit further.

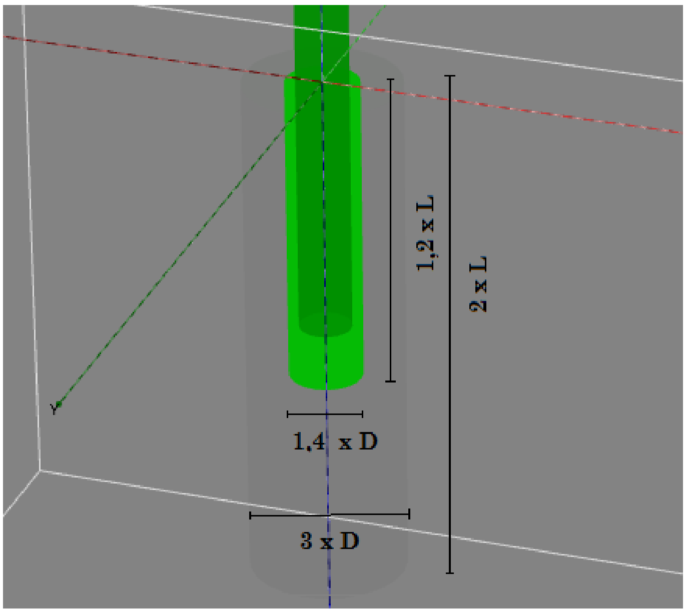

Figure E.5. Chosen soil volumes for refining

The convergence analysis was performed on the main model, so that the sufficient mesh can be chosen for further simulations. After setting the mesh, the same horizontal load is applied and the rotation on the seabed is analyzed. The results can be seen in Figure E.6.

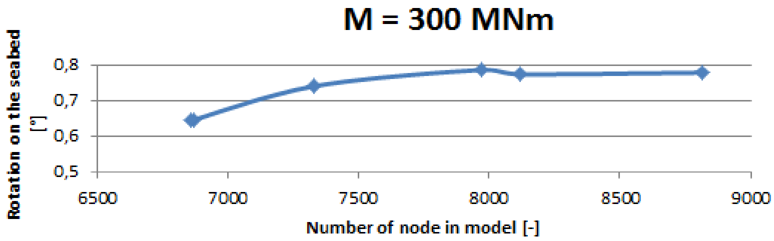

Figure E.6. The covergence analysis for a model

As the results stop changing significantly for models consisting more than 10 000 nodes, it is considered sufficient for the analysis to choose the model with 12 570 nodes. The FinenessFactor for the model are as following:

- FinenessFactor = 0.25 for the plate creating monopile
- FinenessFactor = 0.3536 for the soil volume 1 (closer to the pile)
- FinenessFactor = 0.25 for the soil volume 2

The choice of model boundaries and mesh is made for the dense sand. The decreased friction angle makes the soil weaker, so that the ultimate state will be reached faster, resulting in smaller stresses. Therefore, it is considered that model and mesh is sufficient also for two others sand conditions.

Loading phases

The ULS of sand is analyzed by checking the rotation of the pile on the seabed . The rotation of 4° is set to determine the soil failure. In order to follow the increasing number of loading steps, the calculations point on the pile are chosen, Figure E.7.

The loading phases used in PLAXIS are as following:

- Initial phase: using K_0 procedure the initial soil stresses are found,
- Nil-step phase: without any activations of plates in order to achieve the equilibrium of the soil stress,
- Construction phase: the plates and interfaces are activated in order to simulate the pile installation,
- Loading phase 1: the vertical load on the tower surface is applied to simulate the self-weight of the wind turbine
- Loading phase 2 - final phase: the horizontal load on a given arm is applied to simulate the moment on the seabed coming from the wave and the wind

For all the phases apart of the initial one a plastic calculations are chosen, so that the elasto-plastic deformation analysis can be obtained.

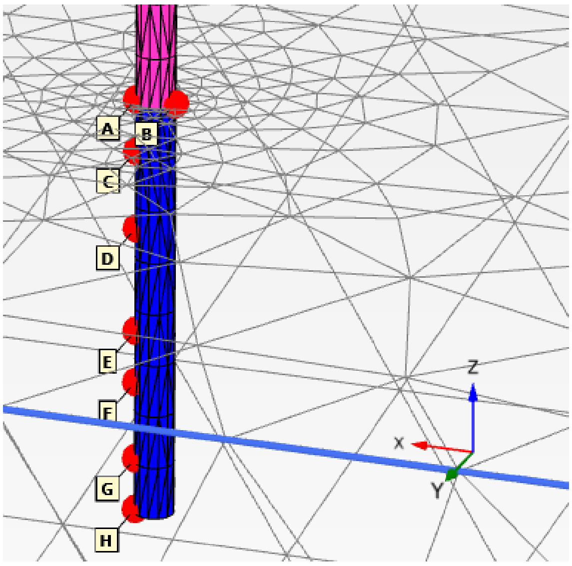

Figure E.7. Localization of chosen points for numerical calculations

The vertical load of 8 MN is chosen to represent the turbine, and it is applied as a surface load. Only for two cases, where the behaviour of monopile between the flexible and the rigid is investigated, the vertical load of 2 MN is applied as a surface load. The magnitude of applied horizontal load is chosen in correspondence to the pile geometry, so that the rotation of 4° on the seabed can be obtained. In cases where the calculations failed due to numerical problems, the tolerated numerical error is slightly increased.

Electronic Appendix F

All the files mentioned in the Electronic Appendix are included on the CD attached to the report. The electronic appendix are divided into two parts: laboratory results and numerical results

Laboratory results

Matlab programs:

"static_test.m" - finding the ultimate capacity for the static tests
"reading_cyclic_data.m", "trimming_data.m", "data_analysis.m" - programs are used in order to prepare data from the laboratory tests and in order to obtain all needed informations
"changing_file_extension.m", "comma2point_overwrite.m" - functions required for the previously mentioned programs
"post_cyclic_resistance.m" - finding the post-cyclic ultimate resistance
"pile_behaviour.m ", "plots_article1.m" , "plots_accumulated_rotation.m" , "plots_stiffness.m", "plots_article2.m" and "stiffness.m" - additional program used for the rest of graphs used in the papers

Excel files:

"all_cyclic_tests.xlsx" - consists an overview of all tests used in the raport
"data for article 2.xlsx" - consists the information about the stiffness and the ultimate resistance changes for the article no 2

Numerical results

Matlab programs:

"soil_parameters_plaxis.m" - program used for calculating the soil parameters
"ULS_all_simulations.m", "pile_deformations.m" , "pile_behaviour.m","static_rotation_plaxis" - programs used in order to display the results from PLAXIS simulations

Maple programs:

"parameters calculations.mw" - calculations of the soil unit weight and the void ratio

Plaxis programs:

”D5L25_40D_20D+L_ULS_4degree.P3D” - D = 5m, L = 25m, e 1.2 L, dense sand
”D6L25_40D_20D+L_ULS_4degree.P3D” - D = 6m, L = 25m, e 1.2 L, dense sand
”D7L25_40D_20D+L_ULS_4degree.P3D” - D = 7m, L = 25m, e 1.2 L, dense sand
”D5L30_40D_20D+L_ULS_4degree.P3D” - D = 5m, L = 30m, e 1.2 L, dense sand
”D5L35_40D_20D+L_ULS_4degree.P3D” - D = 5m, L = 35m, e 1.2 L, dense sand
”D5L25_e1.0L.P3D” - D = 5m, L = 25m, e 1.0 L, dense sand
”D5L25_e1.4L.P3D” - D = 5m, L = 25m, e 1.4 L, dense sand
”D5L11-ULSrigid.P3D” - D = 5m, L = 11 m, e 1.2 L, dense sand
”D1L11-ULSflexible.P3D” - D = 1m, L = 11m, e 1.2 L, dense sand
”D5L25_mediumsand” - D = 5m, L = 25m, e 1.2 L, medium-dense sand
”D5L25_loosesand” - D = 5m, L = 25m, e 1.2 L, loose sand